# **Engineering Activatable Promoters for Scalable and Multi-Input CRISPRa/i Circuits**

Diego Alba Burbano<sup>+,1,2</sup>, Ryan Cardiff<sup>+1</sup>, Benjamin I. Tickman<sup>1,2</sup>, Cholpisit Kiattisewee<sup>1</sup>, Cassandra Maranas<sup>1</sup>, Jesse G. Zalatan<sup>\*1,3</sup>, James M. Carothers<sup>\*,1,2</sup>

1: Molecular Engineering & Sciences Institute and Center for Synthetic Biology University of Washington Seattle, WA 98195 United States

2: Department of Chemical Engineering University of Washington Seattle, WA 98195 United States

3: Department of Chemistry University of Washington Seattle, WA 98195 United States

- +: These authors contributed equally
- \*: Corresponding authors zalatan@uw.edu 206-543-1670

jcaroth@uw.edu 206-221-4902

Proc. Natl. Acad. Sci. USA, In Press.

Classification: Biological Sciences, Applied Biological Sciences

**Keywords:** Activatable promoter engineering, CRISPR activation, gene regulatory networks, genetic circuits, cell-free, optogenetics

# Significance statement

Gene regulatory networks expressed in cell-free systems hold great promise for investigating the limits of biological information processing and developing platforms for molecular biosensing and chemical bioproduction. We address the challenge of engineering gene regulatory networks that can dynamically activate many targets. The work described here enables new classes of deep, wide, and multi-input CRISPR-based genetic circuits. This study represents an important step towards engineered gene regulatory networks with complexities approaching those found in nature.

#### **Abstract**

Dynamic, multi-input gene regulatory networks are ubiquitous in nature. Multi-layer CRISPR-based genetic circuits hold great promise for building gene regulatory networks akin to those found in naturally-occurring biological systems. We develop an approach for creating high-performing activatable promoters that can be assembled into deep, wide, and multi-input CRISPR-activation and -interference (CRISPRa/i) gene regulatory networks. By integrating sequence-based design and in-vivo screening, we engineer activatable promoters that achieve up to 1000-fold dynamic range in an E. coli-based cell-free system. These new components enable CRISPRa gene regulatory networks that are six layers deep and four branches wide. We show the generalizability of the promoter engineering workflow by improving the dynamic range of the light-dependent EL222 optogenetic system from 6-fold to 34-fold. Additionally, high dynamic range promoters enable CRISPRa systems mediated by small molecules and protein-protein interactions. We apply these tools to build input-responsive CRISPRa/i gene regulatory networks, including feedback loops, logic gates, multi-layer cascades, and dynamic pulse modulators. Our work provides a generalizable approach for the design of high dynamic range activatable promoters and enables new classes of gene regulatory functions in cell-free systems.

#### Introduction

Natural biological systems employ complex gene regulatory networks (GRNs) to sense diverse environmental cues and respond to them through the coordinated expression of multiple genes [1]–[3]. Cell-free systems (CFS) have emerged as an attractive chassis for building synthetic biological systems as they allow for rapid prototyping of genetic parts and circuits [4]–[8]. To build increasingly complex CFS capable of sensing and responding to diverse inputs, new approaches for increasing the capabilities of synthetic GRNs are needed [9]–[13]. Advances in GRN engineering will accelerate the use of CFS for building multiplexed biosensors [14]–[16], deploying on-demand bioproduction platforms [17]–[19], and the construction of synthetic cells [20]–[23].

CRISPR-Cas transcriptional regulation has proven a promising framework for building sophisticated genetic circuits across a variety of biological systems [24]–[29]. Transcriptional units containing target sequences for CRISPR activation (CRISPRa) and/or CRISPR interference (CRISPRi), termed CRISPRa/i nodes, can be assembled into circuits with network topologies specified by guide RNAs (gRNAs). Experimental and theoretical analysis indicates that the CRISPRa/i system is well suited to design deep and wide control circuits containing internal nodes connected in series or parallel through orthogonal gRNAs [30]–[32]. Large CRISPRi GRNs with up to 7 gRNAs have been constructed in yeast by implementing low leak promoters and high dynamic range repressors [33]. In *E. coli*-based CFS, CRISPRi genetic control is well established [29], [34], and CRISPRa has recently been incorporated [32], greatly expanding the circuit

design space. However, CRISPRa circuitry is limited by a lack of promoter-gRNA pairs that can be interconnected with minimal signal degradation [32]. Hence, a generalizable approach for engineering activatable promoters with low basal and high activated expression levels would significantly improve CRISPRa and enable the assembly of complex, input-responsive GRNs.

Promoter engineering efforts have traditionally focused on designing constitutive and inducible promoters with predictable expression characteristics [35], [36]. Tuning the strength of constitutive promoters involves designing promoter sequences that achieve a desired level of RNA polymerase (RNAP) recruitment to the promoter [37], [38]. Inducible promoters contain recognition sites for transcriptional activators or repressors that modulate transcriptional levels upon binding [39], [40]. Development of high dynamic range inducible promoters has relied on engineering de-repression based systems [40]–[44], largely due to the difficulty of rationally designing activatable promoters [45], [46]. For effective activation, RNAP recruitment to the promoter should be weak in the absence of an activator, however transcription initiation should be strong upon activator-mediated RNAP recruitment [39], [45]. Hence, tuning RNAP interactions through promoter sequence design could lead to higher dynamic ranges with CRISPRa and other transcriptional activation systems.

We develop an approach integrating sequence-based design and *in-vivo* screening to generate an expandable set of high-performing promoters that exhibit both low basal and high activated expression levels. Through a sequential selection approach, we design activatable promoters with up to 1000-fold dynamic range,

constituting a 33-fold improvement from previous synthetic promoters [32]. These promoters enable complex network topologies with performance levels not previously accessible in CFS [32], including a six-layer deep cascade and a four-branch parallel circuit. By engineering activatable promoters, different inputs can be incorporated into CRISPRa/i CFS circuits. We demonstrate that a blue light-responsive transcriptional activator and three different protein-protein interaction (PPI)-dependent CRISPRa systems can function as circuit inputs. We successfully engineer input-responsive CRISPRa/i circuits operating as multi-layer activation cascades, positive feedback loops, AND-like logic gates, and dynamic two-input pulse modulators. Overall, this work describes a new workflow for engineering activatable promoters and provides a toolbox of versatile components with immediate utility for implementing CRISPRa/i circuits. Together, these developments dramatically expand the ability to assemble large, multi-input GRNs in CFS.

#### Results

We first sought to characterize the impact of sequences affecting RNAP recruitment on both basal and activated expression levels of synthetic activatable promoters. RNAP recruitment is dependent on the affinity of the RNAP sigma subunit (σ) for the -10 and -35 hexamers of the minimal promoter [47], [48] (Figure 1A). Additionally, recruitment is influenced by the GC-content of the intervening sequence between the -10 and -35 sites [47], [48] (Figure 1A). Promoter recognition is enhanced by the AT-rich UP-elements upstream of the minimal promoter, which anchor the α-subunits of RNAP. Collectively, the sequence compositions of these regions influence

RNAP recruitment, binding, and initiation at the promoter. We systematically designed libraries of these discrete promoter regions and used a scalable workflow for screening and isolating library variants in  $E.\ coli$ . The libraries were co-transformed with an aTc-inducible CRISPRa plasmid to enable parallel screening of basal and activated expression levels (Figure 1B, Methods 2) [32]. In the absence of aTc, RNAP recruitment is determined by the promoter basal strength. Upon aTc induction, the MCP-SoxS activator is expressed and localized to a CRISPRa complex at the promoter via a modified gRNA, or scaffold RNA (scRNA), containing the MS2 hairpin. MCP-SoxS then recruits RNAP to the promoter through  $\alpha$ -CTD interactions, activating transcription [49] (Figure 1A). This approach allows us to characterize the impact of individual promoter regions on basal and activated expression simultaneously, and combine variants with low basal and high activated expression to construct high-performing activatable promoters.

# Functional interrogation of promoter regions with CRISPRa

# Impact of Minimal Promoter Region on Activability

Previous work has demonstrated the importance of the minimal promoter region in determining basal and activated expression levels [39], [45], [49]–[51]. We designed two minimal promoter libraries mutagenizing the -10/-35 hexamers and the intervening sequence of the previously identified best-performing minimal promoter (BBa\_J23117) within the J3 synthetic CRISPRa promoter (Figure 1C, Methods 3.1) [45]. These libraries were co-transformed with the aTc-inducible CRISPRa plasmid expressing the J306 scRNA targeting the cognate J3 promoter. Both libraries yielded high promoter

diversity, as measured by RFP expression levels, with basal and activated expression levels ranging from that of a no-reporter control to a strong constitutive promoter (BBa\_J23119) (Figure 1D). The subset of promoters not activated may arise from the generation of sequences resembling tightly regulated native promoters.

The set of minimal promoter variants that maintain both low basal and high activated expression levels can be conceptualized as a Pareto optimal front. In multi-objective optimization, a Pareto front defines the best-performing solutions for which no further improvements in either objective can be achieved without compromising the other (Methods S3) [53]. Three variants from this Pareto front exhibited both lower basal and higher activated expression levels compared to the original BBa\_J23117, indicating the original minimal promoter was not a part of the Pareto front. This finding suggests that promoter mutagenesis can yield improved activatable promoters beyond previous screening methods based on promoter basal strengths alone [45]. By mutagenizing the minimal promoter of CRISPRa promoters, we generated sequences with >100-fold dynamic range in CRISPRa-mediated gene expression (Figure S1).

#### Impact of UP-Element Region on Activatibility

RNAP promoter recognition is enhanced by the AT-rich UP-elements upstream of the minimal promoter, which anchor the  $\alpha$ -subunits of RNAP [39], [47], [54]. For effective CRISPRa, RNAP should only be recruited to the promoter in the presence of an on-target scRNA. Hence, for transcriptional activation with SoxS, improvements in dynamic range could be achieved by minimizing RNAP-UP-element interactions and

lowering basal expression levels [55]. We designed five UP-element libraries mutagenizing the AT-rich E. coli consensus sequence with increasing GC-content (Figure 2A, Methods 3.2). As expected, the consensus UP-element and the AT-rich library had the highest basal expression levels (Figure 2B, left). On average, these libraries showed only 3-fold activation, as compared to 37- to 44-fold activation for the more GC-rich libraries (Figures S2, S3). Qualitatively, we observed a monotonic decrease in basal expression levels and no impact on maximum activated levels with increased GC-content (Figure S2). We identified the optimal variants from each library and found a shift in the Pareto front towards lower basal and higher activated expression levels with increasing UP-element GC-content (Figure 2B, right). Specifically, the median basal and activated expression levels of the GC-rich optimal variants were 59.7-fold lower and 1.7-fold higher than that of the AT-rich optimal variants. The original J3 synthetic promoter, with an UP-element GC content of 50%, sat in between the Pareto fronts consisting of high and low GC-content variants. By mutagenizing the UP-element, we generated promoter variants with >350-fold dynamic range in CRISPRa-mediated gene expression.

# Impact of the scRNA target site region on activatability

Transcriptional activators bind upstream of the minimal promoter region to recruit RNAP to the transcription start site (TSS) [39]. For CRISPRa, the optimal scRNA target site location for SoxS-mediated activation is -81 bp upstream of the TSS [45]. Changing the scRNA target sequence enables rapid generation of orthogonal CRISPRa promoters [56], [57]. Due to the proximity to the UP-element region, we reasoned that

the sequence composition of the scRNA target site may have an impact on basal expression levels. We designed three scRNA target site libraries composed of varying GC-content (Methods 3.3) and measured the basal expression of each library. GC-rich libraries had 4.3-fold lower median basal expression compared to AT-rich libraries (Figure 2C). Additionally, the spread of the basal expression decreased monotonically with increasing GC-content of the scRNA target site sequence (Figure 2C). Together, these results indicate GC-rich scRNA target site sequences lead to low basal expression CRISPRa promoters, perhaps due to reduced interaction with RNAP. To validate the CRISPRa activity at these low basal expression scRNA target sites, we selected 10 GC-rich variants and constructed the corresponding scRNAs. All variants produced a higher fold-activation than the original J306 scRNA (Figure S4), with 3.5-fold average increase in fold-activation.

# Combining promoter regions to engineer high-performing CRISPRa promoters Engineering activatable promoters by combining optimized promoter regions

We proceeded to test if the highest performing variants from the UP-element and minimal promoter screens could be combined to yield activatable promoters with improved performance. We selected three high-performing variants from both the UP-element and minimal promoter screens, as well as the starting J3 UP-element and BBa\_J23117 minimal promoter, and constructed a combinatorial set of 16 promoters. Notably, promoter regions that gave the largest improvements in the original context did not necessarily give the largest improvements when tested in different contexts (Figure S5). For instance, an UP-element that gave 300-fold activation with one minimal

promoter only gave 200-fold activation with a different high-performing minimal promoter (p = 0.003), largely due to an increase in basal expression (Figure S5, right). ANOVA results ( $p = 10^{-5}$ ) support the view that UP-element and minimal promoter contributions affecting activation cannot be isolated from one another (Table S7).

# Engineering activatable promoters through sequential promoter region screening

The results from the previous section highlight the effects that promoter region contexts play in the design of high-performing activatable promoters. Therefore, we tested whether promoters with improved basal and activated expression levels could be achieved by selecting minimal promoters in the context of high-performing UP-elements. We first screened the UP-element region as these libraries had a larger impact than the minimal promoter libraries on the location of the Pareto front (Figures 1D, 2B). We mutagenized the UP-element of a promoter containing the minimal promoter BBa J23117 and a GC-rich scRNA target. We selected three Pareto-optimal UP-element variants which had on average 10% of the original basal and 12% higher activated expression than the J3 promoter (Figure 2D). We then screened minimal promoter libraries in the context of these three selected UP-element variants. We again selected three new promoter variants from the Pareto front, which had on average 17% of the basal and 56% higher activated expression than the J3 promoter (Figure 2D). With this sequential screening approach, we overcame the context effects observed in the previous section and successfully shifted the Pareto front towards lower basal and higher activated expression for both the UP-element and minimal promoter screens.

# Engineering deep and wide circuits with high-performing CRISPRa promoters

In nature, interconnected, multi–layer transcriptional networks coordinate the timing and levels of expression of multiple genes to produce complex responses to environmental stimuli [1], [58], [59]. To develop CRISPRa/i GRNs with complexities approaching those found in nature, components enabling construction of circuits with arbitrary interconnections and minimal signal degradation are needed. CRISPRa promoters with high output dynamic ranges are expected to minimize signal degradation by enabling effective level-matching of the input/output dynamic ranges between sequential CRISPRa/i nodes [32], [33]. Dynamic range improvements achieved at the promoter level should translate into signal propagation improvements at the circuit level and enable construction of increasingly deep and wide CRISPRa circuits.

# Engineering functional CRISPRa/i nodes

We characterized the three promoter variants selected above (Figure 2D, HP1-3) in CFS and observed up to ~1000-fold dynamic range (Figure S6) and a high degree of correspondence with *in vivo* expression levels ( $R^2 = 0.92$ ). We used these promoters to generate a set of orthogonal CRISPRa/i nodes to be assembled into multi-layer circuits following previously-described methods [32]. We combined the highest dynamic range activatable promoter (HP3, Table S1) with previously-screened scRNA target sites to generate orthogonal CRISPRa/i nodes (Figure 3A). Dose-response curves for each orthogonal node made by titrating the plasmid expressing the cognate scRNA showed that these new nodes gave an average activation of 890-fold (Figures 3B, S7; Table S1). Given the context dependence of activation, these nodes could be further improved

through sequential mutagenesis of promoter elements in the context of the corresponding scRNA target sequence.

# Deep CRISPRa Circuits

We investigated whether deep multi-layer cascades could be implemented using the improved CRISPRa/i nodes. We first built a two-layer CRISPRa cascade by tuning the expression levels of the input and internal CRISPRa/i nodes and achieved up to 127-fold activation (Figures S8, S9). An excess of either the input or internal node led to decreased performance of the cascade, potentially due to scRNA competition for binding to dCas9 [30], [60]. Next, we assembled four-layer activation cascades. To compare circuit performance and dynamics in response to scRNA inputs, we measured RFP expression and time to maximum expression rate ( $t_{max}$ ) (Figures 3C, insert; S10) (Methods S3). If the input signal propagates faster than the leak from the rest of the nodes, CRISPRa-dependent expression through the network accelerates, reducing  $t_{max}$ . Therefore, a larger  $t_{max}$  between the +/- input conditions ( $\Delta t_{max}$ ) corresponds with improved circuit function.

For a cascade with equal node concentrations at each layer, we found no input-dependent change in maximum RFP expression and a  $\Delta t_{max}$  of 110 min (Figure 3C, middle). We tuned node concentrations by either decreasing (denoted "D") or increasing (denoted "I") the concentration of each subsequent node as depth increased (Figure 3C, left). These Assemblies D and I had the lowest and highest expression levels, respectively (Figure 3C, middle). These assemblies also had  $t_{max}$  significantly accelerated compared to their no input conditions ( $\Delta t_{max}$  of 85 min and 165 min, and p =

0.01 and  $p = 3 \times 10^{-4}$ , respectively) (Figure 3C, right). When scRNA-promoter dose-response curves were used to inform circuit assembly, we obtained 3-fold higher activated expression than assembly D and 4.5-fold lower basal expression than assembly I, with a similar overall fold-activation and  $\Delta t_{max}$  (Figure 3C).

We interrogated the impact of high-performing promoters on circuit function by exchanging the high-performing promoter of the second internal node for a previously characterized promoter with leakier basal expression [32]. While the leakier promoter was sufficient for constructing functional two-layer cascades [32], the four-layer cascade was no longer input-responsive, as indicated by the fact that expression level and  $t_{max}$  were the same with or without input scRNA. In contrast, all of the assemblies containing high-performing promoters were input-responsive, underscoring the importance of high-performing promoters for building deep transcriptional circuits.

To improve the fold-activation of the four-layer cascade, we tuned the concentrations of individual nodes in the cascade. To reduce the experimental search space, we held the second node constant and tuned the concentrations of the first and third internal nodes. With this approach, the tuned four-layer cascade achieved 16-fold activation compared to 2-fold activation of the initial cascades (Figures 3C, 3D). Qualitatively, higher concentrations of the third node resulted in higher activated states, while lower concentrations of the first node minimized basal expression (Figure S11). Notably, these circuits maintained roughly 80% of their maximal activity even when node concentrations varied by nearly 50% (Figures 3D, S11), showing that they are robust to changes in the amounts of gRNAs and targets. Overall, these results indicate

that timing and expression level of multi-layer, input-responsive circuits can be controlled through node concentration tuning.

We investigated how input signals are communicated through increasingly deep circuits by measuring signal propagation and signal delay at each layer (Figure 3E, left). We quantify the percent of signal propagated by calculating the fold-activation of the full cascade output divided by the activation from the input layer (Methods S3). We define signal delay as the difference between  $t_{maxFC}$  of the cascade input and output layer, where  $t_{maxFC}$  is the time needed to reach the maximum fold-activation (Methods S3). Signal propagation was sustained above 80% until the 4th layer was added, after which it decreased rapidly (Figure 3E, right). Nevertheless, we observed measurable output differences in circuits of up to six layers. The two-layer cascade gave no significant difference in signal delay compared to a single-layer CRISPRa reaction (p = 0.9). This may suggest there is a slow step in output production, such as fluorophore maturation, that masks the effect of the second layer. Beyond two layers, the signal delay increased with subsequent additions of the third, fourth, and sixth layers (Figure 3E, right), averaging ~50 min/layer, but ranging from ~20-100 min.

We investigated whether the signal propagation and signal delay at each layer could be explained by the performance of individual nodes. We used the maximum fold-change of individual nodes from the dose-response curves (Figure S7) to predict the delay and signal propagation at the subsequent level (Methods S4). The model-derived predictions showed high correspondence with the signal propagation and delay at each of the six layers ( $R^2 = 0.92$  and  $R^2 = 0.91$ , respectively) (Figure S12).

These results are consistent with the ideas that high-performing nodes can quickly activate subsequent layers, propagate signals efficiently, and be assembled into deep circuits.

#### Wide CRISPRa Circuits

To identify conditions under which orthogonal nodes can compose wide CRISPRa circuits, we constructed one, two, three, and four parallel three-layer cascades operating in the same CFS reaction. We used a single input to activate the downstream nodes, and measured circuit performance by connecting all of the parallel cascade scRNA outputs to the same RFP node (Figure 3F, left). When we maintained the internal node concentrations constant across parallel cascades, we observed up to 66% decrease in output fold-activation as the width of the circuit increased from one to four cascades (Figure 3F, right). This decrease came largely from higher output levels in the absence of scRNA input (Figure S13), most likely due to higher basal expression of internal scRNAs. We then constructed the same circuits and tuned the node concentrations proportionally to the number of parallel cascades, effectively maintaining the total node concentration constant. When constructed in this manner, we found no statistically significant difference in the fold-activation across cascades of different widths (p = 0.61) (Figure 3F, right). Hence, by tuning the concentration of orthogonal CRISPRa/i nodes, we show an arbitrary number of parallel circuits with as many as nine nodes may be regulated.

# Developing activatable promoters for blue-light responsive CRISPRa/i circuits High-performing blue-light responsive promoters

Having demonstrated that high-performing CRISPRa promoters can be generated through sequential screening, we tested the same approach for engineering activatable promoters responsive to other transcriptional activators. The EL222 transcriptional activator interactions with the RNAP and the DNA binding site are well-characterized, making it a suitable model system for developing optogenetic inputs for CRISPRa/i circuits (Figure 4A) [61]–[64]. Briefly, EL222 binds an 18 bp sequence upstream of the -35 region of the *luxl* promoter and subsequently recruits RNAP through interactions with the  $\alpha$  and  $\sigma$  subunits [64]. We mutagenized the *luxl* minimal promoter (Figure 4A, Methods 3.4), and screened variants in *E. coli* in dark and light to select for high dynamic range (Figure 4B). Starting with a dynamic range of less than 2-fold, we observed up to 4-fold dynamic range in response to blue-light. Similar to our CRISPRa promoter screens, minimal promoters with very low (BBa\_J23113) or very high (BBa\_J23119) basal expressions exhibited low dynamic range in response to blue-light.

We selected 4 variants with >2-fold higher dynamic range than the *luxI* minimal promoter and characterized them in CFS. These variants yielded a 34.1-fold difference in expression between light and dark, compared to just 6.2-fold for the original *luxI* minimal promoter (Figure S14). This improvement comes largely from a reduction in the basal expression from the blue-light promoter, suggesting we successfully minimized the RNAP-minimal promoter interactions without weakening EL222-promoter

interactions. More importantly, these results demonstrate this approach for engineering actionable promoters is applicable to other transcriptional activation systems.

# Blue-light responsive CRISPRa/i circuits

We evaluated whether the engineered blue-light promoter transcription levels were suitable for expressing gRNAs for CRISPRa/i circuits. We titrated gRNA-expressing plasmid concentrations and compared RFP expression across dark and light conditions. For CRISPRi, the highest light-dependent change in repression was 50% (Figure S15). For CRISPRa, the highest light-dependent fold-activation was 11-fold (Figure 4C), which improved to 14-fold upon increasing EL222 plasmid concentration (Figure S16).

We then constructed a light-dependent activation cascade and observed only a 5-fold activation in response to blue light (Figure 4D). To improve the fold-activation, we implemented a positive feedback loop (PFB) in which a downstream node expresses a scRNA directing CRISPRa to an upstream node. We expected the degree of positive feedback in the system to be tunable by titrating the PFB node, with high concentrations of this node resulting in activation in the absence of blue-light. When optimally tuned, the PFB loop increases the light-dependent CRISPRa output levels almost 2-fold (Figure 4D). Excess PFB node led to a 7.6-fold increase in basal expression, decreasing the light-dependent activation to 1.2-fold. These results highlight that rationally designed genetic circuits built from engineered activatable promoters can be used to improve the dynamic range of input-responsive signal processing modules.

# Engineered activatable promoters enable conditional CRISPRa dependent on protein-protein interactions

The versatility of protein-protein interaction (PPI)-mediated genetic regulation for coupling peptide or small-molecule binding to transcriptional outputs has long attracted interest [65]–[71]. In principle, CRISPRa assemblies incorporating dimerizing protein domains could be utilized for PPI-dependent transcriptional activation in bacterial CFS. However, realization of these systems has been limited by strict target site requirements and low dynamic range of activatable promoters [45], [72]. We reasoned that the high dynamic range promoters developed here would allow us to screen for otherwise hard-to-detect functional target sites and component stoichiometries and, if successful, achieve effective conditional, PPI-dependent CRISPRa.

# **Development of Conditional CRISPRa Systems**

As experimental testbeds, we incorporated three previously characterized protein-protein heterodimerization domains into our CRISPRa system: the synthetic coiled-coil SYNZIP 5/6 pairs [73], the abscisic acid (ABA) responsive ABI-PYL1 [65], [74], [75], and the gibberellic acid (GA) responsive GID1-GAI [65], [76]. We fused these heterodimerization domains to SoxS and MCP to enable conditional recruitment of SoxS to the CRISPRa complex. We generated the MCP-SZP6 and SoxS-SZP5 domains for SYNZIP-CRISPRa, the MCP-ABI and SoxS-PYL1 domains for ABA-CRISPRa, and MCP-GAI and SoxS-GID1 for GA-CRISPRa (Figure 5A). In the original J3 promoter context, we observed 5.7-fold activation when cognate SYNZIPs were fused to the C-termini of MCP (MCP-SYNZIP) and SoxS (SoxS-SYNZIP) (Figure S17). This combination of orientations gave the best activation, compared to 2.8-fold

when MCP was fused in the opposite orientation (SYNZIP-MCP & SoxS-SYNZIP), and 1.4-fold when SoxS was fused in the opposite orientation (MCP-SYNZIP & SYNZIP-SoxS) (Figure S17). The fold-activation of ABA-CRISPRa was also maximized when SoxS was at the N-terminus (Figure S17, right), therefore we moved forward with all SoxS N-terminus fusions. For ABA- and GA-CRISPRa, only C-terminus MCP fusions were tested due to the MCP-SYNZIP result and the strong precedent for using C-terminus MCP fusions in CRISPRa systems [49], [77].

CRISPRa operates narrowly within -101:-71 bp from the TSS in a phase-dependent manner [45]. We tested whether the introduction of an additional protein linkage into MCP-SoxS affects the relative scRNA target site requirements [72]. We designed a CRISPRa promoter with densely-packed scRNA target sites every 10 bp [49], as well as variants with 1 bp frameshifts [45], [72] to allow screening with single base pair resolution between -111:-81 bp from the TSS (Figure 5B, Table S1). Surprisingly, SYNZIP-CRISPRa maintains the same preference for the targeting site -81 bp from the TSS and the same stringent 10-11 bp phase dependency seen in conventional CRISPRa (Figure 5B, S18). We then tested SYNZIP-CRISPRa using a high-performing promoter with an optimal target site (HP3, Table S1) and found a 5.4-fold improvement compared to the original J3 promoter (Figure S19).

To create functional systems for coupling peptide or small-molecule binding to CRISPRa-directed transcriptional outputs, we identified permissible small-molecule input and component expression levels. For ABA- and GA-CRISPRa, small-molecule titrations showed that ABA-CRISPRa is responsive between 0.1-10 uM with up to 7.9

fold-activation, and GA-CRISPRa is responsive between 1-1000 uM with up to 9.0 fold-activation (Figure 5C). We screened dimer stoichiometries and expression levels by surveying a range of concentrations for the MCP- and SoxS-fused components. SYNZIP-CRISPRa performs the best of the three systems, giving a maximal activation of 67-fold compared to a control without MCP or SoxS. Even at low concentrations of MCP- and SoxS-fused components, SYNZIP-CRISPRa still achieves 59-fold activation (Figure 5D, left). ABA-CRISPRa gave a maximum activation of 18.6-fold (Figure 5D, middle). For GA-CRISPRa, the maximum activation of 5.9-fold was accessible in a relatively narrow range of component concentrations (Figure 5D, right). For all three PPI-dependent CRISPRa systems, higher expression of the MCP- and SoxS-fused heterodimer components did not necessarily improve activation. In line with the behaviors of natural scaffolds [78], [79], we observed a unique optimal concentration for each PPI-dependent CRISPRa system. The differences between systems may be due to the different affinities of each protein-protein interaction.

# Engineering multi-input CRISPRa/i circuits

#### Multi-layer and multi-input circuits with conditional CRISPRa

We built two types of input-responsive circuits to explore the use of conditional CRISPRa for multi-input and multi-layer input processing: an AND-like logic gate and a CRISPRa cascade. We began by characterizing the scRNA dose-response curve of the novel CRISPRa systems. For both conditional CRISPRa systems, the amount of scRNA needed to saturate the CRISPRa response was similar to that of direct CRISPRa (Figures S7, S20). We tested the orthogonality of the small molecule systems to evaluate if they could be used together for independent gene regulation (Figure 6A).

ABA-CRISPRa is highly specific to its target ligand, showing no significant activation in the presence of GA (p = 0.21). GA-CRISPRa showed 3.1-fold cross-activation from ABA, in line with reports in eukarya [65]. Nonetheless, GA-CRISPRa maintained a 3-fold higher specificity for its cognate ligand, giving 10.5-fold activation from GA. These results suggested that the ABA- and GA-CRISPRa systems could be used for orthogonal gene regulation.

We constructed a multi-input circuit for AND logic by co-expressing components for ABA- and GA-CRISPRa (Figure 6B, left). The addition of either ABA or GA resulted in 2-fold activation compared to the no-ligand condition (p = 0.03). Therefore, we specified that the average of the technical replicates must be above or below 2-fold activation for the circuit to be considered ON or OFF. Consistent with AND-like logic, the circuit generated 4.5-fold activation in the presence of both ligands, a level of activation that was clearly distinct from either of the one-input states (p = 0.03). We built a multi-layer conditional CRISPRa cascade by having both internal layers dependent on ABA. The cascade gave 2.5-fold activation upon addition of ABA, showing that conditional CRISPRa can also support multi-layer information processing (Figure 6B, right).

### Two-input dynamic pulse generator

Synthetic biologists aim to recreate complex, dynamic signaling networks with multiple input-responsive regulators to tightly program the expression timing and magnitude of downstream targets [2], [3], [80]. As a proof of concept, we aimed to engineer a GRN that integrates blue-light CRISPRi with PPI-dependent CRISPRa. The

result would be a tunable pulse generator with two-input control over the level and timing of gene expression (Figure 6C, left). Because SYNZIP-CRISPRa has high-fold activation (Figure S20), we expected that it could be well suited for integration with blue-light CRISPRi.

We first employed simulation analysis to identify system designs for combining two inputs and dynamically regulating reporter gene expression. We built upon a coarse-grained mechanistic model of CRISPRa/i regulation [32] by introducing blue-light pulses regulating gRNA expression (Methods 6). We simulated changes in the pulse width as CRISPRi inputs and scRNA concentration as CRISPRa inputs. By evaluating changes in reporter production rates, our analysis suggested that there are broad ranges of CRISPRi and CRISPRa input parameter values compatible with multi input-responsive regulatory control (Figure 6C, left).

We proceeded to experimentally validate the results of the simulation analysis. To dynamically tune CRISPRi, we changed the blue-light exposure time. To tune SYNZIP-CRISPRa, we changed the scRNA-expressing plasmid concentration. In all cases, we first kept the CFS in the dark for one hour to allow for EL222 expression. As predicted by the model, RFP production rate pulse was tunable by the scRNA plasmid concentration and the blue-light exposure time (Figure 6D). When compared across conditions with the same CRISPRa input, higher CRISPRi input led to 20-56% lower maximum production rates. In conditions with the same CRISPRi input, higher CRISPRa input increased maximum production rates by 20-40 minutes. Collectively,

these results highlight the potential of input-responsive CRISPRa/i GRNs for complex signal processing applications.

#### **Discussion**

Natural biological systems have evolved GRNs containing wide ranges of activatable promoters that enable dynamic responses to changing environmental conditions. Engineering activatable promoters has traditionally been thought to involve a trade-off between basal and activated expression levels [35], [41], [45]. In this work, we show that this trade-off can be relaxed to generate activatable promoters with both lower basal and higher activated expression levels than previously possible (Figures 1B, 2B). Sequential screening of promoter regions allowed us to overcome context effects and identify high-performing activatable promoters (Figure 2D). With this approach, we successfully engineered a suite of orthogonal CRISPRa promoters that match the basal and activated expression levels of the canonical Tet inducible system (Figure S21) and exceed those of the IPTG inducible system [81].

The *E. coli* transcriptional network is governed by a hierarchical structure containing nine layers of regulation [1]. Engineered activatable promoters allowed us to build multi-layer CRISPRa/i GRNs in *E. coli*-based CFS with depths and widths significantly larger than the state of the art [32], [82], approaching the complexity of natural GRNs. Specifically, a 33-fold improvement in promoter dynamic range resulted in 80% lower signal degradation in two-layer cascades [32], and enabled deep GRNs with up to six layers of regulation (Figure 3E). Additionally, we demonstrated wide GRNs regulating up to four parallel cascades (Figure 3F), indicating that the CRISPRa/i framework is well suited for the design of wide control circuits for parallel computing and multi-gene regulation [25]. We also showed that these circuits can be implemented in *E*.

coli by constructing three-layer activation cascades with the internal nodes expressed from either high or low copy number plasmids (Figure S22). The *E. coli* cascades maintained more than 3-fold activation regardless of the copy numbers of the internal node plasmids (Figure S22), demonstrating the high correspondence between CFS and *in vivo* component function [6], [83]. To our knowledge, these represent the deepest CRISPRa cascades in CFS and *in vivo*. Further improvements in GRN complexity may be limited by resource constraints, including upstream gRNAs outcompeting downstream gRNAs for dCas9 binding (Figure S8, Figure S22). Strategies to dynamically regulate upstream gRNA expression, such as reversing CRISPRa complex binding or implementing negative autoregulation motifs [84], could enable even larger GRNs.

Biological systems continuously monitor and process environmental signals by using signal transduction modules as inputs to complex GRNs [85], [86]. Our work provides a general framework for optimizing transcriptional activation systems at the promoter level and integrating them into CRISPRa/i GRNs. Promoter engineering of the optogenetic EL222 system enabled high light-dependent dynamic ranges (Figures 4B, S14), with relevant expression levels for downstream applications (Figures 4C, S15). Through inducible gRNA expression, we demonstrated input signal modulation with various GRN topologies, including positive feedback loops and CRISPRa/i cascades (Figure 4D), as well as integration of different signal transduction modules into the same CRISPRa/i GRN (Figure 6B). Overall, our work highlights the potential for achieving more complex biocomputing functions, including multi-input AND and NOT gates for

targeted therapeutics and next-generation biosensors [87], through multi-input CRISPRa/i GRNs.

Protein-protein interactions have been used widely to execute complex, input-responsive functions in eukaryotes [88]–[92]. Developing similar systems in prokaryotes has been difficult, and the development of high dynamic range promoters allowed us to successfully prototype and optimize conditional CRISPRa systems in *E. coli*-based CFS. Implementation of novel conditional CRISPRa systems may be streamlined by the fact that all systems tested here are effective when targeted -81 bp from the TSS (Figures 5B, S18), despite the presence of additional protein-protein interactions up to 500 amino acids in length. Additionally, conditional CRISPRa fold-activation is proportional to the strength of the protein-protein interaction (Table S2) [73], [76], [93]–[97], informing the *a priori* selection of heterodimers for use in conditional CRISPRa. Collectively, our work suggests that other heterodimerization domains could be implemented, with minimal prototyping, as signal transduction modules for CRISPRa/i GRNs for multiplexed biosensing or screening of PPIs in CFS.

Our workflow for activatable promoter engineering enables the dynamic specification of expression levels for large networks of orthogonal gene targets. The new classes of deep, wide, and input-responsive CRISPRa/i GRNs developed here have immediate application in CFS for investigating the rules of genetic circuit design [10], [13] and biological information processing [20]–[23], as well as for building dynamic, multi-enzyme expression programs for self-assembling bioproduction platforms [17]–[19], [98], [99]. Moreover, CRISPRa/i GRNs could be integrated with existing field-deployable medical diagnostics and environmental monitors to enable

complex, multi-input signal processing [4], [15], [16], [100]. Moving forward, this work could serve as a stepping stone for building entirely synthetic cells and engineered living materials with GRNs that match or go beyond the complexity of natural systems.

#### Methods

# 1. Plasmid and Library Preparation

Details regarding plasmid and library construction are presented in Methods S6. Plasmids were transformed into chemically competent NEB Turbo *E. coli.* 10 uL of the outgrowth with transformed libraries was diluted 1:20 with LB and plated onto LB-agar with carbenicillin to check library complexity. The remaining outgrowth was seeded into 5 mL of LB with carbenicillin or gentamicin. Cells were grown overnight ~16 hours at 37 °C. Single colonies were picked from plates and grown overnight in LB with carbenicillin. Single colonies and culture were sequence verified. Plasmids were isolated from subcultures using a DNA miniprep kit (QIAprep Spin Miniprep Kit) and Sanger sequenced (Genewiz inc.).

# 2. E. coli Experiments

dCas9, MCP-SoxS, and scRNA are on a p15A ori plasmid while reporter construct is located on a pSC101\*\* ori plasmid. For experiments involving more than two plasmids, competent cells were first made from cells carrying the reporter plasmid and the CRISPRa plasmid (including either on- or off-target input scRNAs). The appropriate plasmids expressing internal scRNAs were transformed into the competent cells. Details regarding culturing conditions and quantification are provided in Methods S8.

#### 3. Design of Promoter Region Libraries

#### 3.1 Minimal Promoter Libraries

MP1 was designed by rationally mutagenizing specific bases that are known contacts of RNAP within the minimal promoter. MP2 was made by randomly mutagenizing within

the intervening sequence. Since the libraries yielded similar Pareto fronts, we combined these mutations into MP3, used in the sequential screening process (Table S3).

# 3.2 UP-Element Libraries

We designed five UP-element libraries mutagenizing the AT-rich *E. coli* consensus sequence with increasing GC-content. We generated 5 libraries from 0% to 100% GC-content, and a library representing the *E. coli* consensus sequence (Table S3).

# 3.3 scRNA Target Site Libraries

We generated three scRNA target site libraries with varying compositions of GC-content (0%, 50%, and 100%) (Table S3). These libraries were used in tandem with a GC-rich UP-element.

# 3.4 EL222 Minimal Promoter Libraries

Starting with the native *luxl* minimal promoter, we introduced rational mutations to make it resemble a synthetic activatable promoter (J23117). We then randomly mutagenized within the -10:-35 region (Table S3).

# 4. Cell-Free System Preparation

CFS was acquired from Arbor Biosciences (myTXTL). The CFS used for an experiment was thawed on ice and pooled into a 1.5 ml Eppendorf tube, vortexed, and spun-down using a mini benchtop centrifuge to ensure sample homogeneity. Details about plasmid preparation are provided in Methods S1, and details about the CFS reaction are provided in Methods S5..

# 5. Optogenetic Experiments

*E. coli* cultures and CFS reactions were prepared as described above. The incubation conditions were modified to include a blue-light illumination source (UVP Visi-Blue UV Transilluminator, 8 Watts, 460/470 nm). Details about optogenetic setup are provided in Methods S7.

# 6. CFS Blue-light CRISPRa/i modeling

The CFS blue-light CRISPRa/i model was expanded from the previously described CFS CRISPRa/i model [32]. The model constitutes a series of first order chemical reactions for protein and guide RNA production, CRISPR complex assembly, and DNA targeting. All model details are described in Methods S2.

# 7. Quantification and statistical analysis

# 7.1 Data analysis

Throughout this work all measured RFP levels in *E. coli* were normalized by measured OD600 with appropriate propagation of uncertainties. All metrics are described in Methods S3.

#### 7.2 Statistics

Statistical significance was calculated using two-tailed unpaired Welch's *t*-tests. Asterisks in Figures indicate a statistically significant difference (\*: p-value < 0.05, \*\*: p-value < 0.01, \*\*\*: p-value < 0.001).

#### **Author Information**

# **Corresponding Authors**

James M. Carothers - Department of Chemical Engineering, Molecular Engineering & Sciences Institute and Center for Synthetic Biology, University of Washington, Seattle, WA 98195; Email: <a href="mailto:jcaroth@uw.edu">jcaroth@uw.edu</a>

Jesse G. Zalatan- Department of Chemistry, Molecular Engineering & Sciences Institute and Center for Synthetic Biology, University of Washington, Seattle, WA 98195; Email: <a href="mailto:zalatan@uw.edu">zalatan@uw.edu</a>

#### Authors

**Diego Alba Burbano** - Department of Chemical Engineering, Molecular Engineering & Sciences Institute and Center for Synthetic Biology, University of Washington, Seattle, WA 98195

**Ryan Cardiff** - Molecular Engineering & Sciences Institute and Center for Synthetic Biology, University of Washington, Seattle, WA 98195

**Benjamin I. Tickman** - Department of Chemical Engineering, Molecular Engineering & Sciences Institute and Center for Synthetic Biology, University of Washington, Seattle, WA 98195

**Cholpisit Kiattisewee** - Molecular Engineering & Sciences Institute and Center for Synthetic Biology, University of Washington, Seattle, WA 98195

Cassandra Maranas - Molecular Engineering & Sciences Institute and Center for Synthetic Biology, University of Washington, Seattle, WA 98195

#### **Author Contributions**

D.A.B., R.C., B.I.T., J.G.Z., and J.M.C. designed the research. D.A.B., R.C., and C.M. performed experiments. D.A.B., R.C., B.I.T., C.K., and C.M. analyzed the data. D.A.B., R.C., J.G.Z., and J.M.C. wrote the manuscript with input from all of the authors.

# **Acknowledgements**

We thank members of the Carothers and Zalatan groups for advice, materials, and comments on the manuscript. We also thank the Thachuk and Baker labs for access to their Echo instruments.

# **Competing interests**

D.A.B., R.C., J.G.Z., and J.M.C are inventors on patents and/or patent applications filed by the University of Washington that describe promoter engineering, conditional CRISPRa technologies, and CRISPRa/i circuits in prokaryotic systems. J.G.Z. and J.M.C are members of the Wayfinder Biosciences scientific advisory board.

# Data sharing plans

Data supporting the findings of this work are available within the paper and its supporting information files. All data and code are available on GitHub at: https://github.com/carothersresearch/CRISPRai\_Circuits\_2022

#### **Funding information**

This work was supported by US National Science Foundation (NSF) Award MCB 2032794 (J.M.C. and J.G.Z.), NSF Award CBET 1844152 (J.M.C.), NSF Award EF-1935087 (J.M.C.), US Department of Energy (DOE) BETO DE-EE0008927 (J.M.C. and J.G.Z.) and DOE ARPA-E DE-AR00002387-1567 (J.M.C). This material is based upon work supported by the NSF Graduate Research Fellowship Program under Grant No. DGE-2140004 (D.A.B.). Any opinions, findings, and conclusions or recommendations expressed in this material are those of the author(s) and do not necessarily reflect the views of the NSF.

#### References

- [1] H.-W. Ma, B. Kumar, U. Ditges, F. Gunzer, J. Buer, and A.-P. Zeng, "An extended transcriptional regulatory network of Escherichia coli and analysis of its hierarchical structure and network motifs," *Nucleic Acids Res.*, vol. 32, no. 22, pp. 6643–6649, 2004, doi: 10.1093/nar/gkh1009.
- [2] L. Cai, C. K. Dalal, and M. B. Elowitz, "Frequency-modulated nuclear localization bursts coordinate gene regulation," *Nature*, vol. 455, no. 7212, Art. no. 7212, Sep. 2008, doi: 10.1038/nature07292.
- [3] D. Benzinger, S. Ovinnikov, and M. Khammash, "Synthetic gene networks recapitulate dynamic signal decoding and differential gene expression," *Cell Syst.*, p. S2405471222000825, Mar. 2022, doi: 10.1016/j.cels.2022.02.004.
- [4] J. K. Jung et al., "Cell-free biosensors for rapid detection of water contaminants," Nat. Biotechnol., vol. 38, no. 12, Art. no. 12, Dec. 2020, doi: 10.1038/s41587-020-0571-7.
- [5] A. S. Karim et al., "In vitro prototyping and rapid optimization of biosynthetic enzymes for cell design," Nat. Chem. Biol., vol. 16, no. 8, pp. 912–919, Aug. 2020, doi: 10.1038/s41589-020-0559-0.
- [6] F.-X. Lehr et al., "Cell-Free Prototyping of AND-Logic Gates Based on Heterogeneous RNA Activators," ACS Synth. Biol., vol. 8, no. 9, pp. 2163–2173, Sep. 2019, doi: 10.1021/acssynbio.9b00238.
- [7] S. J. Moore *et al.*, "Rapid acquisition and model-based analysis of cell-free transcription–translation reactions from nonmodel bacteria," *Proc. Natl. Acad. Sci.*, vol. 115, no. 19, pp. E4340–E4349, May 2018, doi: 10.1073/pnas.1715806115.
- [8] Z. Swank and S. J. Maerkl, "CFPU: A Cell-Free Processing Unit for High-Throughput, Automated In Vitro Circuit Characterization in Steady-State Conditions," *BioDesign Res.*, vol. 2021, Mar. 2021, doi: 10.34133/2021/2968181.
- [9] M. C. Bassalo, R. Liu, and R. T. Gill, "Directed evolution and synthetic biology applications to microbial systems," *Curr. Opin. Biotechnol.*, vol. 39, pp. 126–133, Jun. 2016, doi: 10.1016/j.copbio.2016.03.016.
- [10] J. A. N. Brophy and C. A. Voigt, "Principles of genetic circuit design," *Nat. Methods*, vol. 11, no. 5, Art. no. 5, May 2014, doi: 10.1038/nmeth.2926.
- [11] Z. Swank, N. Laohakunakorn, and S. J. Maerkl, "Cell-free gene-regulatory network engineering with synthetic transcription factors," *Proc. Natl. Acad. Sci.*, vol. 116, no. 13, pp. 5892–5901, Mar. 2019, doi: 10.1073/pnas.1816591116.
- [12] P.-F. Xia, H. Ling, J. L. Foo, and M. W. Chang, "Synthetic genetic circuits for programmable biological functionalities," *Biotechnol. Adv.*, vol. 37, no. 6, p. 107393, Nov. 2019, doi: 10.1016/j.biotechadv.2019.04.015.
- [13] U. Alon, "Network motifs: theory and experimental approaches," *Nat. Rev. Genet.*, vol. 8, no. 6, pp. 450–461, Jun. 2007, doi: 10.1038/nrg2102.
- [14] J. K. Jung et al., "Cell-free biosensors for rapid detection of water contaminants," Nat. Biotechnol., vol. 38, no. 12, pp. 1451–1459, Dec. 2020, doi: 10.1038/s41587-020-0571-7.
- [15] J. K. Jung, C. M. Archuleta, K. K. Alam, and J. B. Lucks, "Programming cell-free

- biosensors with DNA strand displacement circuits," *Nat. Chem. Biol.*, vol. 18, no. 4, pp. 385–393, Apr. 2022, doi: 10.1038/s41589-021-00962-9.
- [16] P. Q. Nguyen *et al.*, "Wearable materials with embedded synthetic biology sensors for biomolecule detection," *Nat. Biotechnol.*, vol. 39, no. 11, pp. 1366–1374, Nov. 2021, doi: 10.1038/s41587-021-00950-3.
- [17] K. Pardee *et al.*, "Portable, On-Demand Biomolecular Manufacturing," *Cell*, vol. 167, no. 1, pp. 248-259.e12, Sep. 2016, doi: 10.1016/j.cell.2016.09.013.
- [18] J. C. Stark *et al.*, "On-demand biomanufacturing of protective conjugate vaccines," *Sci. Adv.*, vol. 7, no. 6, p. eabe9444, Feb. 2021, doi: 10.1126/sciadv.abe9444.
- [19] C. Zhou, X. Lin, Y. Lu, and J. Zhang, "Flexible on-demand cell-free protein synthesis platform based on a tube-in-tube reactor," *React. Chem. Eng.*, vol. 5, no. 2, pp. 270–277, 2020, doi: 10.1039/C9RE00394K.
- [20] K. P. Adamala, D. A. Martin-Alarcon, K. R. Guthrie-Honea, and E. S. Boyden, "Engineering genetic circuit interactions within and between synthetic minimal cells," *Nat. Chem.*, vol. 9, no. 5, pp. 431–439, May 2017, doi: 10.1038/nchem.2644.
- [21] L. Aufinger, J. Brenner, and F. C. Simmel, "Complex dynamics in a synchronized cell-free genetic clock," *Nat. Commun.*, vol. 13, no. 1, Art. no. 1, May 2022, doi: 10.1038/s41467-022-30478-2.
- [22] J. Garamella, D. Garenne, and V. Noireaux, "TXTL-based approach to synthetic cells," *Methods Enzymol.*, vol. 617, pp. 217–239, 2019, doi: 10.1016/bs.mie.2018.12.015.
- [23] E. Karzbrun, A. M. Tayar, V. Noireaux, and R. H. Bar-Ziv, "Synthetic biology. Programmable on-chip DNA compartments as artificial cells," *Science*, vol. 345, no. 6198, pp. 829–832, Aug. 2014, doi: 10.1126/science.1255550.
- [24] D. Banerjee *et al.*, "Genome-scale metabolic rewiring improves titers rates and yields of the non-native product indigoidine at scale," *Nat. Commun.*, vol. 11, no. 1, p. 5385, Dec. 2020, doi: 10.1038/s41467-020-19171-4.
- [25] H. Kim, D. Bojar, and M. Fussenegger, "A CRISPR/Cas9-based central processing unit to program complex logic computation in human cells," *Proc. Natl. Acad. Sci.*, vol. 116, no. 15, pp. 7214–7219, Apr. 2019, doi: 10.1073/pnas.1821740116.
- [26] J. Landberg, N. R. Wright, T. Wulff, M. J. Herrgård, and A. T. Nielsen, "CRISPR interference of nucleotide biosynthesis improves production of a single-domain antibody in Escherichia coli," *Biotechnol. Bioeng.*, vol. 117, no. 12, pp. 3835–3848, 2020, doi: 10.1002/bit.27536.
- [27] A. C. Reis *et al.*, "Simultaneous repression of multiple bacterial genes using nonrepetitive extra-long sgRNA arrays," *Nat. Biotechnol.*, vol. 37, no. 11, pp. 1294–1301, Nov. 2019, doi: 10.1038/s41587-019-0286-9.
- [28] J. Santos-Moreno and Y. Schaerli, "CRISPR-based gene expression control for synthetic gene circuits," *Biochem. Soc. Trans.*, vol. 48, no. 5, pp. 1979–1993, Oct. 2020, doi: 10.1042/BST20200020.
- [29] A. Westbrook *et al.*, "Distinct timescales of RNA regulators enable the construction of a genetic pulse generator," *Biotechnol. Bioeng.*, vol. 116, no. 5, pp. 1139–1151, May 2019, doi: 10.1002/bit.26918.
- [30] S. Clamons and R. Murray, "Modeling predicts that CRISPR-based activators, unlike CRISPR-based repressors, scale well with increasing gRNA competition and

- dCas9 bottlenecking," Synthetic Biology, preprint, Jul. 2019. doi: 10.1101/719278.
- [31] J. Nielsen and J. D. Keasling, "Engineering Cellular Metabolism," *Cell*, vol. 164, no. 6, pp. 1185–1197, Mar. 2016, doi: 10.1016/j.cell.2016.02.004.
- [32] B. I. Tickman et al., "Multi-layer CRISPRa/i circuits for dynamic genetic programs in cell-free and bacterial systems," Cell Syst., p. S2405471221004191, Nov. 2021, doi: 10.1016/j.cels.2021.10.008.
- [33] M. W. Gander, J. D. Vrana, W. E. Voje, J. M. Carothers, and E. Klavins, "Digital logic circuits in yeast with CRISPR-dCas9 NOR gates," *Nat. Commun.*, vol. 8, no. 1, Art. no. 1, May 2017, doi: 10.1038/ncomms15459.
- [34] R. Marshall and V. Noireaux, "Quantitative modeling of transcription and translation of an all- E. coli cell-free system," *Sci. Rep.*, vol. 9, no. 1, Art. no. 1, Aug. 2019, doi: 10.1038/s41598-019-48468-8.
- [35] H. Alper, C. Fischer, E. Nevoigt, and G. Stephanopoulos, "Tuning genetic control through promoter engineering," *Proc. Natl. Acad. Sci. U. S. A.*, vol. 102, no. 36, pp. 12678–12683, Sep. 2005, doi: 10.1073/pnas.0504604102.
- [36] J. R. Kelly *et al.*, "Measuring the activity of BioBrick promoters using an in vivo reference standard," *J. Biol. Eng.*, vol. 3, p. 4, Mar. 2009, doi: 10.1186/1754-1611-3-4.
- [37] R. C. Brewster, D. L. Jones, and R. Phillips, "Tuning Promoter Strength through RNA Polymerase Binding Site Design in Escherichia coli," *PLOS Comput. Biol.*, vol. 8, no. 12, p. e1002811, Dec. 2012, doi: 10.1371/journal.pcbi.1002811.
- [38] T. L. Fleur, A. Hossain, and H. M. Salis, "Automated Model-Predictive Design of Synthetic Promoters to Control Transcriptional Profiles in Bacteria," Synthetic Biology, preprint, Sep. 2021. doi: 10.1101/2021.09.01.458561.
- [39] D. J. Lee, S. D. Minchin, and S. J. W. Busby, "Activating Transcription in Bacteria," Annu. Rev. Microbiol., vol. 66, no. 1, pp. 125–152, Oct. 2012, doi: 10.1146/annurev-micro-092611-150012.
- [40] T. C. Yu *et al.*, "Multiplexed characterization of rationally designed promoter architectures deconstructs combinatorial logic for IPTG-inducible systems," *Nat. Commun.*, vol. 12, no. 1, p. 325, Jan. 2021, doi: 10.1038/s41467-020-20094-3.
- [41] B. F. Cress *et al.*, "Rapid generation of CRISPR/dCas9-regulated, orthogonally repressible hybrid T7-lac promoters for modular, tuneable control of metabolic pathway fluxes in Escherichia coli," *Nucleic Acids Res.*, vol. 44, no. 9, pp. 4472–4485, May 2016, doi: 10.1093/nar/gkw231.
- [42] T. M. Groseclose, R. E. Rondon, Z. D. Herde, C. A. Aldrete, and C. J. Wilson, "Engineered systems of inducible anti-repressors for the next generation of biological programming," *Nat. Commun.*, vol. 11, no. 1, Art. no. 1, Sep. 2020, doi: 10.1038/s41467-020-18302-1.
- [43] X. Liu *et al.*, "De novo design of programmable inducible promoters," *Nucleic Acids Res.*, vol. 47, no. 19, pp. 10452–10463, Nov. 2019, doi: 10.1093/nar/gkz772.
- [44] I. J. Roney, A. D. Rudner, J.-F. Couture, and M. Kærn, "Improvement of the reverse tetracycline transactivator by single amino acid substitutions that reduce leaky target gene expression to undetectable levels," *Sci. Rep.*, vol. 6, p. 27697, Jun. 2016, doi: 10.1038/srep27697.
- [45] J. Fontana et al., "Effective CRISPRa-mediated control of gene expression in

- bacteria must overcome strict target site requirements," *Nat. Commun.*, vol. 11, no. 1, p. 1618, Dec. 2020, doi: 10.1038/s41467-020-15454-y.
- [46] Y. Chen *et al.*, "Tuning the dynamic range of bacterial promoters regulated by ligand-inducible transcription factors," *Nat. Commun.*, vol. 9, no. 1, p. 64, Dec. 2018, doi: 10.1038/s41467-017-02473-5.
- [47] W. Ross, S. E. Aiyar, J. Salomon, and R. L. Gourse, "Escherichia coli promoters with UP elements of different strengths: modular structure of bacterial promoters," *J. Bacteriol.*, vol. 180, no. 20, pp. 5375–5383, Oct. 1998, doi: 10.1128/JB.180.20.5375-5383.1998.
- [48] R. K. Shultzaberger, Z. Chen, K. A. Lewis, and T. D. Schneider, "Anatomy of Escherichia coli σ 70 promoters," *Nucleic Acids Res.*, vol. 35, no. 3, pp. 771–788, Feb. 2007, doi: 10.1093/nar/gkl956.
- [49] C. Dong, J. Fontana, A. Patel, J. M. Carothers, and J. G. Zalatan, "Synthetic CRISPR-Cas gene activators for transcriptional reprogramming in bacteria," *Nat. Commun.*, vol. 9, no. 1, Art. no. 1, Jun. 2018, doi: 10.1038/s41467-018-04901-6.
- [50] I. G. Hook-Barnard and D. M. Hinton, "Transcription Initiation by Mix and Match Elements: Flexibility for Polymerase Binding to Bacterial Promoters," *Gene Regul. Syst. Biol.*, vol. 1, pp. 275–293, Dec. 2007.
- [51] M. S. Paget and J. D. Helmann, "The σ70family of sigma factors," *Genome Biol.*, vol. 4, no. 1, p. 203, Jan. 2003, doi: 10.1186/gb-2003-4-1-203.
- [52] L. S. Qi *et al.*, "Repurposing CRISPR as an RNA-guided platform for sequence-specific control of gene expression," *Cell*, vol. 152, no. 5, pp. 1173–1183, Feb. 2013, doi: 10.1016/j.cell.2013.02.022.
- [53] Y. Censor, "Pareto optimality in multiobjective problems," *Appl. Math. Optim.*, vol. 4, no. 1, pp. 41–59, Mar. 1977, doi: 10.1007/BF01442131.
- [54] S. T. Estrem, T. Gaal, W. Ross, and R. L. Gourse, "Identification of an UP element consensus sequence for bacterial promoters," *Proc. Natl. Acad. Sci. U. S. A.*, vol. 95, no. 17, pp. 9761–9766, Aug. 1998.
- [55] T. Gaal *et al.*, "DNA-binding determinants of the alpha subunit of RNA polymerase: novel DNA-binding domain architecture," *Genes Dev.*, vol. 10, no. 1, pp. 16–26, Jan. 1996, doi: 10.1101/gad.10.1.16.
- [56] J. Fontana, D. Sparkman-Yager, J. G. Zalatan, and J. M. Carothers, "Challenges and opportunities with CRISPR activation in bacteria for data-driven metabolic engineering," *Curr. Opin. Biotechnol.*, vol. 64, pp. 190–198, Aug. 2020, doi: 10.1016/j.copbio.2020.04.005.
- [57] J. Lian, M. HamediRad, S. Hu, and H. Zhao, "Combinatorial metabolic engineering using an orthogonal tri-functional CRISPR system," *Nat. Commun.*, vol. 8, no. 1, p. 1688, Nov. 2017, doi: 10.1038/s41467-017-01695-x.
- [58] H. Bolouri and E. H. Davidson, "Transcriptional regulatory cascades in development: Initial rates, not steady state, determine network kinetics," *Proc. Natl. Acad. Sci.*, vol. 100, no. 16, pp. 9371–9376, Aug. 2003, doi: 10.1073/pnas.1533293100.
- [59] F. Banuett, "Signalling in the Yeasts: An Informational Cascade with Links to the Filamentous Fungi," *Microbiol. Mol. Biol. Rev.*, vol. 62, no. 2, pp. 249–274, Jun. 1998, doi: 10.1128/MMBR.62.2.249-274.1998.

- [60] P.-Y. Chen, Y. Qian, and D. Del Vecchio, "A Model for Resource Competition in CRISPR-Mediated Gene Repression," in 2018 IEEE Conference on Decision and Control (CDC), Dec. 2018, pp. 4333–4338. doi: 10.1109/CDC.2018.8619016.
- [61] D. Camsund, A. Jaramillo, and P. Lindblad, "Engineering of a Promoter Repressed by a Light-Regulated Transcription Factor in Escherichia coli," *BioDesign Res.*, vol. 2021, Sep. 2021, doi: 10.34133/2021/9857418.
- [62] P. Jayaraman, K. Devarajan, T. K. Chua, H. Zhang, E. Gunawan, and C. L. Poh, "Blue light-mediated transcriptional activation and repression of gene expression in bacteria," *Nucleic Acids Res.*, vol. 44, no. 14, pp. 6994–7005, Aug. 2016, doi: 10.1093/nar/gkw548.
- [63] L. B. Motta-Mena *et al.*, "An optogenetic gene expression system with rapid activation and deactivation kinetics," *Nat. Chem. Biol.*, vol. 10, no. 3, pp. 196–202, Mar. 2014, doi: 10.1038/nchembio.1430.
- [64] B. D. Zoltowski, L. B. Motta-Mena, and K. H. Gardner, "Blue light-induced dimerization of a bacterial LOV-HTH DNA-binding protein," *Biochemistry*, vol. 52, no. 38, pp. 6653–6661, Sep. 2013, doi: 10.1021/bi401040m.
- [65] Y. Gao, X. Xiong, S. Wong, E. J. Charles, W. A. Lim, and L. S. Qi, "Complex transcriptional modulation with orthogonal and inducible dCas9 regulators," *Nat. Methods*, vol. 13, no. 12, pp. 1043–1049, Dec. 2016, doi: 10.1038/nmeth.4042.
- [66] P. K. Jain *et al.*, "Development of Light-Activated CRISPR Using Guide RNAs with Photocleavable Protectors," *Angew. Chem. Int. Ed.*, vol. 55, no. 40, pp. 12440–12444, 2016, doi: 10.1002/anie.201606123.
- [67] K. Kundert et al., "Controlling CRISPR-Cas9 with ligand-activated and ligand-deactivated sgRNAs," Nat. Commun., vol. 10, no. 1, Art. no. 1, May 2019, doi: 10.1038/s41467-019-09985-2.
- [68] Y. Nihongaki, F. Kawano, T. Nakajima, and M. Sato, "Photoactivatable CRISPR-Cas9 for optogenetic genome editing," *Nat. Biotechnol.*, vol. 33, no. 7, pp. 755–760, Jul. 2015, doi: 10.1038/nbt.3245.
- [69] L. R. Polstein and C. A. Gersbach, "A light-inducible CRISPR-Cas9 system for control of endogenous gene activation," *Nat. Chem. Biol.*, vol. 11, no. 3, pp. 198–200, Mar. 2015, doi: 10.1038/nchembio.1753.
- [70] Z.-M. Ying, F. Wang, X. Chu, R.-Q. Yu, and J.-H. Jiang, "Activatable CRISPR Transcriptional Circuits Generate Functional RNA for mRNA Sensing and Silencing," *Angew. Chem. Int. Ed.*, vol. 59, no. 42, pp. 18599–18604, 2020, doi: 10.1002/anie.202004751.
- [71] Y. Yu *et al.*, "Engineering a far-red light–activated split-Cas9 system for remote-controlled genome editing of internal organs and tumors," *Sci. Adv.*, vol. 6, no. 28, p. eabb1777, Jul. 2020, doi: 10.1126/sciadv.abb1777.
- [72] M. C. Villegas Kcam, A. J. Tsong, and J. Chappell, "Rational engineering of a modular bacterial CRISPR–Cas activation platform with expanded target range," *Nucleic Acids Res.*, vol. 49, no. 8, pp. 4793–4802, May 2021, doi: 10.1093/nar/gkab211.
- [73] K. E. Thompson, C. J. Bashor, W. A. Lim, and A. E. Keating, "SYNZIP Protein Interaction Toolbox: in Vitro and in Vivo Specifications of Heterospecific Coiled-Coil Interaction Domains," ACS Synth. Biol., vol. 1, no. 4, pp. 118–129, Apr. 2012, doi:

- 10.1021/sb200015u.
- [74] D. Cunningham-Bryant, J. Sun, B. Fernandez, and J. G. Zalatan, "CRISPR–Cas-Mediated Chemical Control of Transcriptional Dynamics in Yeast," *ChemBioChem*, vol. 20, no. 12, pp. 1519–1523, 2019, doi: 10.1002/cbic.201800823.
- [75] F.-S. Liang, W. Q. Ho, and G. R. Crabtree, "Engineering the ABA Plant Stress Pathway for Regulation of Induced Proximity," *Sci. Signal.*, vol. 4, no. 164, p. rs2, Mar. 2011, doi: 10.1126/scisignal.2001449.
- [76] T. Miyamoto *et al.*, "Rapid and Orthogonal Logic Gating with a Gibberellin-induced Dimerization System," *Nat. Chem. Biol.*, vol. 8, no. 5, pp. 465–470, Mar. 2012, doi: 10.1038/nchembio.922.
- [77] J. G. Zalatan *et al.*, "Engineering Complex Synthetic Transcriptional Programs with CRISPR RNA Scaffolds," *Cell*, vol. 160, no. 1, pp. 339–350, Jan. 2015, doi: 10.1016/j.cell.2014.11.052.
- [78] E. F. Jr. Douglass, C. J. Miller, G. Sparer, H. Shapiro, and D. A. Spiegel, "A Comprehensive Mathematical Model for Three-Body Binding Equilibria," *J. Am. Chem. Soc.*, vol. 135, no. 16, pp. 6092–6099, Apr. 2013, doi: 10.1021/ja311795d.
- [79] A. Levchenko, J. Bruck, and P. W. Sternberg, "Scaffold proteins may biphasically affect the levels of mitogen-activated protein kinase signaling and reduce its threshold properties," *Proc. Natl. Acad. Sci.*, vol. 97, no. 11, pp. 5818–5823, May 2000, doi: 10.1073/pnas.97.11.5818.
- [80] B. Wang, M. Barahona, and M. Buck, "Engineering modular and tunable genetic amplifiers for scaling transcriptional signals in cascaded gene networks," *Nucleic Acids Res.*, vol. 42, no. 14, pp. 9484–9492, Aug. 2014, doi: 10.1093/nar/gku593.
- [81] T. S. Lee et al., "BglBrick vectors and datasheets: A synthetic biology platform for gene expression," J. Biol. Eng., vol. 5, no. 1, p. 12, Dec. 2011, doi: 10.1186/1754-1611-5-12.
- [82] J. Garamella, R. Marshall, M. Rustad, and V. Noireaux, "The All E. coli TX-TL Toolbox 2.0: A Platform for Cell-Free Synthetic Biology," *ACS Synth. Biol.*, vol. 5, no. 4, pp. 344–355, Apr. 2016, doi: 10.1021/acssynbio.5b00296.
- [83] O. Borkowski, C. Bricio, M. Murgiano, B. Rothschild-Mancinelli, G.-B. Stan, and T. Ellis, "Cell-free prediction of protein expression costs for growing cells," *Nat. Commun.*, vol. 9, no. 1, p. 1457, Apr. 2018, doi: 10.1038/s41467-018-03970-x.
- [84] D. A. Specht, L. B. Cortes, and G. Lambert, "Overcoming Leak Sensitivity in CRISPRi Circuits Using Antisense RNA Sequestration and Regulatory Feedback," ACS Synth. Biol., Aug. 2022, doi: 10.1021/acssynbio.2c00155.
- [85] S. Kaplan, A. Bren, A. Zaslaver, E. Dekel, and U. Alon, "Diverse Two-Dimensional Input Functions Control Bacterial Sugar Genes," *Mol. Cell*, vol. 29, no. 6, pp. 786–792, Mar. 2008, doi: 10.1016/j.molcel.2008.01.021.
- [86] S. Krishna, L. Orosz, K. Sneppen, S. Adhya, and S. Semsey, "Relation of Intracellular Signal Levels and Promoter Activities in the gal Regulon of Escherichia coli," *J. Mol. Biol.*, vol. 391, no. 4, pp. 671–678, Aug. 2009, doi: 10.1016/j.jmb.2009.06.043.
- [87] H. R. Kempton, L. E. Goudy, K. S. Love, and L. S. Qi, "Multiple Input Sensing and Signal Integration Using a Split Cas12a System," *Mol. Cell*, vol. 78, no. 1, pp.

- 184-191.e3, Apr. 2020, doi: 10.1016/j.molcel.2020.01.016.
- [88] J. Beltrán *et al.*, "Rapid biosensor development using plant hormone receptors as reprogrammable scaffolds," *Nat. Biotechnol.*, pp. 1–7, Jun. 2022, doi: 10.1038/s41587-022-01364-5.
- [89] G. W. Foight *et al.*, "Multi-input chemical control of protein dimerization for programming graded cellular responses," *Nat. Biotechnol.*, vol. 37, no. 10, Art. no. 10, Oct. 2019, doi: 10.1038/s41587-019-0242-8.
- [90] G. Guntas *et al.*, "Engineering an improved light-induced dimer (iLID) for controlling the localization and activity of signaling proteins," *Proc. Natl. Acad. Sci.*, vol. 112, no. 1, pp. 112–117, Jan. 2015, doi: 10.1073/pnas.1417910112.
- [91] Z. Huang *et al.*, "Creating Red Light-Switchable Protein Dimerization Systems as Genetically Encoded Actuators with High Specificity," *ACS Synth. Biol.*, vol. 9, no. 12, pp. 3322–3333, Dec. 2020, doi: 10.1021/acssynbio.0c00397.
- [92] D. I. Piraner, M. H. Abedi, B. A. Moser, A. Lee-Gosselin, and M. G. Shapiro, "Tunable thermal bioswitches for in vivo control of microbial therapeutics," *Nat. Chem. Biol.*, vol. 13, no. 1, pp. 75–80, Jan. 2017, doi: 10.1038/nchembio.2233.
- [93] J. Carey, V. Cameron, P. L. De Haseth, and O. C. Uhlenbeck, "Sequence-specific interaction of R17 coat protein with its ribonucleic acid binding site," *Biochemistry*, vol. 22, no. 11, pp. 2601–2610, May 1983, doi: 10.1021/bi00280a002.
- [94] F. Dupeux *et al.*, "A thermodynamic switch modulates abscisic acid receptor sensitivity," *EMBO J.*, vol. 30, no. 20, pp. 4171–4184, Oct. 2011, doi: 10.1038/emboj.2011.294.
- [95] K. Miyazono *et al.*, "Structural basis of abscisic acid signalling," *Nature*, vol. 462, no. 7273, Art. no. 7273, Dec. 2009, doi: 10.1038/nature08583.
- [96] M. Ueguchi-Tanaka et al., "GIBBERELLIN INSENSITIVE DWARF1 encodes a soluble receptor for gibberellin," *Nature*, vol. 437, no. 7059, Art. no. 7059, Sep. 2005, doi: 10.1038/nature04028.
- [97] H. Yoshida *et al.*, "Evolution and diversification of the plant gibberellin receptor GID1," *Proc. Natl. Acad. Sci.*, vol. 115, no. 33, pp. E7844–E7853, Aug. 2018, doi: 10.1073/pnas.1806040115.
- [98] W. S. Grubbe, B. J. Rasor, A. Krüger, M. C. Jewett, and A. S. Karim, "Cell-free styrene biosynthesis at high titers," *Metab. Eng.*, vol. 61, pp. 89–95, Sep. 2020, doi: 10.1016/j.ymben.2020.05.009.
- [99] N. S. Kruyer *et al.*, "Membrane Augmented Cell-Free Systems: A New Frontier in Biotechnology," *ACS Synth. Biol.*, vol. 10, no. 4, pp. 670–681, Apr. 2021, doi: 10.1021/acssynbio.0c00625.
- [100] J. A. Peruzzi, N. R. Galvez, and N. P. Kamat, "Engineering transmembrane signal transduction in synthetic membranes using two-component systems," Synthetic Biology, preprint, Oct. 2022. doi: 10.1101/2022.10.30.514420.

## **Figure Legends**

## Figure 1: Functional interrogation of promoter regions with CRISPRa

- A. Schematic of RNAP interactions with the CRISPRa complex and target promoter.  $\sigma^{70}$  affinity for the minimal promoter and  $\alpha$ -CTD affinity for the UP-element determines RNAP recruitment to a promoter. When CRISPRa is targeted to a promoter with a complementary scRNA target site, the RNAP  $\alpha$ -CTD domain is recruited by the SoxS transcriptional activator. RNAP-promoter and CRISPRa-promoter interactions can be modulated by modifying the DNA sequence of the different promoter regions.
- B. Workflow for the assembly and characterization of libraries of activatable promoters. A library of RFP genes with varying promoters is generated through PCR (Methods 1.1). The library is then co-transformed into *E. coli* with an aTc-inducible CRISPRa plasmid. Colonies are then seeded overnight, and subsequently diluted into media with appropriate concentrations of aTc. For each promoter variant in the libraries, basal and activated RFP levels were measured with 0 nM and 200 nM aTc, respectively (Methods 2).
- C. Schematic of RNAP interaction with the minimal promoter and library design.  $\sigma^{70}$  recognizes specific positions in the extended -10 and -35 regions of the minimal promoter, which informed the design of the library MP1.  $\sigma^{70}$  binding is also influenced by the GC-content, the length, and the <sup>-15</sup>TGn<sup>-1</sup> motif of the intervening sequence, which informed the design of library MP2 (Methods 3.1).
- D. Minimal promoter effect on expression levels. **Left:** Inducible CRISPRa system and minimal promoter libraries of the J3 synthetic promoter. MCP-SoxS is expressed

from the aTc-inducible pTet promoter. dCas9 and J306 scRNA are constitutively expressed. **Right:** Activated and basal RFP/OD<sub>600</sub> for the two minimal promoter libraries ( $n_{MP1}$  = 89,  $n_{MP2}$  = 84). Red dash line defines the Pareto front containing the best performing promoter variants (Methods S3), for which no further improvements in basal or activated levels can be achieved without compromising the other. Gray dash line defines promoter variants with equal activated and basal expression levels, indicating they are not activated by CRISPRa. The J23117 minimal promoter (green, triplicates) is included as a standard reference for CRISPRa efficiency. The J23119 minimal promoter (red, triplicates) is an example of a non-activatable promoter due to high basal expression levels. A plasmid without RFP (black, triplicates) indicates the background fluorescence of the system.

## Figure 2: Combining promoter regions to engineer high-performing CRISPRa promoters

- A. Schematic of RNAP interactions with the UP-element and library design.  $\alpha$ -CTD affinity for AT-rich UP-elements upstream of the minimal promoter helps recruit RNAP. Upon targeting with CRISPRa, UP-element RNAP recruitment contributions are largely replaced by SoxS-RNAP  $\alpha$ -CTD interactions. UP-element libraries with increasing GC-content were designed to minimize  $\alpha$ -CTD interactions (Methods 3.2).
- B. UP-element GC-content effect on expression levels is shown through activated and basal RFP/OD<sub>600</sub> for the six UP-element libraries (n<sub>UP1</sub> = n<sub>UP2</sub> = ... = n<sub>UP6</sub> = 110). **Left:** Increasing GC-content in the UP-element lowers the range of basal expression level, while maintaining the full range of activated expression levels. Gray dash line defines promoter variants with equal activated and basal expression levels. **Right:** Colored dash lines define the Pareto front for each UP-element library (Methods S3). Increasing the UP-element GC-content effectively shifts the Pareto front towards lower basal expression levels.
- C. scRNA target site composition effect on basal expression. Comparison of three scRNA libraries with increasing GC-content ( $n_{S1} = n_{S2} = n_{S3} = 93$ ) (Methods 3.3). Basal expression levels are normalized to the standard J3 promoter basal expression level. Red lines indicate the median expression level of each distribution. The interquartile range (IQR) is calculated as the difference between the upper and lower quartiles and measures the spread of the distribution.
- D. Sequential construction of activatable promoters. **Left:** Activatable promoters were constructed by sequential library mutagenesis screens starting from the J3 promoter

with a GC-rich scRNA target site. Three Pareto optimal UP-elements were selected after promoter mutagenesis with a GC-rich UP-element library (1). We then mutagenized the minimal promoter of the three previously selected variants (2), and again selected three Pareto optimal variants. **Right:** Basal and activated expression levels for all mutagenesis variants normalized to the standard J3 promoter expression levels (green). Yellow points represent variants from the UP-element mutagenesis ( $n_{\text{UP6}} = 192$ ) (1), while purple points represent variants from the minimal promoter mutagenesis ( $n_{\text{MP3}} = 279$ ) (2). Red circles indicate selected variants from each screen, and solid lines depict the Pareto optimal fronts. Each sequential mutagenesis led to variants with both lower basal and higher activated expression levels.

## Figure 3: Engineering deep and wide circuits with high-performing CRISPRa promoters

- A. Schematic of orthogonal CRISPRa/i nodes for use in cell-free circuits. Internal nodes contain an orthogonal scRNA target site and express orthogonal scRNAs.

  Output nodes contain orthogonal scRNA target sites and express RFP. All nodes contain the same UP-element and minimal promoter (HP3).
- B. High-throughput characterization of scRNA components in CFS. **Left:** Plasmids encoding each CRISPRa component are mixed using an acoustic liquid handling robot and expressed in CFS. **Right:** scRNA-dose response curves for each node are generated by titrating the amount of scRNA plasmid from 0.5 pM to 5 nM.
- C. Comparison of assembly strategies for building a four-layer CRISPRa cascade. **Left:** Internal node concentrations either decreased from 200 pM to 32 pM as depth increased, were held constant at 200 pM, or increased from 200 pM to 1.25 nM as depth increased. A fourth assembly method was tested in which internal node concentrations were 40, 200, and 170 pM, based on individual scRNA-dose response characteristics. A fifth cascade was included in which the high-performing promoter of the second internal node was replaced with the leaky J2 promoter. Input and output node concentrations were held constant across all strategies at 0 or 15 pM and 10 nM, respectively. **Center:** Cascade output RFP expression for each assembly strategy with scRNA input (red) and without (black), relative to RFP basal expression. **Right:** Change in time to maximum expression rate ( $\Delta t_{max}$ ) for each assembly strategy (Methods S3).

- D. Rapid fold change optimization of a four-layer CRISPRa cascade. **Left:** The first and third internal nodes of the cascade were varied between 40 and 160 pM, and 85 and 340 pM, respectively. The input node, second internal node, and output node were held constant at 0 or 15 pM, 0.2 nM, and 10 nM, respectively. **Right:** Fold change between with and without scRNA input for each CRISPRa cascade.
- E. Signal propagation through deep CRISPRa/i circuits. **Left:** CRISPRa cascades with increasing depth. Input and output node concentrations were held constant across all cascades at 0 or 15 pM and 10 nM, respectively. All of the parallel cascade scRNA outputs are connected to the same RFP node. All node concentrations are tabulated in Table S5. **Right:** Propagation efficiency and signal delay are shown as a function of circuit depth (Methods S3).
- F. Construction of wide CRISPRa/i circuits. **Left:** CRISPRa cascades with increasing width. Input and output node concentrations were held constant across all cascades at 0 or 15 pM and 10 nM, respectively. **Right:** The concentration of each internal node was held at 0.2 nM as circuit width increased (blue), or the internal node concentration was scaled down proportionally to the width of the circuit (red), such that each internal node concentration is 0.2/n nM, where n is the number of parallel cascades. Fold-activation is given relative to a single CRISPRa cascade (Methods S3).

For all panels, values represent the mean ± standard deviation of three technical replicates.

## Figure 4: Developing activatable promoters for blue-light responsive CRISPRa/i circuits

- A. Schematic of EL222 light-responsive promoter system and library design. EL222 transcription factor dimerizes in response to 470 nm light and binds a specific sequence upstream of the minimal promoter. EL222 then recruits RNAP through interactions with the α-CTD domain. Minimal promoter library design is based on the original *luxI* promoter and previous minimal promoter libraries (Methods 3.4).
- B. Characterization of light responsive promoters in *E. coli.* Left: Blue-light promoter screening (Methods 5). EL222 protein and promoter library are expressed from a single plasmid. Assembly and screening are carried out as previously described. Basal and activated expression levels are measured from cultures not exposed or continuously exposed to blue-light, respectively. Right: Basal expression and dynamic range of blue-light promoter variants (n<sub>MP3</sub> = 96). Gray dash line defines promoter variants with equal activated and basal expression levels, indicating they are not activated by EL222. The J23119 minimal promoter (red) and J23113 (black) are examples of non-activatable promoters. Variants with improved performance (red circles) compared to the original *luxl* promoter (green) were selected for use in CFS.
- C. Light-responsive CRISPRa in CFS. Left: EL222 scRNA expression from an engineered blue-light promoter and downstream CRISPRa. Reactions contain 8nM and 10 nM of EL222 and RFP plasmids respectively. Right: Titration of blue-light inducible scRNA plasmid concentration to maximize the fold change

between blue-light dependent CRISPRa (blue) and CRISPRa due to scRNA leak in the dark (black).

D. Improvement of blue-light CRISPRa dynamic range through the construction of a positive feedback circuit. Left: Blue-light responsive CRISPRa cascade with positive feedback (PFB). PFB is achieved by including a downstream node that expresses a scRNA targeting an upstream node Reactions contain 15nM and 10 nM of EL222 and RFP plasmids respectively. Right: Blue-light dependent CRISPRa (blue) and CRISPRa due to scRNA leak in the dark (black). The amount of positive feedback was tuned by adjusting the concentration of the PFB node. "No", "Low", and "High" PFB concentrations correspond to 0, 3 pM, and 2 nM, respectively.

For all panels, values represent the mean ± standard deviation of three technical replicates.

### Figure 5: Engineered activatable promoters enable PPI-dependent conditional CRISPRa

- A. Schematic of different PPI-dependent CRISPRa systems. MCP-SoxS fusion is split and the two proteins are instead fused to one end of a heterodimerization domain. The heterodimerization domains used to build PPI-dependent CRISPRa systems are the SYNZIP5/SYNZIP6 pair, the abscisic acid (ABA)-responsive ABI/PYL1 domain, and the gibberellic acid (GA)-responsive GAI/GID1 domain.
- B. Distance requirements of PPI-dependent CRISPRa. **Left:** Engineered promoter containing densely-packed scRNA target sites and single base pair 5' additions allows for CRISPRa targeting between -81 and -111 bp from the TSS. **Right:** Testing SYNZIP-CRISPRa between -81 and -91 bp from the TSS. SYNZIP-CRISPRa components are expressed at 5 nM. Fold change is calculated relative to an off-target scRNA for each promoter variant.
- C. Tuning conditional CRISPRa response through titration of small molecule concentration. For ABA- and GA- CRISPRa, the corresponding small molecule was titrated between 0 and 10 or 0 and 10<sup>3</sup> µM respectively to find the optimal concentration. ABA- and GA-CRISPRa components are expressed at 10 nM.
- D. Improving PPI-dependent and conditional CRISPRa response by optimizing component stoichiometries. The concentration of the plasmids expressing the MCP and SoxS components for each dimerization system were varied 1-25 nM and tested combinatorially to find the best ratio of the two heterodimers. ABA is added at 10 μM and GA is added at 10<sup>3</sup> μM. Fold change is given relative to a reaction with no MCP and SoxS plasmids added.

## Figure 6: Engineering multi-input CRISPRa/i Circuits

- A. Conditional CRISPRa response to non-cognate ligands. The orthogonality of the small molecule-responsive conditional CRISPRa systems was tested by adding either the corresponding or non-corresponding small molecule to cell-free reactions containing the components for ABA- or GA-CRISPRa. All components are added at their respective optimal screened concentrations. ABA is added at 10 μM and GA is added at 10<sup>3</sup> μM.
- B. Assembly of conditional CRISPRa circuits. For both circuits, all components are added at their respective optimal screened concentrations. ABA is added at 10 μM and GA is added at 10<sup>3</sup> μM. **Left:** AND-like behavior was constructed by adding the components for both ABA- and GA- CRISPRa in a cell-free reaction. **Right:** The CRISPRa cascade was assembled by using ABA-CRISPRa to activate expression of both the first and second node in an activation cascade. The first node was added at either 0.05 or 0 nM, and the internal and output nodes were added at 10 nM.
- C. Simulation analysis of a two-input CRISPRa/i circuit using SYNZIP5/SYNZIP6 heterodimerization mediated-CRISPRa and blue-light CRISPRi (Methods 6).
- D. SYNZIP-CRISPRa and blue-light CRISPRi were integrated to construct a tunable pulse generator. The amount of CRISPRa was tuned by adding either 0.2 nM or 1 nM of constitutively expressed scRNA plasmid to the CFS reaction. The sgRNA targeting RFP for CRISPRi was driven from the blue-light responsive engineered EL222 promoter. The amount of CRISPRi was tuned by adjusting the time of

blue-light exposure between 45 and 135 min. RFP production rates (Methods S3) are plotted as a function of CRISPRa and CRISPRi inputs.

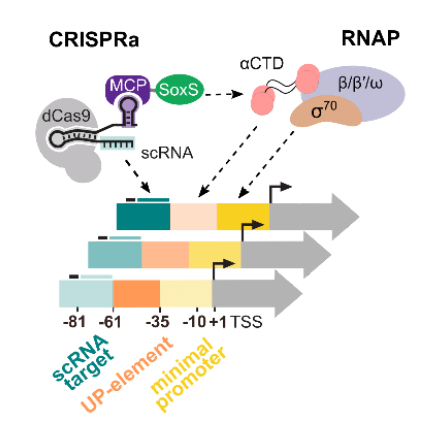
For all panels, values represent the mean ± standard deviation of three technical replicates.

# **Engineering Activatable Promoters for Scalable and Multi-Input CRISPRa/i Circuits**

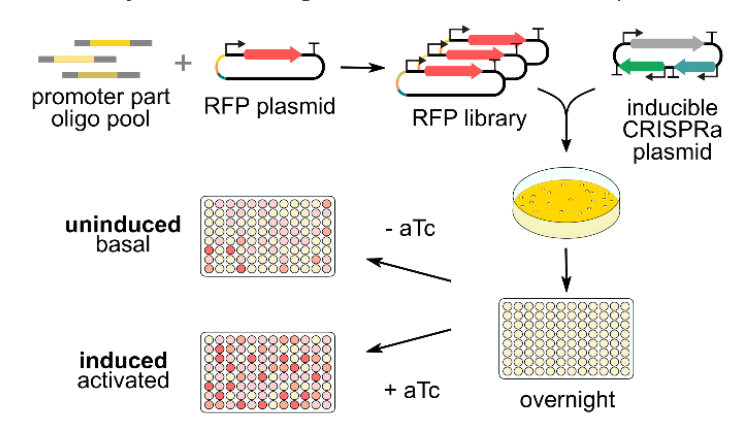
**Main Text Figures** 

Figure 1: Functional interrogation of promoter regions with CRISPRa

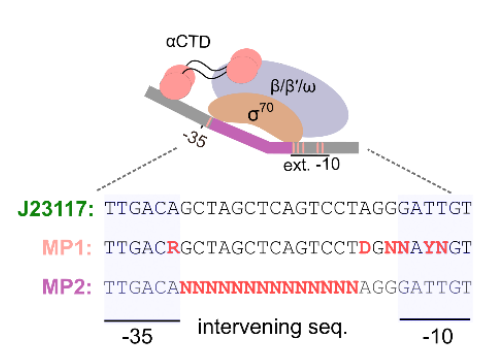
A RNAP recruitment contributions



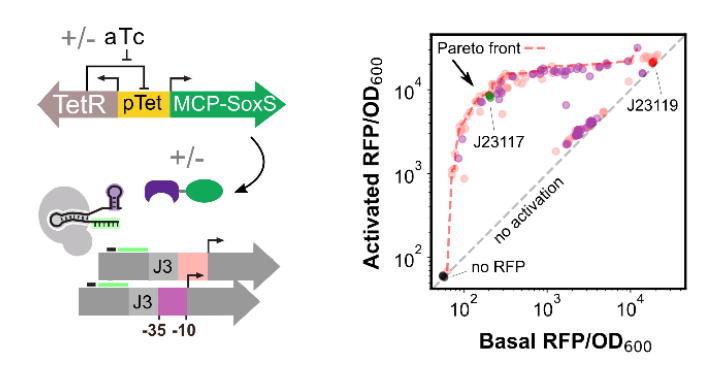
B Assembly and screening of libraries of activatable promoters



C Minimal promoter libray design



**D** Minimal promoter effect on basal and activated expression



- A. Schematic of RNAP interactions with the CRISPRa complex and target promoter.  $\sigma^{70}$  affinity for the minimal promoter and  $\alpha$ -CTD affinity for the UP-element determines RNAP recruitment to a promoter. When CRISPRa is targeted to a promoter with a complementary scRNA target site, the RNAP  $\alpha$ -CTD domain is recruited by the SoxS transcriptional activator. RNAP-promoter and CRISPRa-promoter interactions can be modulated by modifying the DNA sequence of the different promoter regions.
- B. Workflow for the assembly and characterization of libraries of activatable promoters.

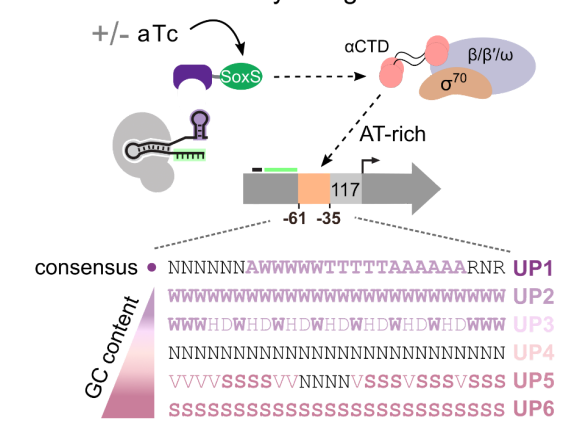
  A library of RFP genes with varying promoters is generated through PCR (Methods 1.1). The library is then co-transformed into *E. coli* with an aTc-inducible CRISPRa

plasmid. Colonies are then seeded overnight, and subsequently diluted into media with appropriate concentrations of aTc. For each promoter variant in the libraries, basal and activated RFP levels were measured with 0 nM and 200 nM aTc, respectively (Methods 2).

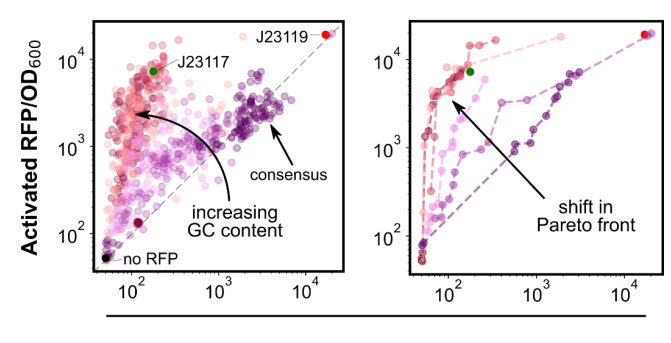
- C. Schematic of RNAP interaction with the minimal promoter and library design.  $\sigma^{70}$  recognizes specific positions in the extended -10 and -35 regions of the minimal promoter, which informed the design of the library MP1.  $\sigma^{70}$  binding is also influenced by the GC-content, the length, and the <sup>-15</sup>TGn<sup>-1</sup> motif of the intervening sequence, which informed the design of library MP2 (Methods 3.1).
- D. Minimal promoter effect on expression levels. **Left:** Inducible CRISPRa system and minimal promoter libraries of the J3 synthetic promoter. MCP-SoxS is expressed from the aTc-inducible pTet promoter. dCas9 and J306 scRNA are constitutively expressed. **Right:** Activated and basal RFP/OD<sub>600</sub> for the two minimal promoter libraries (n<sub>MP1</sub> = 89, n<sub>MP2</sub> = 84). Red dash line defines the Pareto front containing the best performing promoter variants (Methods S3), for which no further improvements in basal or activated levels can be achieved without compromising the other. Gray dash line defines promoter variants with equal activated and basal expression levels, indicating they are not activated by CRISPRa. The J23117 minimal promoter (green, triplicates) is included as a standard reference for CRISPRa efficiency. The J23119 minimal promoter (red, triplicates) is an example of a non-activatable promoter due to high basal expression levels. A plasmid without RFP (black, triplicates) indicates the background fluorescence of the system.

Figure 2: Combining promoter regions to engineer high-performing CRISPRa promoters

#### A UP-element library design

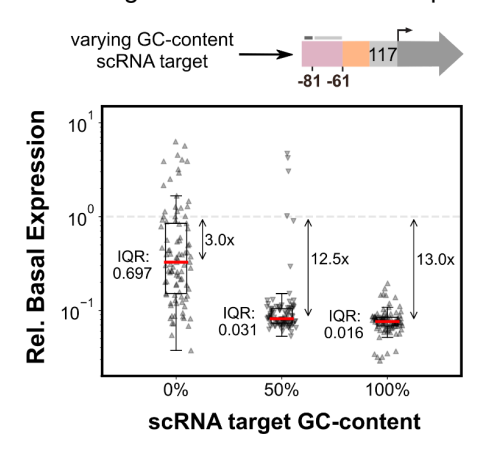


**B** UP-element effect on basal and activated expression

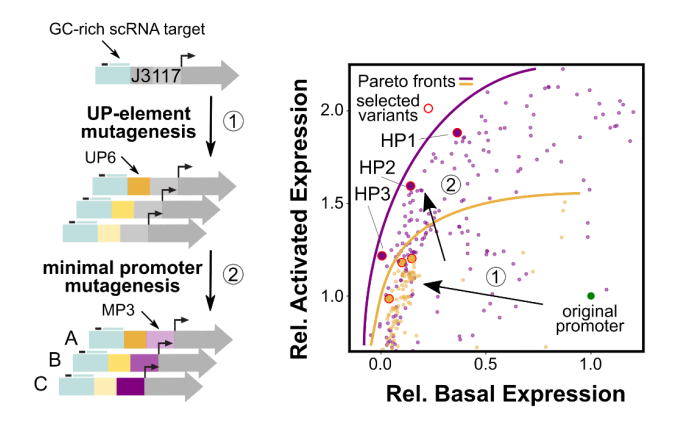


Basal RFP/OD<sub>600</sub>

C scRNA target site effect on basal expression



**D** Sequential construction of activatable promoters



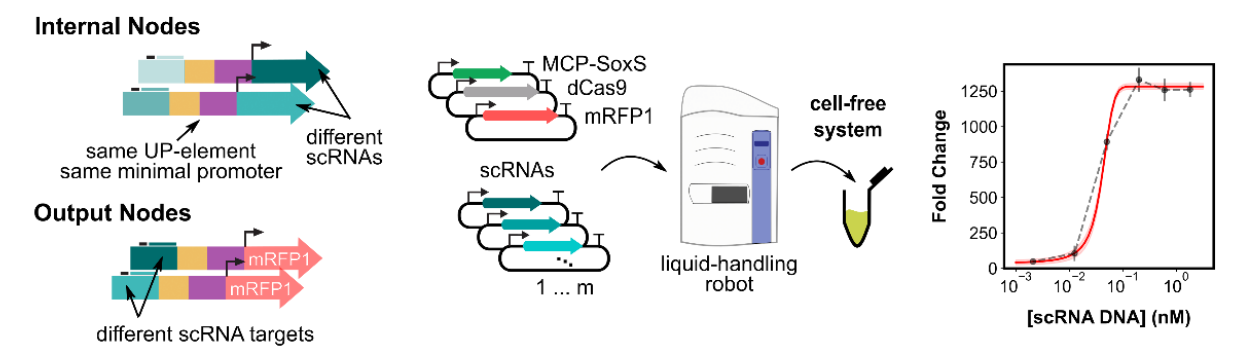
- A. Schematic of RNAP interactions with the UP-element and library design.  $\alpha$ -CTD affinity for AT-rich UP-elements upstream of the minimal promoter helps recruit RNAP. Upon targeting with CRISPRa, UP-element RNAP recruitment contributions are largely replaced by SoxS-RNAP  $\alpha$ -CTD interactions. UP-element libraries with increasing GC-content were designed to minimize  $\alpha$ -CTD interactions (Methods 3.2).
- B. UP-element GC-content effect on expression levels is shown through activated and basal RFP/OD<sub>600</sub> for the six UP-element libraries ( $n_{UP1} = n_{UP2} = ... = n_{UP6} = 110$ ). **Left:** Increasing GC-content in the UP-element lowers the range of basal expression level, while maintaining the full range of activated expression levels. Gray dash line

defines promoter variants with equal activated and basal expression levels. **Right:**Colored dash lines define the Pareto front for each UP-element library (Methods S3).
Increasing the UP-element GC-content effectively shifts the Pareto front towards lower basal expression levels.

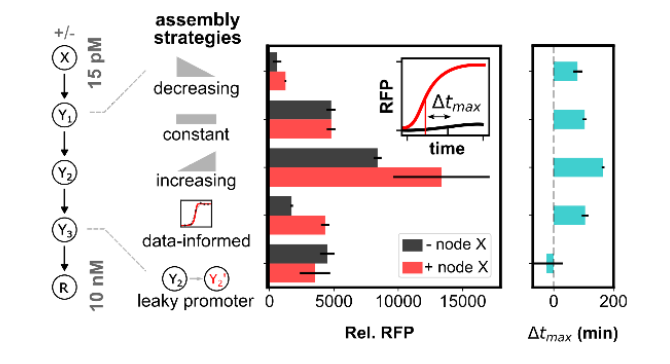
- C. scRNA target site composition effect on basal expression. Comparison of three scRNA libraries with increasing GC-content ( $n_{S1} = n_{S2} = n_{S3} = 93$ ) (Methods 3.3). Basal expression levels are normalized to the standard J3 promoter basal expression level. Red lines indicate the median expression level of each distribution. The interquartile range (IQR) is calculated as the difference between the upper and lower quartiles and measures the spread of the distribution.
- D. Sequential construction of activatable promoters. **Left:** Activatable promoters were constructed by sequential library mutagenesis screens starting from the J3 promoter with a GC-rich scRNA target site. Three Pareto optimal UP-elements were selected after promoter mutagenesis with a GC-rich UP-element library (1). We then mutagenized the minimal promoter of the three previously selected variants (2), and again selected three Pareto optimal variants. **Right:** Basal and activated expression levels for all mutagenesis variants normalized to the standard J3 promoter expression levels (green). Yellow points represent variants from the UP-element mutagenesis (n<sub>UP6</sub> = 192) (1), while purple points represent variants from the minimal promoter mutagenesis (n<sub>MP3</sub> = 279) (2). Red circles indicate selected variants from each screen, and solid lines depict the Pareto optimal fronts. Each sequential mutagenesis led to variants with both lower basal and higher activated expression levels.

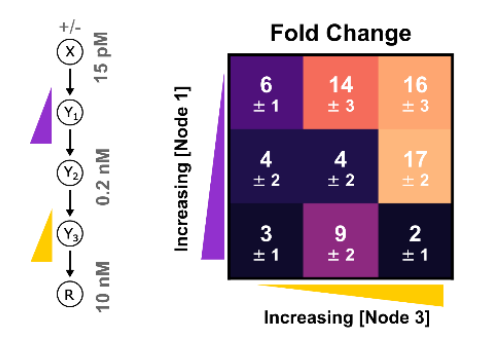
Figure 3: Engineering deep and wide circuits with high-performing CRISPRa promoters

A Orthogonal node generation B High-throughput part characterization in CFS

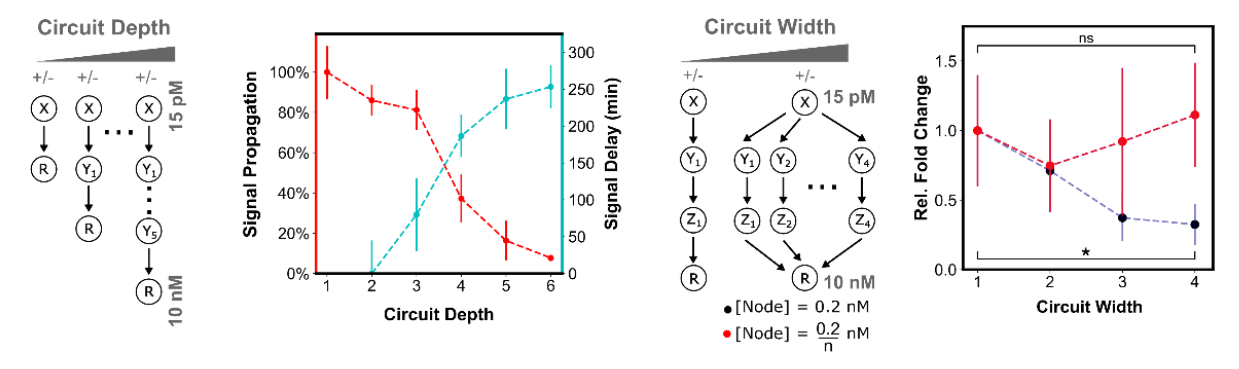


- C Assembly strategies for building CRISPRa/i circuits
- **D** Rapid optimization of circuit function





- E Signal propagation through deep circuits
- **F** Parallel regulation capacity in wide circuits



- A. Schematic of orthogonal CRISPRa/i nodes for use in cell-free circuits. Internal nodes contain an orthogonal scRNA target site and express orthogonal scRNAs.

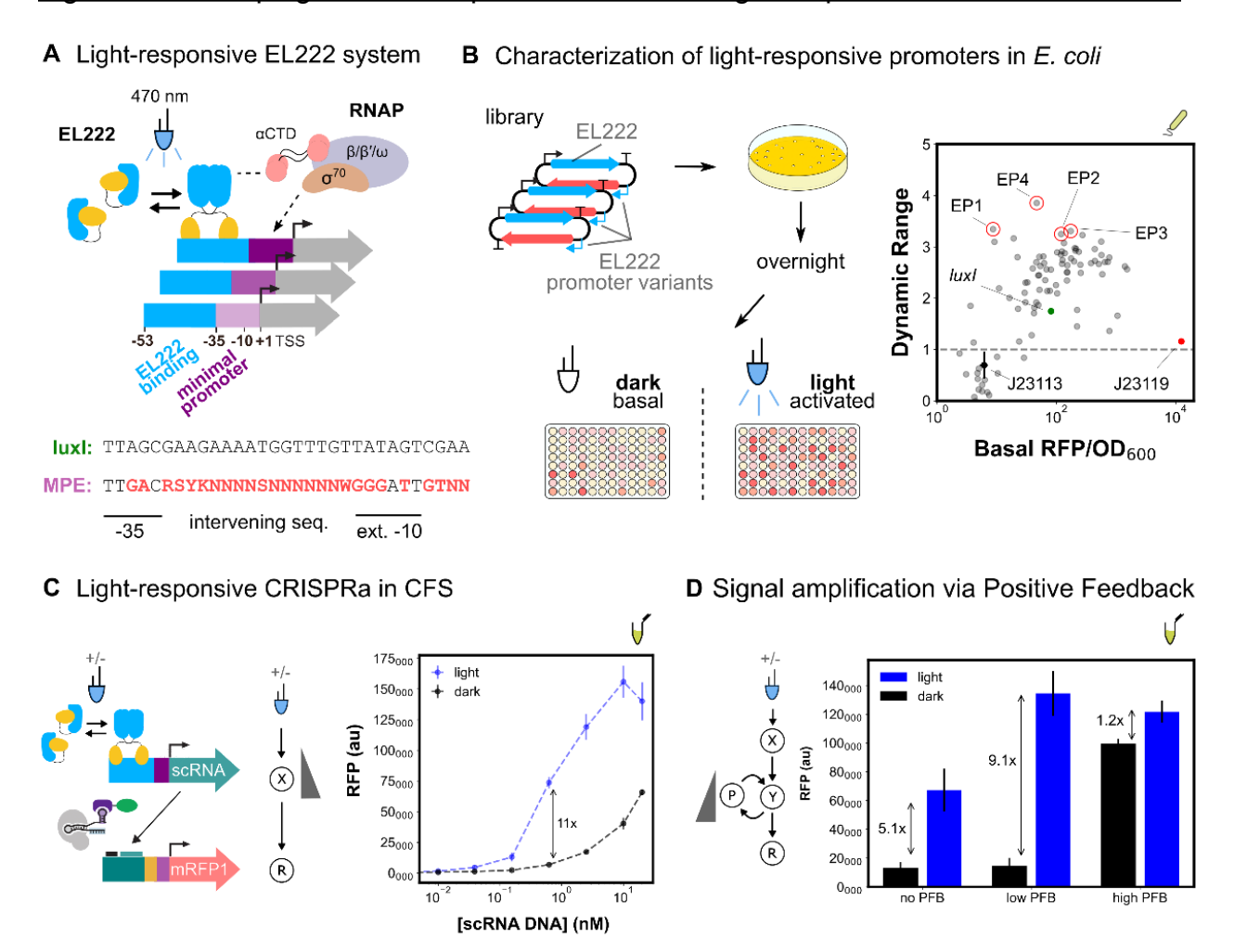
  Output nodes contain orthogonal scRNA target sites and express RFP. All nodes contain the same UP-element and minimal promoter (HP3).
- B. High-throughput characterization of scRNA components in CFS. **Left:** Plasmids encoding each CRISPRa component are mixed using an acoustic liquid handling

- robot and expressed in CFS. **Right:** scRNA-dose response curves for each node are generated by titrating the amount of scRNA plasmid from 0.5 pM to 5 nM.
- C. Comparison of assembly strategies for building a four-layer CRISPRa cascade. **Left:** Internal node concentrations either decreased from 200 pM to 32 pM as depth increased, were held constant at 200 pM, or increased from 200 pM to 1.25 nM as depth increased. A fourth assembly method was tested in which internal node concentrations were 40, 200, and 170 pM, based on individual scRNA-dose response characteristics. A fifth cascade was included in which the high-performing promoter of the second internal node was replaced with the leaky J2 promoter. Input and output node concentrations were held constant across all strategies at 0 or 15 pM and 10 nM, respectively. **Center:** Cascade output RFP expression for each assembly strategy with scRNA input (red) and without (black), relative to RFP basal expression. **Right:** Change in time to maximum expression rate ( $\Delta t_{max}$ ) for each assembly strategy (Methods S3).
- D. Rapid fold change optimization of a four-layer CRISPRa cascade. **Left:** The first and third internal nodes of the cascade were varied between 40 and 160 pM, and 85 and 340 pM, respectively. The input node, second internal node, and output node were held constant at 0 or 15 pM, 0.2 nM, and 10 nM, respectively. **Right:** Fold change between with and without scRNA input for each CRISPRa cascade.
- E. Signal propagation through deep CRISPRa/i circuits. **Left:** CRISPRa cascades with increasing depth. Input and output node concentrations were held constant across all cascades at 0 or 15 pM and 10 nM, respectively. All of the parallel cascade scRNA outputs are connected to the same RFP node. All node

- concentrations are tabulated in Table S5. **Right:** Propagation efficiency and signal delay are shown as a function of circuit depth (Methods S3).
- F. Construction of wide CRISPRa/i circuits. **Left:** CRISPRa cascades with increasing width. Input and output node concentrations were held constant across all cascades at 0 or 15 pM and 10 nM, respectively. **Right:** The concentration of each internal node was held at 0.2 nM as circuit width increased (blue), or the internal node concentration was scaled down proportionally to the width of the circuit (red), such that each internal node concentration is 0.2/n nM, where n is the number of parallel cascades. Fold-activation is given relative to a single CRISPRa cascade (Methods S3).

For all panels, values represent the mean ± standard deviation of three technical replicates.

Figure 4: Developing activatable promoters for blue-light responsive CRISPRa/i circuits



- A. Schematic of EL222 light-responsive promoter system and library design. EL222 transcription factor dimerizes in response to 470 nm light and binds a specific sequence upstream of the minimal promoter. EL222 then recruits RNAP through interactions with the  $\alpha$ -CTD domain. Minimal promoter library design is based on the original *luxI* promoter and previous minimal promoter libraries (Methods 3.4).
- B. Characterization of light responsive promoters in *E. coli*. **Left:** Blue-light promoter screening (Methods 5). EL222 protein and promoter library are expressed from a single plasmid. Assembly and screening are carried out as previously described. Basal and activated expression levels are measured from cultures not exposed

or continuously exposed to blue-light, respectively. **Right:** Basal expression and dynamic range of blue-light promoter variants ( $n_{MP3}$  = 96). Gray dash line defines promoter variants with equal activated and basal expression levels, indicating they are not activated by EL222. The J23119 minimal promoter (red) and J23113 (black) are examples of non-activatable promoters. Variants with improved performance (red circles) compared to the original *lux1* promoter (green) were selected for use in CFS.

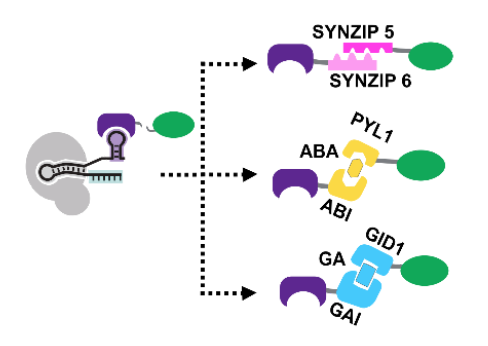
- C. Light-responsive CRISPRa in CFS. Left: EL222 scRNA expression from an engineered blue-light promoter and downstream CRISPRa. Reactions contain 8nM and 10 nM of EL222 and RFP plasmids respectively. Right: Titration of blue-light inducible scRNA plasmid concentration to maximize the fold change between blue-light dependent CRISPRa (blue) and CRISPRa due to scRNA leak in the dark (black).
- D. Improvement of blue-light CRISPRa dynamic range through the construction of a positive feedback circuit. Left: Blue-light responsive CRISPRa cascade with positive feedback (PFB). PFB is achieved by including a downstream node that expresses a scRNA targeting an upstream node Reactions contain 15nM and 10 nM of EL222 and RFP plasmids respectively. Right: Blue-light dependent CRISPRa (blue) and CRISPRa due to scRNA leak in the dark (black). The amount of positive feedback was tuned by adjusting the concentration of the PFB node. "No", "Low", and "High" PFB concentrations correspond to 0, 3 pM, and 2 nM, respectively.

For all panels, values represent the mean  $\pm$  standard deviation of three technical replicates.

Figure 5: Engineered activatable promoters enable PPI-dependent conditional CRISPRa

A PPI-dependent CRISPRa

**C** Conditional CRISPRa is sensitive to ligand concentration



ABA

ABA

3500

\*
3500

\*
3500

\*
3500

\*
3500

\*
3500

\*
3500

\*
3500

\*
3000

\*
3000

\*
3000

\*
3000

\*
3000

\*
3000

\*
3000

\*
3000

\*
3000

\*
3000

\*
3000

\*
3000

\*
3000

\*
3000

\*
3000

\*
3000

\*
3000

\*
3000

\*
3000

\*
3000

\*
3000

\*
3000

\*
3000

\*
3000

\*
3000

\*
3000

\*
3000

\*
3000

\*
3000

\*
3000

\*
3000

\*
3000

\*
3000

\*
3000

\*
3000

\*
3000

\*
3000

\*
3000

\*
3000

\*
3000

\*
3000

\*
3000

\*
3000

\*
3000

\*
3000

\*
3000

\*
3000

\*
3000

\*
3000

\*
3000

\*
3000

\*
3000

\*
3000

\*
3000

\*
3000

\*
3000

\*
3000

\*
3000

\*
3000

\*
3000

\*
3000

\*
3000

\*
3000

\*
3000

\*
3000

\*
3000

\*
3000

\*
3000

\*
3000

\*
3000

\*
3000

\*
3000

\*
3000

\*
3000

\*
3000

\*
3000

\*
3000

\*
3000

\*
3000

\*
3000

\*
3000

\*
3000

\*
3000

\*
3000

\*
3000

\*
3000

\*
3000

\*
3000

\*
3000

\*
3000

\*
3000

\*
3000

\*
3000

\*
3000

\*
3000

\*
3000

\*
3000

\*
3000

\*
3000

\*
3000

\*
3000

\*
3000

\*
3000

\*
3000

\*
3000

\*
3000

\*
3000

\*
3000

\*
3000

\*
3000

\*
3000

\*
3000

\*
3000

\*
3000

\*
3000

\*
3000

\*
3000

\*
3000

\*
3000

\*
3000

\*
3000

\*
3000

\*
3000

\*
3000

\*
3000

\*
3000

\*
3000

\*
3000

\*
3000

\*
3000

\*
3000

\*
3000

\*
3000

\*
3000

\*
3000

\*
3000

\*
3000

\*
3000

\*
3000

\*
3000

\*
3000

\*
3000

\*
3000

\*
3000

\*
3000

\*
3000

\*
3000

\*
3000

\*
3000

\*
3000

\*
3000

\*
3000

\*
3000

\*
3000

\*
3000

\*
3000

\*
3000

\*
3000

\*
3000

\*
3000

\*
3000

\*
3000

\*
3000

\*
3000

\*
3000

\*
3000

\*
3000

\*
3000

\*
3000

\*
3000

\*
3000

\*
3000

\*
3000

\*
3000

\*
3000

\*
3000

\*
3000

\*
3000

\*
3000

\*
3000

\*
3000

\*
3000

\*
3000

\*
3000

\*
3000

\*
3000

\*
3000

\*
3000

\*
3000

\*
3000

\*
3000

\*
3000

\*
3000

\*
3000

\*
3000

\*
3000

\*
3000

\*
3000

\*
3000

\*
3000

\*
3000

\*
3000

\*
3000

\*
3000

\*
3000

\*
3000

\*
3000

\*
3000

\*
3000

\*
3000

\*
3000

\*
3000

\*
3000

\*
3000

\*
3000

\*
3000

\*
3000

\*
3000

\*
3000

\*
3000

\*
3000

\*
3000

\*
3000

\*
3000

\*
3000

\*
3000

\*
3000

\*
3000

\*
3000

\*
3000

\*
3000

\*
3000

\*
3000

\*
3000

\*
3000

\*
3000

\*
3000

\*
3000

\*
3000

\*
3000

\*
3000

\*
3000

\*
3000

\*
3000

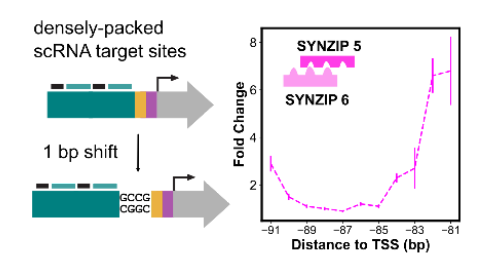
\*
3000

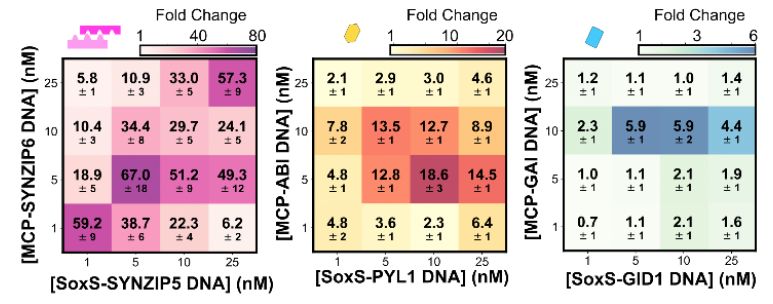
\*
3000

\*
3000

**B** PPI-dependent CRISPRa mantains distance requirements

D PPI-dependent CRISPRa systems exhibit unique stoichiometric preferences



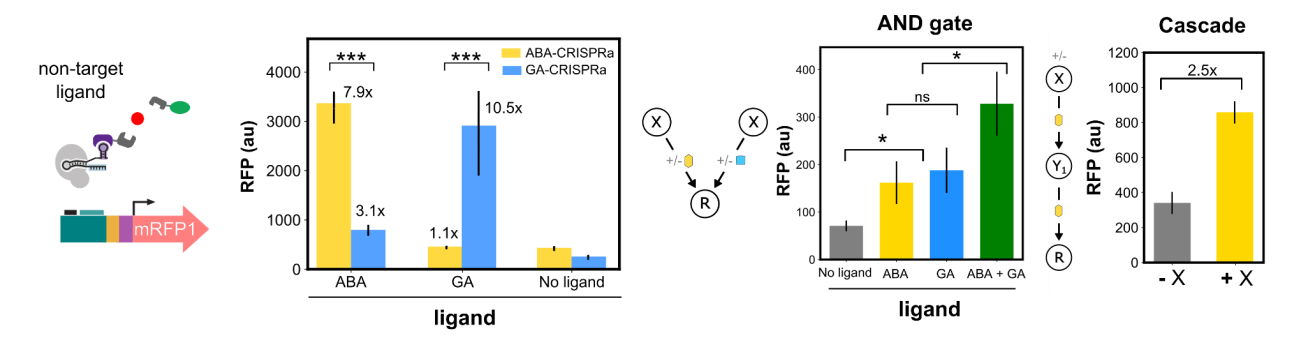


- A. Schematic of different PPI-dependent CRISPRa systems. MCP-SoxS fusion is split and the two proteins are instead fused to one end of a heterodimerization domain. The heterodimerization domains used to build PPI-dependent CRISPRa systems are the SYNZIP5/SYNZIP6 pair, the abscisic acid (ABA)-responsive ABI/PYL1 domain, and the gibberellic acid (GA)-responsive GAI/GID1 domain.
- B. Distance requirements of PPI-dependent CRISPRa. **Left:** Engineered promoter containing densely-packed scRNA target sites and single base pair 5' additions allows for CRISPRa targeting between -81 and -111 bp from the TSS. **Right:** Testing SYNZIP-CRISPRa between -81 and -91 bp from the TSS. SYNZIP-CRISPRa components are expressed at 5 nM. Fold change is calculated relative to an off-target scRNA for each promoter variant.

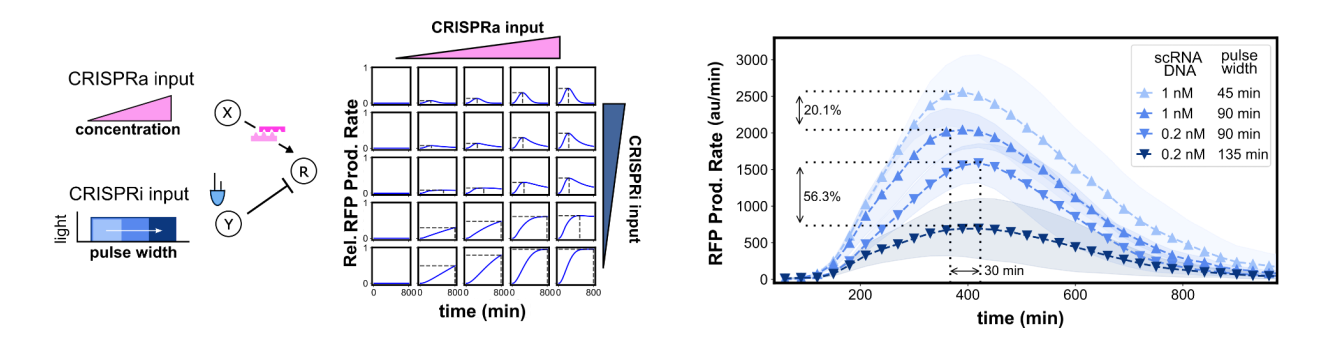
- C. Tuning conditional CRISPRa response through titration of small molecule concentration. For ABA- and GA- CRISPRa, the corresponding small molecule was titrated between 0 and 10 or 0 and 10<sup>3</sup> µM respectively to find the optimal concentration. ABA- and GA-CRISPRa components are expressed at 10 nM.
- D. Improving PPI-dependent and conditional CRISPRa response by optimizing component stoichiometries. The concentration of the plasmids expressing the MCP and SoxS components for each dimerization system were varied 1-25 nM and tested combinatorially to find the best ratio of the two heterodimers. ABA is added at 10  $\mu$ M and GA is added at 10<sup>3</sup>  $\mu$ M. Fold change is given relative to a reaction with no MCP and SoxS plasmids added.

Figure 6: Engineering multi-input CRISPRa/i Circuits

A Conditional CRISPRa systems are largely orthogonal B Assembly of conditional CRISPRa circuits



- c Simulation analysis of two-input CRISPRa/i circuit
- **D** Dynamic two-input pulse generator in CFS



- A. Conditional CRISPRa response to non-cognate ligands. The orthogonality of the small molecule-responsive conditional CRISPRa systems was tested by adding either the corresponding or non-corresponding small molecule to cell-free reactions containing the components for ABA- or GA-CRISPRa. All components are added at their respective optimal screened concentrations. ABA is added at  $10 \, \mu M$  and GA is added at  $10^3 \, \mu M$ .
- B. Assembly of conditional CRISPRa circuits. For both circuits, all components are added at their respective optimal screened concentrations. ABA is added at 10 μM and GA is added at 10<sup>3</sup> μM. **Left:** AND-like behavior was constructed by adding the components for both ABA- and GA- CRISPRa in a cell-free reaction. **Right:** The CRISPRa cascade was assembled by using ABA-CRISPRa to

- activate expression of both the first and second node in an activation cascade. The first node was added at either 0.05 or 0 nM, and the internal and output nodes were added at 10 nM.
- C. Simulation analysis of a two-input CRISPRa/i circuit using SYNZIP5/SYNZIP6 heterodimerization mediated-CRISPRa and blue-light CRISPRi (Methods 6).
- D. SYNZIP-CRISPRa and blue-light CRISPRi were integrated to construct a tunable pulse generator. The amount of CRISPRa was tuned by adding either 0.2 nM or 1 nM of constitutively expressed scRNA plasmid to the CFS reaction. The sgRNA targeting RFP for CRISPRi was driven from the blue-light responsive engineered EL222 promoter. The amount of CRISPRi was tuned by adjusting the time of blue-light exposure between 45 and 135 min. RFP production rates (Methods S3) are plotted as a function of CRISPRa and CRISPRi inputs.

For all panels, values represent the mean ± standard deviation of three technical replicates.

## Supplemental Information

## **Engineering Activatable Promoters for Scalable and Multi-Input CRISPRa/i Circuits**

Diego Alba Burbano<sup>+,1,2</sup>, Ryan Cardiff<sup>+1</sup>, Benjamin I. Tickman<sup>2</sup>, Cholpisit Kiattisewee<sup>1</sup>, Cassandra Maranas<sup>1</sup>, Jesse G. Zalatan<sup>\*1,3</sup>, James M. Carothers<sup>\*,1,2</sup>

1: Molecular Engineering & Sciences Institute and Center for Synthetic Biology University of Washington Seattle, WA 98195 United States

2: Department of Chemical Engineering University of Washington Seattle, WA 98195 United States

3: Department of Chemistry University of Washington Seattle, WA 98195 United States

- +: These authors contributed equally
- \*: Corresponding authors zalatan@uw.edu 206-543-1670

jcaroth@uw.edu 206-221-4902

Proc. Natl. Acad. Sci. USA, In Press.

#### **Supplementary Figures**

Figure S1: Minimal promoter effect on fold-change

Figure S2: UP-element libraries RFP distributions

Figure S3: UP-element libraries fold-change distributions

Figure S4: CRISPRa activity validation of high GC-content scRNAs

Figure S5: Combinatorial construction of activatable promoters

Figure S6: Activatable promoter characterization in CFS

Figure S7: scRNA dose-response characterizations

Figure S8: Titration of middle node in two-layer activation cascade

Figure S9: Signal propagation in a two-layer activation cascade

**Figure S10:** Time course for four-layer activation cascade assembly strategies

Figure S11: Four-layer activation cascade basal and activated RFP expression

**Figure S12:** Signal propagation and signal delay model accuracy

Figure \$13: Wide circuit basal and activated RFP expression

Figure S14: Blue-light promoter characterization in CFS

Figure \$15: Blue-light CRISPRi

Figure \$16: EL222 titration in blue-light CRISPRa

Figure S17: Fusion orientation preference for SYNZIP and ABI/PYL1

Figure \$18: Dependence of SYNZIP-CRISPRa on distance to TSS

Figure S19: Improvements in SYNZIP-CRISPRa from engineered promoters

Figure S20: Conditional CRISPRa scRNA dose-response

Figure S21: Comparisons of CRISPRa promoters to pTet

Figure S22: Three-layer activation cascade in *E. coli* 

#### Supplementary Tables

**Table S1:** Promoters generated in this paper

**Table S2:** Dimerization domains affinity

**Table S3:** Primers for promoter mutagenesis

**Table S4:** Plasmids used in this work

**Table S5:** Deep cascades concentration

**Table S6:** Component sequences

## **Table S7:** ANOVA analysis of combinatorial promoter screens

## **Supplementary Methods**

**Methods S1:** Plasmid Preparation for Cell-Free System

Methods S2: CFS Blue-light CRISPRa/i modeling

Methods S3: Quantification and Statistical Analysis

**Methods S4:** Relationship between signal delay and signal propagation

Methods S5: Cell-Free Gene Expression Reactions

Methods S6: Plasmid and Library Construction

**Methods S7:** Optogenetic Illumination Setup

Methods S8: E. coli experiments culturing and quantification conditions

## **Supplementary Figures**

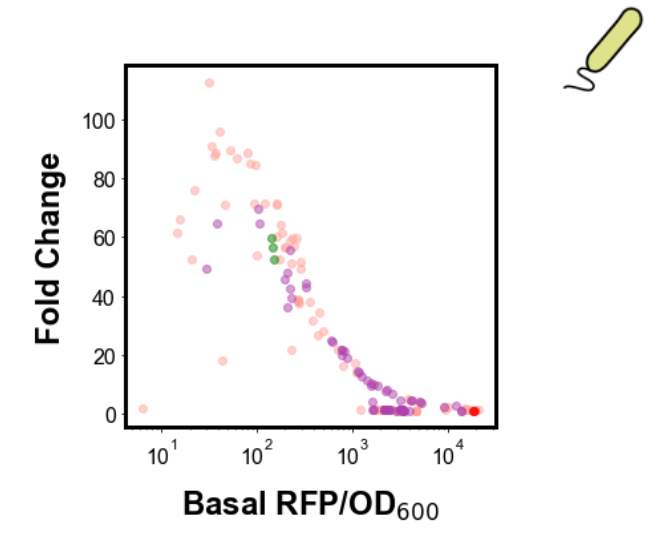


Figure S1: Minimal promoter effect on fold-change

Basal RFP/OD<sub>600</sub> and fold change for the two minimal promoter libraries ( $n_{MP1}$  = 89,  $n_{MP2}$  = 84). The J23117 minimal promoter (green, triplicates) is included as a standard reference for CRISPRa efficiency. The J23119 minimal promoter (red, triplicates) is an example of a non-activatable promoter due to high basal expression levels.

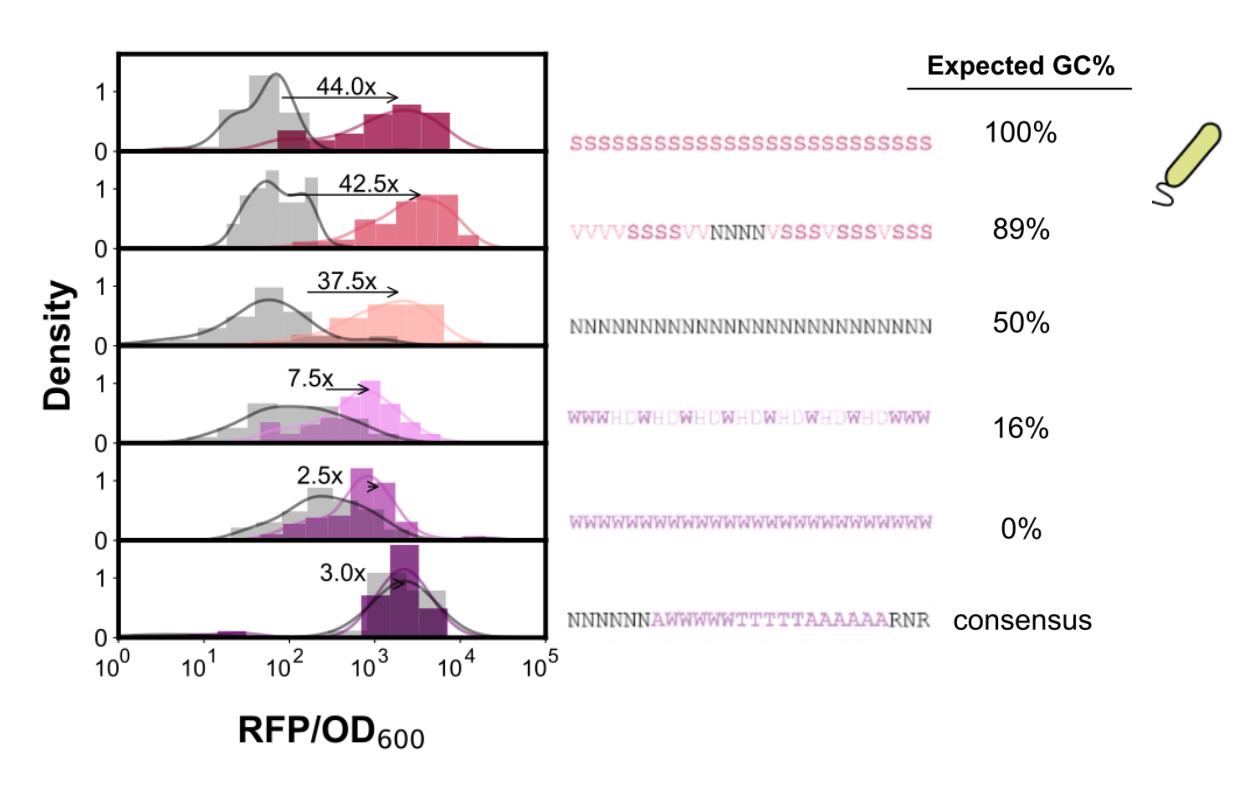


Figure S2: UP-element libraries RFP distributions

Histograms and probability density functions for basal expression (gray) and activated expression (colored) for six UP-element libraries with increasing GC-content. Median fold change is calculated as the ratio of median activation and media basal expression levels.

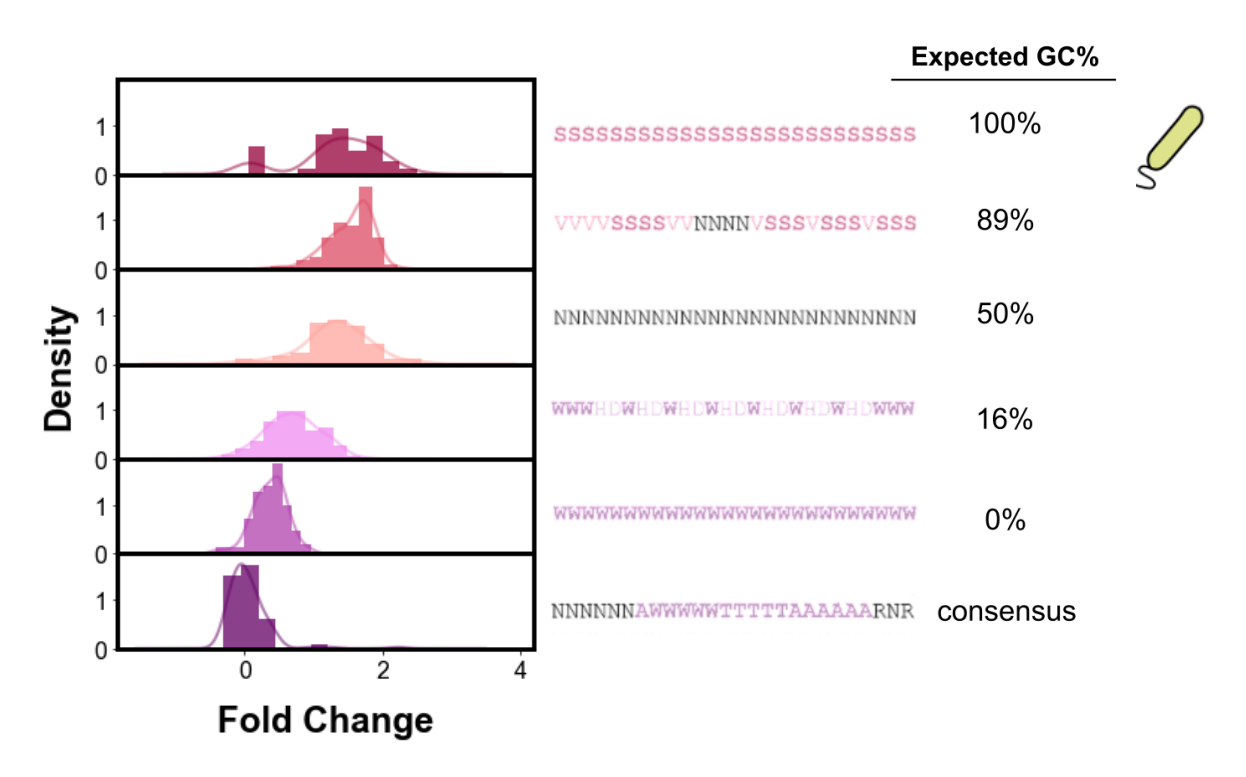


Figure S3: UP-element libraries fold-change distributions

Histograms and probability density functions for ford change for six UP-element libraries with increasing GC-content.

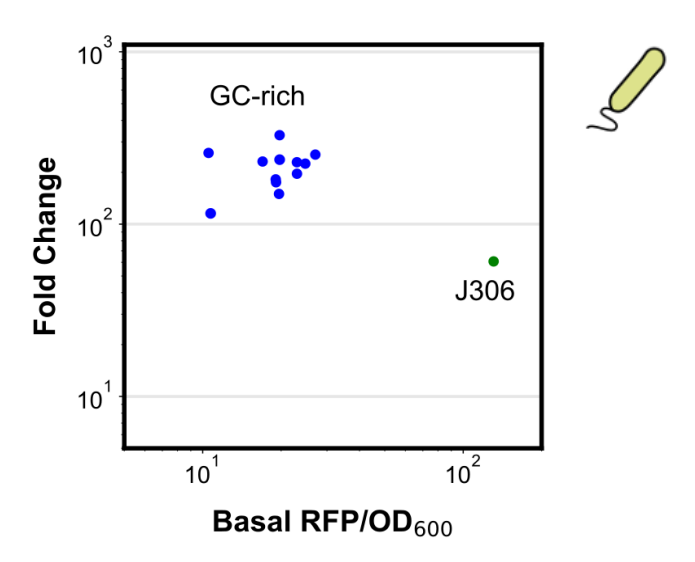


Figure S4: CRISPRa activity validation of high GC-content scRNAs

Fold change upon aTc induction and basal expression. scRNA target site sequences were initially selected based on low expression leak in *E. coli* and the corresponding scRNAs were constructed for use in CFS. Selected scRNAs were benchmarked against the standard J306 scRNA (green).

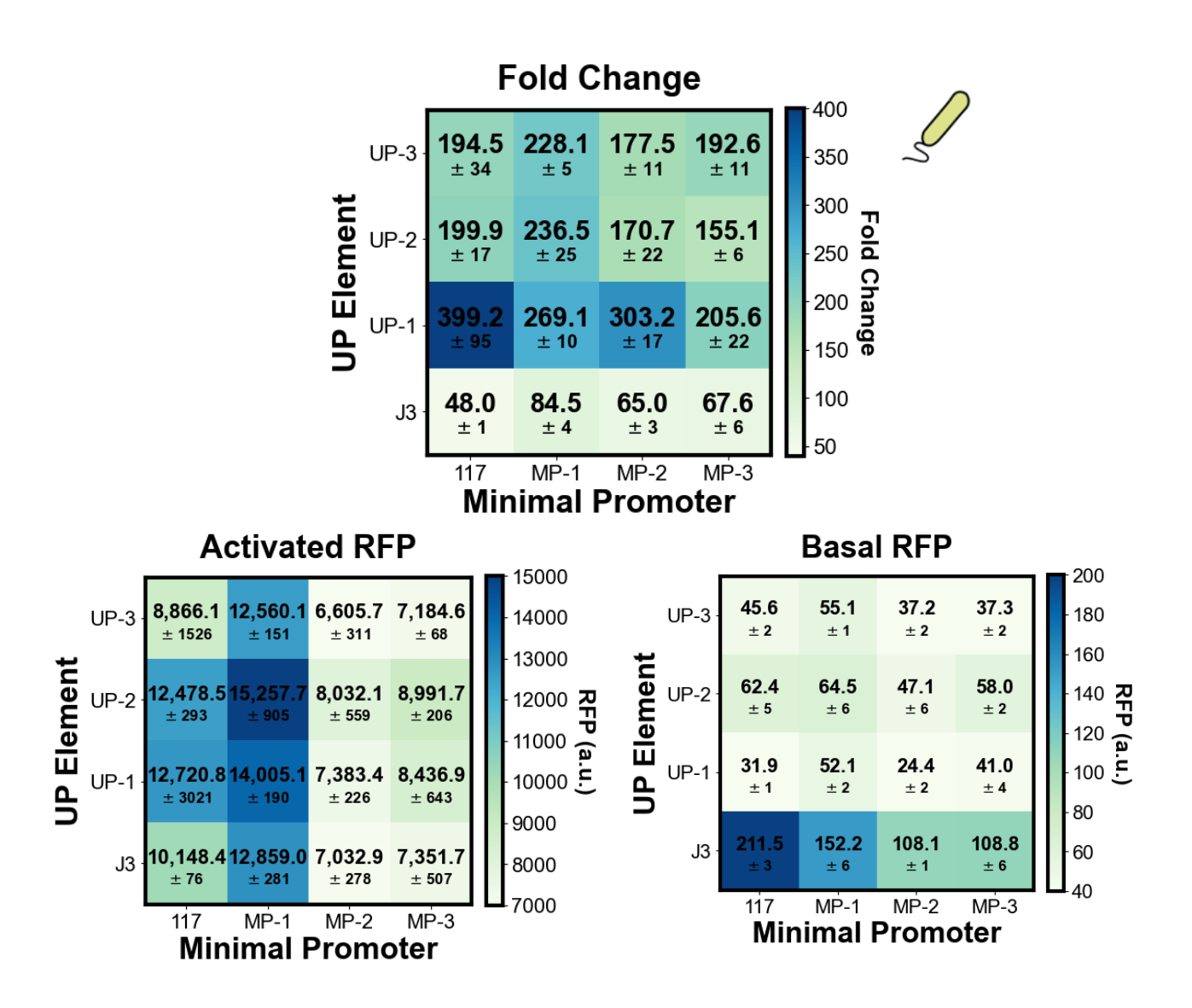


Figure S5: Combinatorial construction of activatable promoters

In addition to the J3.J23117 benchmark, three high performing variants each from the UP element and minimal promoter libraries were tested in a combinatorial manner for a total of 16 UP element/minimal promoter combinations screened in *E. coli*. We quantified the basal and activation expression of the 16 promoters with the same scRNA (bottom). Activation ratio is calculated by dividing the activated RFP expression from the inducible CRISPRa system by the basal RFP expression from each promoter (top). Values represent the mean ± standard deviation of three technical replicates.

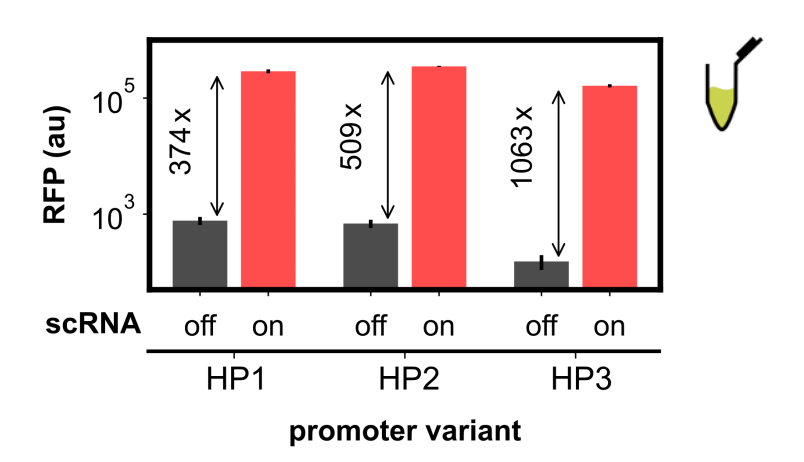


Figure S6: Activatable promoter characterization in CFS

Characterization of selected promoter variants in CFS. CRISPRa-mediated RFP expression levels (red, 0.4 nM scRNA DNA) and RFP basal expression levels (black, 0 nM scRNA DNA). Reactions contain 10 nM of RFP plasmid. Values represent the mean ± standard deviation of three technical replicates.

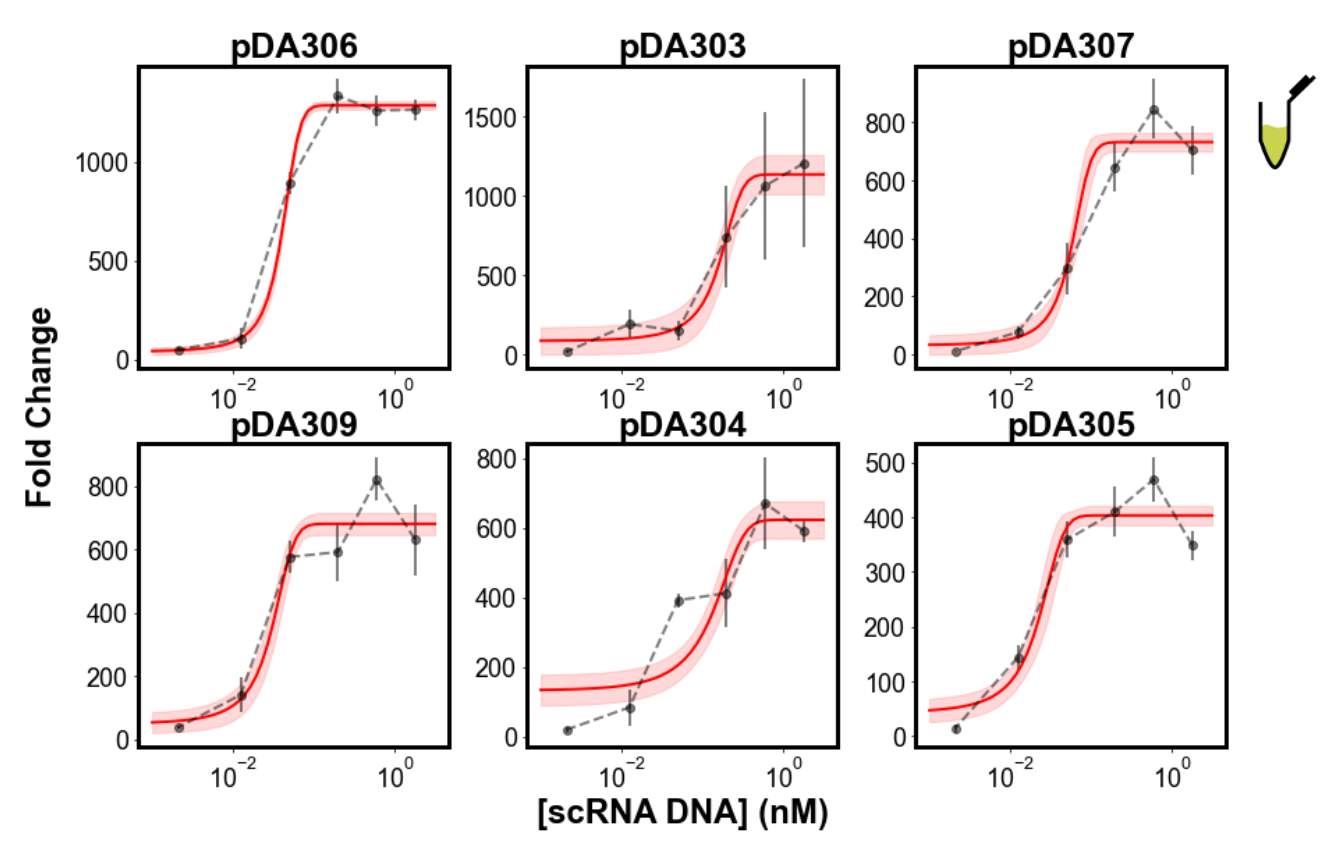


Figure S7: scRNA dose-response characterizations

scRNA dose-response curves are shown for orthogonal promoter-scRNA pairs in CFS. The scRNA-dose response curve is characterized through titrating the amount of scRNA DNA added to the CFS reaction. Reactions contain 10 nM of RFP plasmid. Red line indicates a logistic fit to the data. Values represent the mean ± standard deviation of three technical replicates.

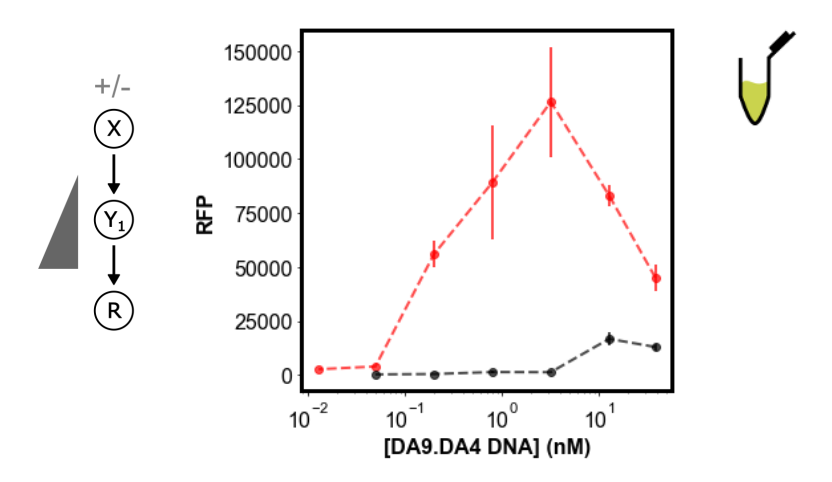


Figure S8: Titration of middle node in two-layer activation cascade

Two-layer activation cascade with high-performing components to identify the best performing internal node concentration. **Left:** Circuit schematic for measuring output RFP and fold change as a function of input scRNA. **Right:** Cascade RFP output with scRNA input (15 pM, red) and without (0 pM, black). Output node concentration is held constant at 10 nM. Values represent the mean  $\pm$  standard deviation of three technical replicates.

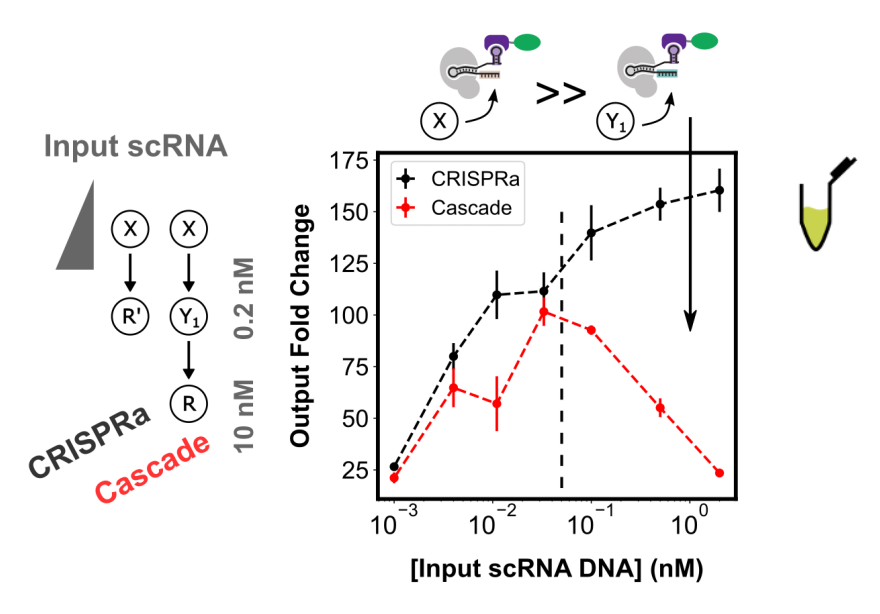


Figure S9: Signal propagation in a two-layer activation cascade

gRNA competition impact on circuit function. **Left:** Circuit schematic for measuring output fold change as a function of input scRNA for both CRISPRa (black) and CRISPRa cascade (red). Internal node concentration and output node concentration are held constant at 0.2 nM and 10 nM, respectively. **Right:** Input scRNA plasmid concentration was titrated between 1 pM and 2 nM. Black dashed line indicates saturation of CRISPRa complexes with input scRNA. Values represent the mean ± standard deviation of three technical replicates.

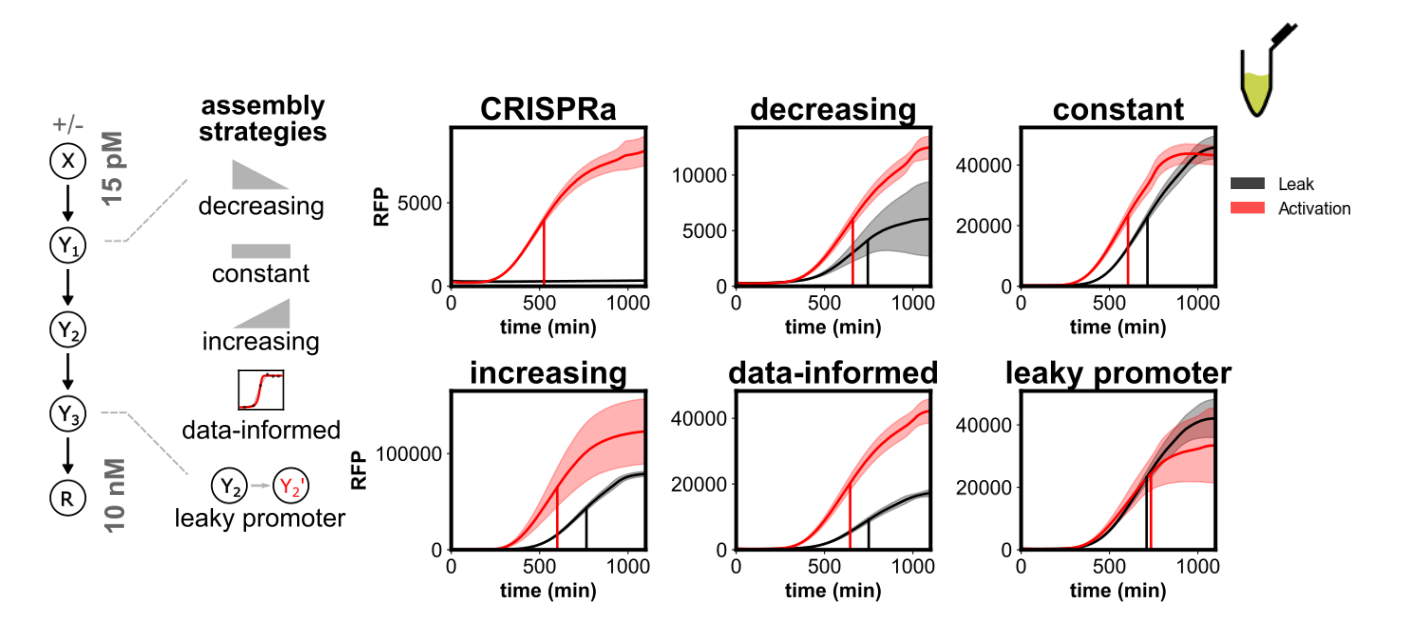


Figure S10: Time course for four-layer activation cascade assembly strategies

Comparison of the dynamics of four-layer CRISPRa cascade assemblies. **Left:** Internal node concentrations either decreased from 200 pM to 32 pM as depth increased, were held constant at 200 pM, or increased from 200 pM to 1.25 nM as depth increased. A fourth assembly method was tested in which internal node concentrations were 40, 200, and 170 pM, based on individual scRNA-dose response characteristics. A fifth cascade was included in which the high-performing promoter of the second internal node was replaced with the leaky J2 promoter. Input and output node concentrations were held constant across all strategies at 0 or 15 pM and 10 nM, respectively. **Right:** Output RFP expression for each assembly strategy with scRNA input (red) and without (black). Values represent the mean  $\pm$  standard deviation of three technical replicates. Time to maximum expression rate ( $t_{max}$ ) for each assembly strategy is calculated by finding the time to reach maximum RFP production rate between (Methods 7.1).

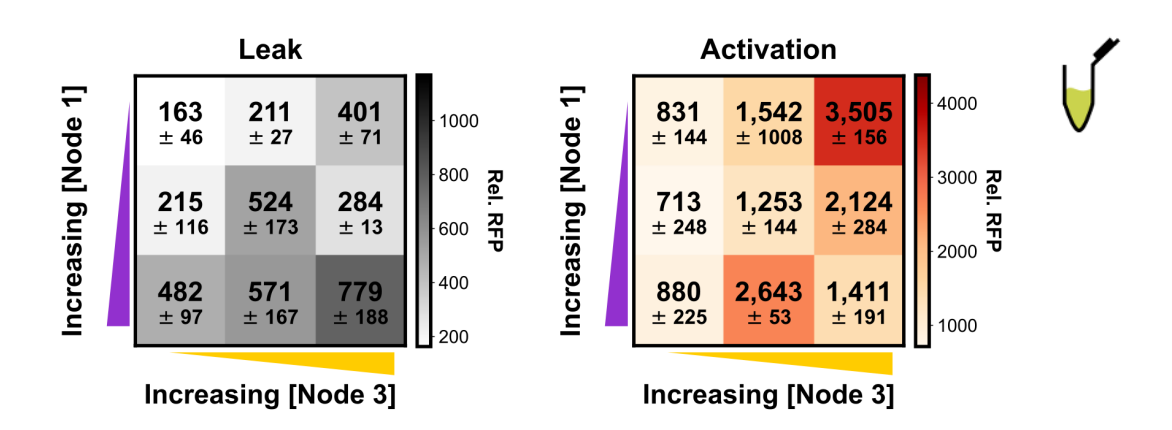


Figure S11: Four-layer activation cascade basal and activated RFP expression

**Left:** Basal expression levels for cascades titrating the first and third layers between 40 and 160 pM, and 85 and 340 pM, respectively. **Right:** Activated expression levels for the same cascades. The input node, second internal node, and output node were held constant at 0 or 15 pM, 0.2 nM, and 10 nM, respectively. Values are not background subtracted. Values represent the mean ± standard deviation of three technical replicates.

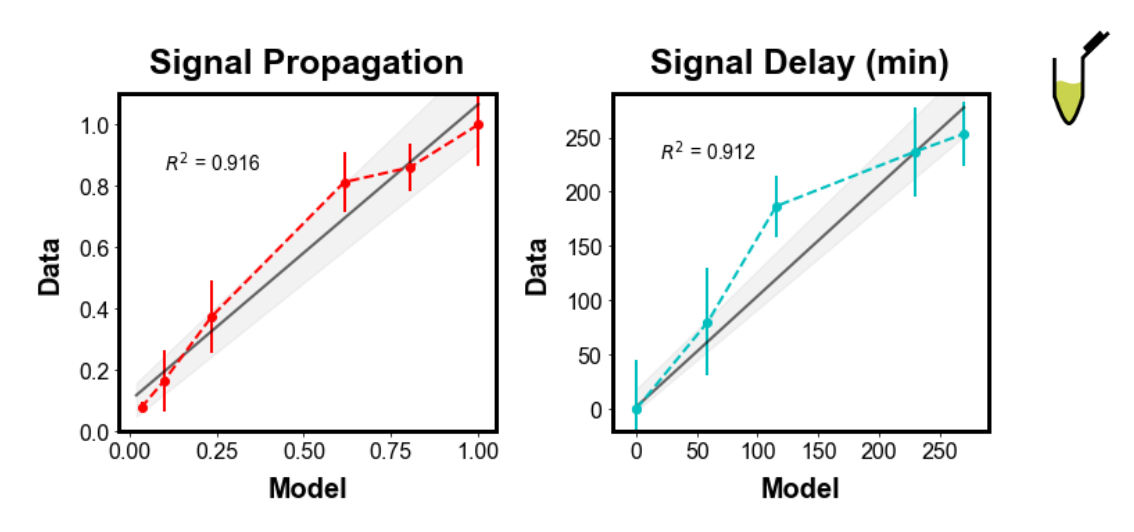


Figure S12: Signal propagation and signal delay model accuracy

Comparisons of measured and predicted signal propagation (left) and signal delay (right) for activation cascades of different depths. Signal propagation is calculated by dividing the fold-activation of the cascade output by the fold-activation from the input layer. (Methods 7.2). Signal delay is calculated as the difference between the cascade output and input layer in time to reach the maximum fold-activation (Methods 7.2). Both measures are presented as the mean ± standard deviation of three technical replicates. The fold-change from the individual promoters' dose-response curves (Figure S7) are used to iteratively predict the delay and signal propagation at the next layer (Methods S4). Black line represents the mean ± standard deviation of linear regression model measuring goodness-of-fit between model predictions and experimental data.

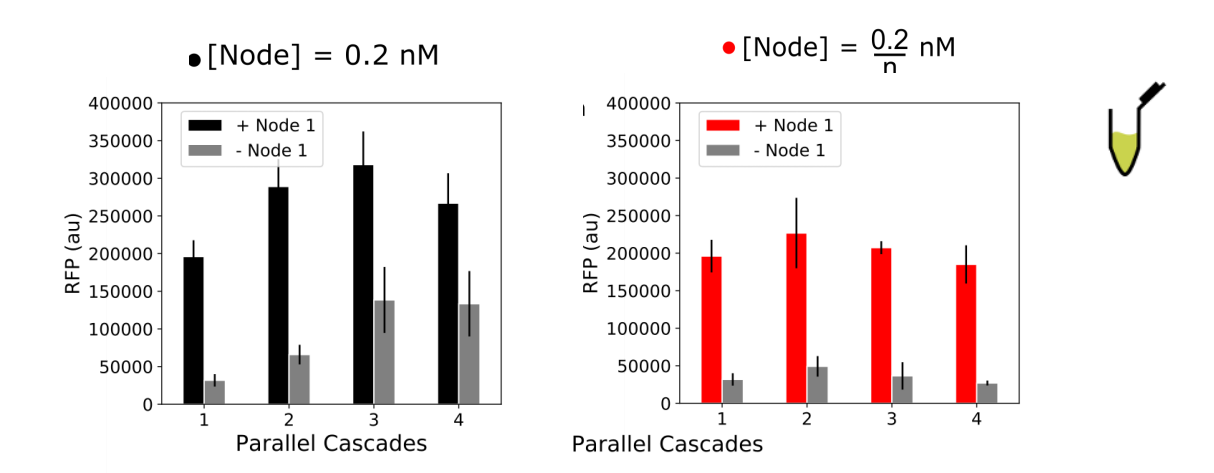


Figure S13: Wide circuit basal and activated RFP expression

Up to four parallel three-layer cascades were constructed. **Left:** The concentration of each internal node was held at 0.2 nM as circuit width increased. **Right:** The internal node concentration is scaled down proportionally to the width of the circuit, such that each internal node concentration is 0.2/n nM, where n is the number of parallel cascades.

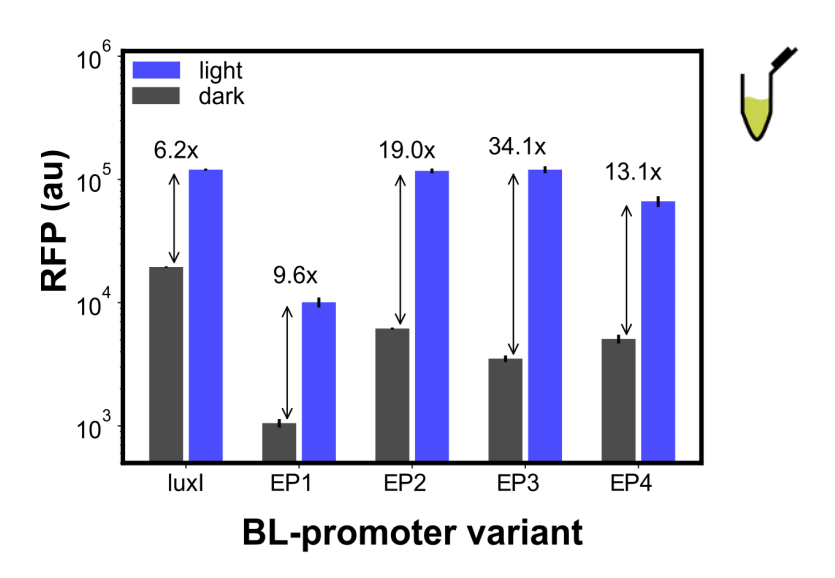


Figure S14: Blue-light promoter characterization in CFS

Characterization of selected promoter variants in CFS. Reactions contain 8 nM and 10 nM of EL222 and RFP plasmids respectively. EL222-mediated RFP expression levels (blue) and RFP basal expression levels (black). Values represent the mean  $\pm$  standard deviation of three technical replicates.

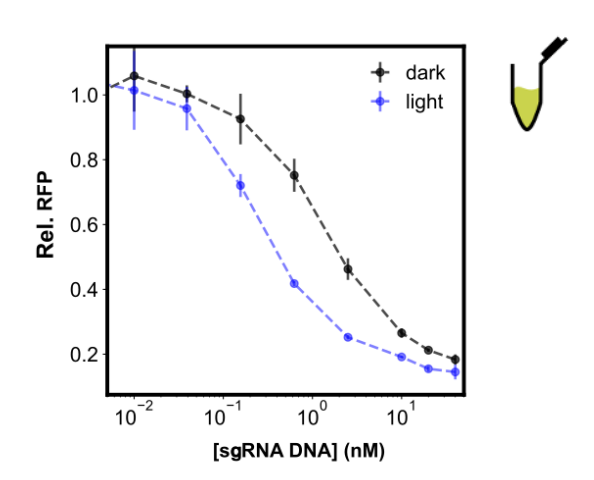


Figure S15: Blue-light CRISPRi

Titration of blue-light inducible sgRNA plasmid concentration to maximize the fold repression between blue-light dependent CRISPRi (blue) and CRISPRi due to sgRNA leak in the dark (black). Reactions contain 8 nM and 1 nM of EL222 and RFP plasmids respectively. Values represent the mean ± standard deviation of three technical replicates.

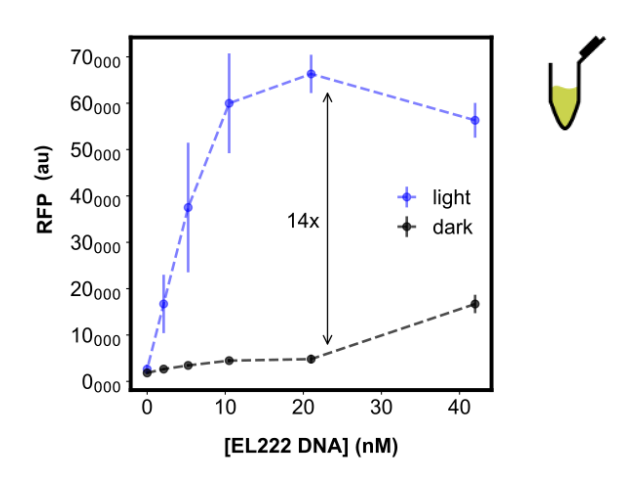


Figure S16: EL222 titration in blue-light CRISPRa

Titration of EL222 plasmid concentration to maximize the fold change between blue-light dependent CRISPRa (blue) and CRISPRa due to scRNA leak in the dark (black). Reactions contain 10 nM RFP plasmid. Values represent the mean ± standard deviation of three technical replicates.

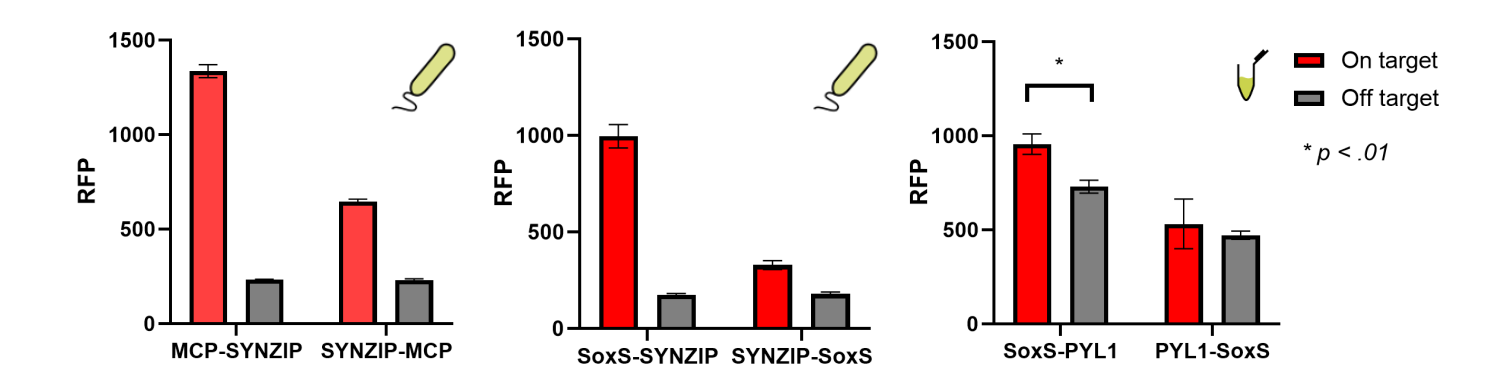


Figure S17: Fusion orientation preference for SYNZIP and ABI/PYL1

**Left, Middle:** MCP and SoxS fusion orientations were tested for the SYNZIP-CRISPRa system in *E. coli* using the J306 spacer at -81 bp from the TSS. The MCP test was done using SoxS-SYNZIP and the SoxS test was done using MCP-SYNZIP. **Right:** SoxS fusions were tested for the abscisic acid (ABA) CRISPRa system using MCP-ABI. The ABA constructs were tested in CFS using the R206 spacer at -81 bp from the TSS. ABA components were expressed at 5 nM. Off-target represents reactions containing a scRNA with no cognate target. Values represent the mean ± standard deviation of three technical replicates.

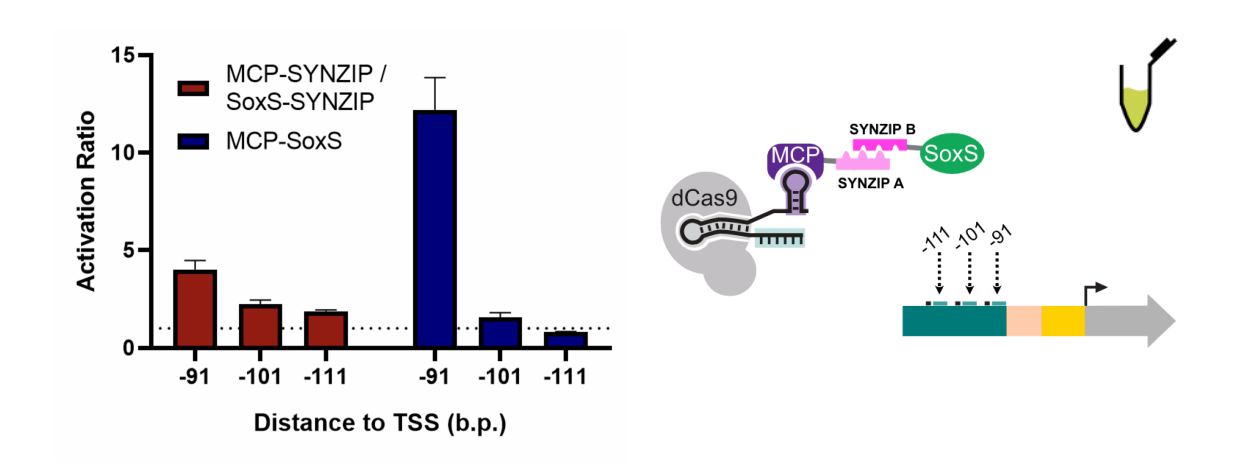


Figure S18: Dependence of SYNZIP-CRISPRa on distance to TSS

SYNZIP-CRISPRa and CRISPRa were tested at various target sites with increasing distance from the TSS in 10 bp intervals using a CRISPRa promoter with densely packed scRNA target sites. Plasmids expressing SYNZIP components are added at 5 nM each. Values represent the mean ± standard deviation of three technical replicates.

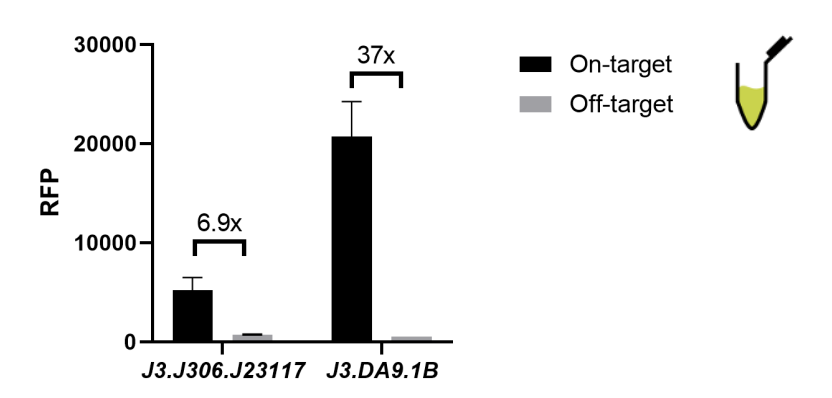


Figure S19: Improvements in SYNZIP-CRISPRa from engineered promoters

Comparison of SYNZIP-CRISPRa scRNA-dependent fold change with the previous synthetic promoter used to survey target sites and an engineered high dynamic range promoter. Off-target represents reactions containing a scRNA with no cognate target. In each reaction, the concentration of reporter DNA was 10 nM. SYNZIP components are added at 5 nM each. Reactions are background subtracted from a cell-free reaction containing no DNA. Values represent the mean ± standard deviation of three technical replicates.

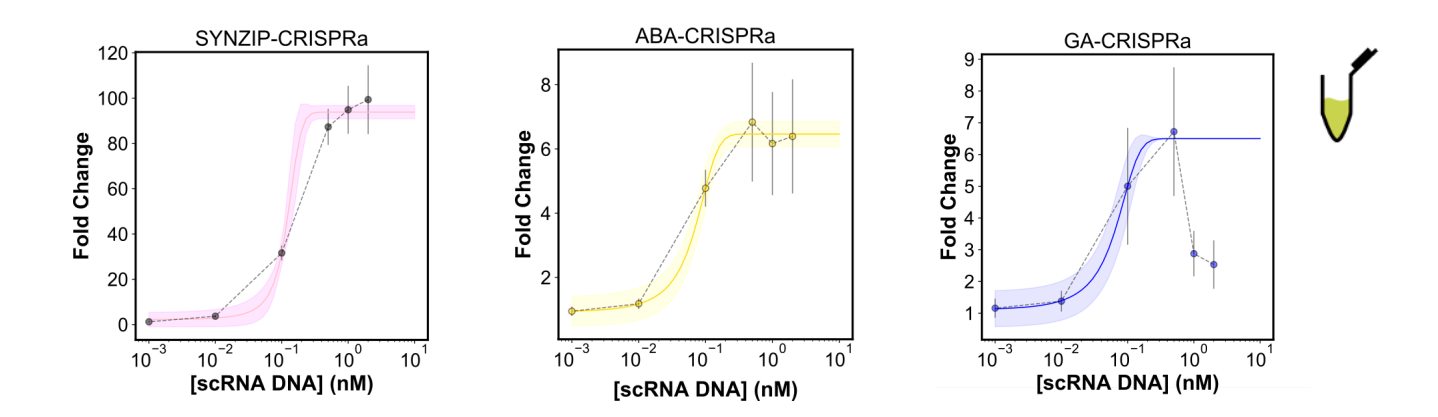


Figure S20: Conditional CRISPRa scRNA dose-response

scRNA-dose response curves were collected for conditional CRISPRa systems. scRNA concentrations were titrated between  $10^{-3}$  and  $10^1$  nM. Fold activation was calculated relative to the no scRNA condition. For all conditions, ABA is added at  $10~\mu M$  and GA is added at  $10^3~\mu M$ . SYNZIP-CRISPRa components were both added at 5~nM, MCP-ABI and SoxS-PYL1 were added at 5~and~10~nM respectively, and GA-CRISPRa components were both added at 10~nM. Colored lines indicate a logistic fit to the data. Values represent the mean  $\pm$  standard deviation of three technical replicates.

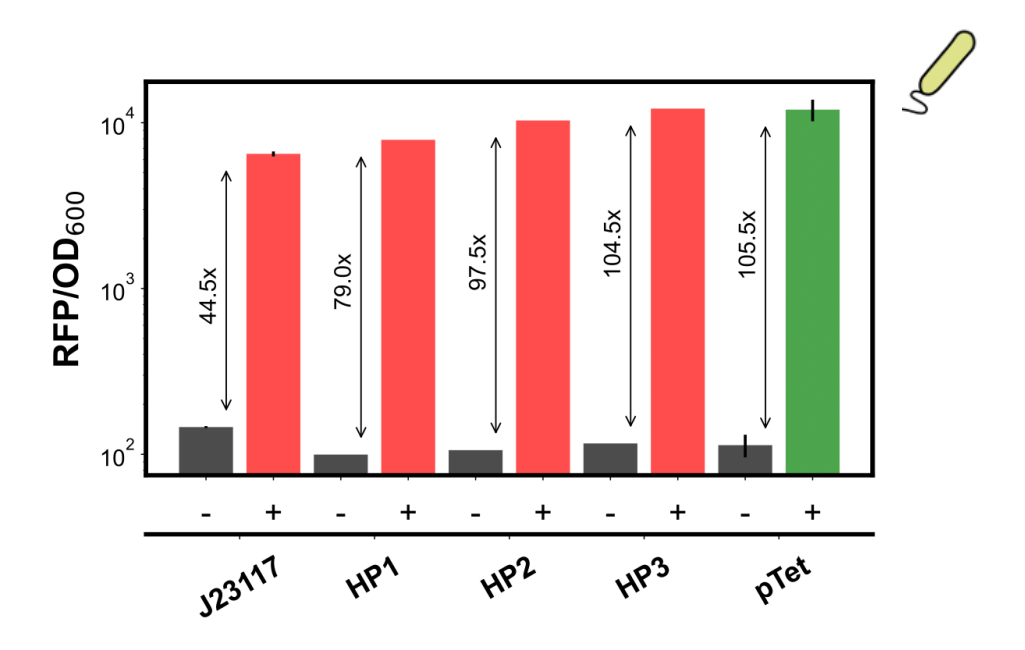


Figure S21: Comparison of CRISPRa promoters to pTet

Comparison of RFP expression levels of different CRISPRa promoters (red) to the pTet system (green). In both systems, RFP plasmid copy number and RBS remained constant. Basal expression level ("-") is measured with off-target scRNAs for the CRISPRa promoters, and 0 nM aTc for pTet. Activated expression level ("+") is measured with on-target scRNAs for the CRISPRa promoters, and 200 nM aTc for pTet. The J23117 and pTet values represent the mean ± standard deviation of three technical replicates, whereas HP1-3 values correspond to the individual variants from the sequential screen (Figure 2D).

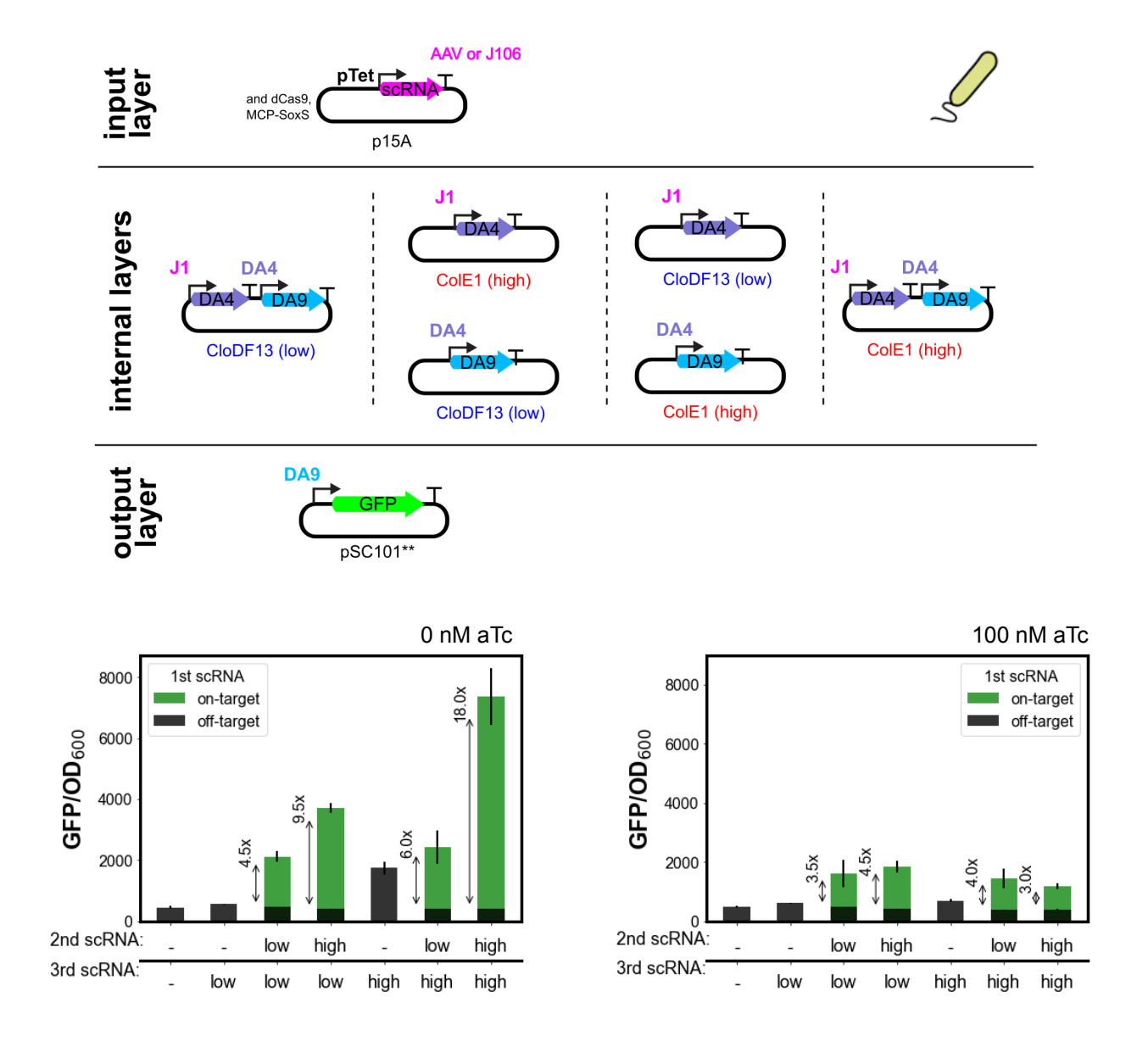


Figure S22: Three-layer activation cascades in E. coli

Three-layer activation cascades in *E. coli* with the input controlled by pTet and internal nodes expressed from different copy number plasmids. **Top:** Schematic of plasmids used for the different nodes. Input and output layers were kept constant across conditions, and the copy number of the plasmids encoding the two internal layers was varied between ColE1 (high copy) and CloDF13 (low copy). **Bottom, left:** GFP output for the different activation cascades at 0 nM aTc. Leak is minimized in the system when the third scRNA is expressed from a low copy number plasmid. Leak is also lowered when the second scRNA is present due to gRNA competition with the third scRNA.

Expressing the second scRNA from a high copy number resulted in higher fold-activation. **Bottom, right:** When induced with 100 nM aTc, cascade output is reduced, likely due to competition of the first scRNA with downstream scRNAs. Values represent the mean ± standard deviation of three technical replicates

# Supplementary Tables

Table S1: Promoters generated in this paper

Promoter	scRNA target	UP-element	Minimal Promoter	Basal	Activated
HP1_J3. DA9.2A		CCGGCGGCGCGG CTGCCGCGCGGCG	TTGACAGTTTTACGATGT GTTGGGATTGTGCTAGC	773.66 ± 123.99	289908.0 ± 22289.67
		CCGCGGGGCGCCG CTGCCGGGGGCGCG	TTGACACTTCCGGCACGA AAAGGGATTGTGCTAGC	690.33 ± 112.43	351826.66 ± 7551.20
HP3_J3. DA9.1B		CCGCGGGGCGCCG CTGCCGGGGGCGCG	TTGACGCCTCCTTCTTTC TTAGGGATTGTGCTAGC	153.33 ± 43.81	163114.33 ± 10141.27
J3.DA2. 1B		CCGCGGGGCGCCG CTGCCGGGGGCGCG	TTGACGCCTCCTTCTTTC TTAGGGATTGTGCTAGC	567.33 ± 20.21	380117.0 ± 73224.73
J3.DA3. 1B		CCGCGGGGCGCCG CTGCCGGGGGCGCG	TTGACGCCTCCTTCTTTC TTAGGGATTGTGCTAGC	595.0 ± 39.05	279047.33 ± 14991.68
J3.DA4. 1B		CCGCGGGGCGCCG CTGCCGGGGGCGCG	TTGACGCCTCCTTCTTTC TTAGGGATTGTGCTAGC	263.66 ± 9.18	332795.33 ± 7755.96
J3.DA6. 1B		CCGCGGGGCGCCG CTGCCGGGGGCGCG	TTGACGCCTCCTTCTTTC TTAGGGATTGTGCTAGC	370.66 ± 40.35	313809.33 ± 15988.97
J3.DA9. 1B		CCGCGGGGCGCCG CTGCCGGGGGCGCG	TTGACGCCTCCTTCTTTC TTAGGGATTGTGCTAGC	186.0 ± 79.92	224187.33 ± 20739.19
		CCGCGGGGCGCCG CTGCCGGGGGCGCG	TTGACGCCTCCTTCTTTC TTAGGGATTGTGCTAGC	425.33 ± 29.86	349136.66 ± 15853.45
EP1	-	TCGGTAGCCTTTA GTCCATG	TTGACGCTGTATTCAGGC AAAGGGATTGTGCTAGC	1053.66 ± 82.92	10081.91 ± 940.10
EP2	-	TCGGTAGCCTTTA GTCCATG	TTGACAGTGCGTACGCAG GGAGGGATTGTGCTAGC	6170.33 ± 113.42	117299.0 ± 5279.40
EP3	I	TCGGTAGCCTTTA GTCCATG	TTGACGGTGAAGAGTATC AGAGGGATTGTGCTAGC	3516.66 ± 217.243	120075.33 ± 7740.25
EP4	I	TCGGTAGCCTTTA GTCCATG	TTGACAGCTCAGTGAGTA GTAGGGATTGTGCTAGC	5079.66 ± 417.91	66449.16 ± 6693.89
R2.E8. R206	(-81) TCGGCTCACT TATGCACGGC		TTGACAAAGCTATGGCCG GCAGGGATTGTCACAGC	250.67 ± 21.2	6287.67 ± 670.47
R2.E8. R208	(-91) TCCCTGACCC TCGGCTCACT	CCGGCCCCCCG CTGCCGCGGGCCG	TTGACAAAGCTATGGCCG GCAGGGATTGTCACAGC	250.67 ± 21.2	3056.67 ± 414.77
R2.E8. R210	(-101) ACCCTTTCCT TCCCTGACCC		TTGACAAAGCTATGGCCG GCAGGGATTGTCACAGC	250.67 ± 21.2	394.67 ± 56.89
R2.E8. R212	(-111) TTCCTCTCCT ACCCTTTCCT		TTGACAAAGCTATGGCCG GCAGGGATTGTCACAGC	250.67 ± 21.2	206.67 ± 4.51

Table S2: Dimerization domain affinity

Domain	K <sub>d</sub>	Method of measurement	Ref
MS2:MCP	.0033uM	Filter binding assay	(Carey et al., 1983)
SYNZIP5: SYNZIP6	<.015uM	Fluorescence polarization	(Thompson et al., 2012)
PYL1:ABA	1 - 52uM	Isothermal titration calorimetry, Surface plasmon resonance	(Dupeux et al., 2011; Miyazono et al., 2009)
PYL1:ABA:ABI	.030uM	Isothermal titration calorimetry	(Dupeux et al., 2011)
GID1:GA	.2 - 4uM	Radioactivity assay with isotopically labeled GA, <i>In vitro</i> FRET binding assay, Surface plasmon resonance	(Miyamoto et al., 2012; Ueguchi-Tanaka et al., 2005; Yoshida et al., 2018)
GAI:GA:GID1	.180uM	Surface plasmon resonance	(Yoshida et al., 2018)

Table S3: Primers for promoter mutagenesis

Minimal Promoter	
oMP1	CGATTATAGATTGACRGCTAGCTCAGTCCTDGNNAYNGTGCTAGCGAATTCATTAAAG AG
oMP2	CGATTATAGATTGACTTGACANNNNNNNNNNNNNNNAGGGATTGTNNNAGCGAATTCAT TAAAGAG
oMP3_S2	CGCTAGCACAATCCCWNNNNNNSNNNNMRSYGTCAAGCCGGGAGAGCTGGTTCCATTG CGATTGCAGCCACGTGTGAGAGTT
oMP3_S2	CGCTAGCACAATCCCWNNNNNNSNNNNMRSYGTCAACGCCGCCCGGCAGCCGGCGGGGGGGGGGGGGGGG
oMP3_S2	CGCTAGCACAATCCCWNNNNNNSNNNNMRSYGTCAACGCCGCGGCGGCAGCCGCCG

	CCGGTGCAGCCACGTGTGAGAGTT
LID alamant	
UP-element	
oUP1	GCTAGCTGTCAAYNYTTTTTTAAAAAWWWWWTNNNNNTTGTGTCCAGAACGCTCCGT
	AG
oUP2	GCTAGCTGTCAAWWWWWWWWWWWWWWWWWWWWWWWWWWWTTGTGTCCAGAACGCTCCGT
001 2	AG
oUP3	GCTAGCTGTCAAWWWHDWHDWHDWHDWWDWHWWHDWWWTTGTGTCCAGAACGCTCCGT
0013	AG
oUP4	GCTAGCTGTCAANNNNNNNNNNNNNNNNNNNNNNNTTGTGTCCAGAACGCTCCGT
00F4	AG
aLIDE	GCTAGCTGTCAABBBBSSSSBBNNNNBSSSBSSSBSSSTTGTGTCCAGAACGCTCCGT
oUP5	AG
oUP6	GCTAGCTGTCAASSSSSSSSSSSSSSSSSSSSSSSTTGTGTCCAGAACGCTCCGT
0000	AG
-LID0 04	GCTAGCTGTCAASSSSSSSSSSSSSSSSSSSSSSSTGCAGCCACGTGTGAGAGTT
oUP6_S1	AG
scRNA	
target site	
	GCTCGTCTCCTCACTTCTCCTWWWWWWWWWWWWWWWWWWW
oTS1	CGCGGGCCGTTGACAGCTCAGTCCTAGG
	GCTCGTCTCCTCACTTCTCCTNNNNNNNNNNNNNNNNNNN
oTS2	CGCGGGCCGTTGACAGCTCAGTCCTAGG
	GCTCGTCTCCTCACTTCTCCTSSSSSSSSSSSSSSSSSSS
oTS3	CGCGGGCCGTTGACAGCTCAGTCCTAGG
EL222	
promoter	
oMPE	CCTCTTTAATGAATTCGCTNNNACAATCCCWNNNNNNSNNNNMRSYGTCAACATGGAC
	TAAAGGCTACCTATAAA

## Table S4: Plasmids used in this work

Plasmid	J-Pro moter	scRNA target		Minimal Promoter	RBS	RBS CDS		Terminator	res *	ori **
pJF143. J3	J3	J306	J3	J23117	Bujard	mRFP1	Х	dbl term	Α	S

pCK389. gRNA	Х	X	X	Sp.Cas9, pTet, J23119	, Bujard, X	Sp.Cas9, MCP-Sox S (R93A,S1 01A)	J306, AAV, DA9	Dbl term, BBa_B1002, TrrnB	С	Α
pJF182. gRNA	Х	×	X	Sp.Cas9, J23107, J23119	, Bujard, X	Sp.Cas9, MCP-Sox S (R93A,S1 01A)	J306, AAV	dbl term, BBa_B1002, TrrnB	С	А
pDA010. 188	Х	Х	х	J23107	Bujard	Sp. dCas9	X	ECK120033 736	Α	Е
pRC029	x	X	Х	J23107	Bujard	MCP-Sox S (R93A,S1 01A)	Х	ECK120033 736	Α	E
pRC011	Х	X	Х	J23107	Bujard	MCP-SY NZIP6	Х	ECK120033 736	Α	Е
pRC012	Х	Х	Х	J23107	Bujard	SoxS-SY NZIP5	Х	ECK120033 736	Α	Е
pRC025	Х	X	Х	J23107	Bujard	MCP-ABI	Х	ECK120033 736	Α	Е
pRC027	Х	X	Х	J23107	Bujard	SoxS-PY L1	Х	ECK120033 736	Α	Е
pRC042	Х	X	Х	J23107	Bujard	MCP-GAI	Х	ECK120033 736	Α	Е
pRC043	Х	X	Х	J23107	Bujard	SoxS-GI D1	Х	ECK120033 736	Α	Е
pWS025 .BLNNN- RFP	Х	Х	X, EL222_Bi nding_re gion	J23119, N	BBa_B0 034, Bujard	EL222, mRFP1	Х	BBa_B0015_ dblT, dbl term	Α	S

pDA010. EL222	Х	Х	х	J23106	BBa_B0 034	EL222	X	BBa_B0015_ dblT	Α	E
pDA040. BLD7-m RFP	х	X	EL222_Bi nding_re gion	D7	X	mRFP1	X	ECK120033 736	Α	E
pDA040. BLD7-D A9	х	X	EL222_Bi nding_re gion	D7	X	X	DA9	ECK120033 736	Α	E
pDA040. BLD7-R R2	Х	Х	EL222_Bi nding_re gion	D7	x	X	RR2	ECK120033 736	Α	E
pDA303	J3	DA9	1	В	Bujard	mRFP1	Х	ECK120033 736	Α	Е
pDA304	J3	DA2	1	В	Bujard	mRFP1	Х	ECK120033 736	Α	Е
pDA305	J3	DA3	1	В	Bujard	mRFP1	Х	ECK120033 736	Α	Е
pDA306	J3	DA4	1	В	Bujard	mRFP1	Х	ECK120033 736	Α	Е
pDA307	J3	DA6	1	В	Bujard	mRFP1	Х	ECK120033 736	Α	Е
pDA309	J3	DA10	1	В	Bujard	mRFP1	Х	ECK120033 736	Α	Е
pDA310	J3	DA9	1	В	Х	Х	DA2	ECK120033 736	Α	Е
pDA311	J3	DA9	1	В	X	Х	DA3	ECK120033 736	Α	Е
pDA312	J3	DA9	1	В	X	Х	DA4	ECK120033 736	Α	Е
pDA313	J3	DA9	1	В	×	х	DA6	ECK120033 736	Α	Е

pDA314	J3	DA9	1	В	х	Х	DA8	ECK120033 736	Α	Е
pDA315	J3	DA2	1	В	х	Х	DA10	ECK120033 736	Α	Е
pDA316	J3	DA3	1	В	х	Х	DA10	ECK120033 736	Α	Е
pDA317	J3	DA4	1	В	Х	Х	DA10	ECK120033 736	Α	Е
pDA318	J3	DA6	1	В	Х	Х	DA10	ECK120033 736	Α	Е
pDA319	J3	DA8	1	В	Х	Х	DA10	ECK120033 736	Α	Е
pDA320	J3	DA9	1	В	Х	Х	DA2	ECK120033 736	Α	Е
pDA321	J3	DA2	1	В	Х	Х	DA3	ECK120033 736	Α	Е
pDA322	J3	DA3	1	В	Х	Х	DA4	ECK120033 736	Α	Е
pDA323	J3	DA4	1	В	Х	Х	DA6	ECK120033 736	Α	Е
pDA324	J3	DA6	1	В	Х	Х	DA8	ECK120033 736	Α	Е
pDA325	J3	DA8	1	В	Х	Х	DA10	ECK120033 736	Α	Е
pRC014. (0-4)	R2	R206 (-81), R208 (-91), R210 (-101), R212 (-111)	E	8	Bujard	mRFP	x	ECK120033 736	Α	E

pCK956. gRNA	Х	x	Х	J23107, J23107, pTet	Bujard, Bujard, X	Sp.Cas9, MCP-Sox S (R93A,S1 01A)	J106, AAV	Dbl term, BBa_B1002, TrrnB	С	Α
pDA506. gRNA	X	gRNA	1	В	Bujard	sfGFP	X	dbl term	K	s
pCK957	Х	J106	1	В	Х	X	DA4	Sht TermA	C, S	E, D
pCK958	Х	J106, DA4	1	В	Х	X	DA4, DA9	Sht TermA	C, S	E, D
pCK960	Х	DA4	1	В	Х	х	DA9	Sht TermA	C, S	E, D

Table S5: Deep cascade concentrations

Cascade/ Plasmid	D1 -	D1 +	D2 -	D2 +	D3 -	D3 +	D4 -	D4 +	D5 -	D5 +	D6 -	D6 +
pDA010. 188	4	4	4	4	4	4	4	4	4	4	4	4
pRC029	4	4	4	4	4	4	4	4	4	4	4	4
pBT009.J1	0	.015	0	.015	0	.015	0	.015	0	.015	0	.015

<sup>\*</sup>Resistance marker: C stands for chloramphenicol, A stands for ampicillin, S stands for spectinomycin, K stands for kanamycin

<sup>\*\*</sup>Origin of replication:. E stands for ColE1, A stands for p15A, and S stands for sc101\*\*, and D stand for CloDF13

.119.DA4												
pDA332			0.2	0.2	0.04	0.04	0.04	0.04	0.04	0.04	0.04	0.04
pDA320					0.2	0.2	0.2	0.2	0.2	0.2	0.2	0.2
pDA315							0.34	0.34	0.34	0.34	0.34	0.34
pDA335									0.13	0.13	0.13	0.13
pDA336											.093	.093
pDA306	10	10										
pDA303			10	10								
pDA304					10	10						
pDA309							10	10				
pDA307									10	10		
pDA305											10	10

All plasmid concentrations are in nM.

## Table S6: Component sequences

pRC011: J23107.Buj.MCP-SYNZIP6

tttacggctagctcagccctaggtattatgctagcGAATTCATTAAAGAGGAGAAAGGTACCatggggccc
gcttctaactttactcagttcgttctcgtcgacaatggcggaactggcgacgtgactgtcgcccaagcaacttcgctaacgg
gatcgctgaatggatcagctctaactcgcgttcacaggcttacaaagtaacctgtagcgttcgtcagagctctgcgcagaat
cgcaaatacaccatcaaagtcgaggtgcctaaaggcgcctggcgttcgtacttaaatatggaactaaccattccaattttcg
ccacgaattccgactgcgagcttattgttaaggcaatgcaaggtctcctaaaagatggaaacccgattccctcagcaatcg
cagcaaactccggcatctacGGTGGCGGAGGTAGCCAAAAAGTTGCGCAGCTGAAAAACCG
TGTTGCGTACAAACTGAAAGAAAACGCGAAGCTGGAGAACATCGTGGCGCGTCTG
GAAAACGACAATGCGAACCTGGAGAAAAGACATTGCGAATCTCGAAAAAGGACATCGC
AAATCTGGAACGTGACGTTGCGCGTTAAGCGGCCGCcacgcaaaaaaaccccgcttcggcggg
gttttttcgc

pRC012: J23107.Buj.SoxS-SYNZIP5

tttacggctagctcagccctaggtattatgctagcGAATTCATTAAAGAGGAGAAAGGTACCATGTCC
CATCAGAAAATTATTCAGGATCTTATCGCATGGATTGACGAGCATATTGACCAGCCGC
TTAACATTGATGTAGTCGCAAAAAAAATCAGGCTATTCAAAGTGGTACTTGCAACGAAT
GTTCCGCACGGTGACGCATCAGACGCTTGGCGATTACATTCGCCAACGCCGCCTG
TTACTGGCCGCCGTTGAGTTGCGCACCACCGAGCGTCCGATTTTTGATATCGCAAT
GGACCTGGGTTATGTCTCGCAGCAGACCTTCTCCCGCGTTTTCGCGCGGCAGTTT
GATCGCACTCCCGCGGATTATCGCCACCGCCTG
GGTGGCGAGGTAGCAACCCG
TTAAAGAACTGAAAAACTACATCCAGGAGCTGGAAGAGCGTAACGCTGAACTCAAA
AACCTGAAGGAACACCTGAAATTCGCAAAAGCGGAACTGGAATTCGAACTGGCGG
CTCACAAATTCGAGTAAGGCGCCCCCCacgcaaaaaaaccccgcttcggcggggttttttcgc

pRC025: J23107.Buj.MCP-ABI

tttacggctagctcagccctaggtattatgctagcGAATTCATTAAAGAGGAGAAAGGTACCatggggccc gcttctaactttactcagttcgttctcgtcgacaatggcggaactggcgacgtgactgtcgccccaagcaacttcgctaacgg gatcgctgaatggatcagctctaactcgcgttcacaggcttacaaagtaacctgtagcgttcgtcagagctctgcgcagaat cgcaaatacaccatcaaagtcgaggtgcctaaaggcgcctggcgttcgtacttaaatatggaactaaccattccaattttcg ccacgaattccgactgcgagcttattgttaaggcaatgcaaggtctcctaaaagatggaaacccgattccctcagcaatcg cagcaaactccggcatctac GGTGGCGGAGGTAGCACGCGTGTGCCTTTGTATGGTTTTACT TCGATTTGTGGAAGAAGACCTGAGATGGAAGcTGCTGTTTCGACTATACCAAGATTC CTTCAATCTTCCTCTGGTTCGATGTTAGATGGTCGGTTTGATCCTCAATCCGCCGCT CATTTCTTCGGTGTTTACGACGGCCATGGCGGTTCTCAGGTAGCGAACTATTGTAGA GAGAGGATGCATTTGGCTTTGGCGGAGGAGATAGCTAAGGAGAAACCGATGCTCT GCGATGGTGATACGTGGCTGGAGAAGTGGAAGAAGCTCTTTTCAACTCGTTCCTG AGAGTTGACTCGGAGATTGAGTCAGTTGCGCCGGAGACGGTTGGGTCAACGTCGG TGGTTGCCGTTTTTCCCGTCTCACATCTTCGTCGCTAACTGCGGTGACTCTAGA GCCGTTCTTTGCCGCGGCAAAACTGCACTTCCATTATCCGTTGACCATAAACCGGAT AGAGAAGATGAAGCTGCGAGGATTGAAGCCGCAGGAGGGAAAGTGATTCAGTGGA TGAAACCATCCATCATTCCTGATCCGGAAGTGACGGCTGTGAAGAGAGTAAAAGAA AGCGTGTGAGATGGCAAGGAAGCGGATTCTCTTGTGGCACAAGAAAAACGCGGTG CGGCGATGTCCGCGGCTGAGTATTTGTCAAAGCTGGCGATACAGAGAGGAAGCAA AGACAACATAAGTGTGGTGGTTGATTTGAAGTAAGGCGCGCCCacgcaaaaaaccc cgcttcggcggggttttttcgc

pRC027: J23107.Buj.SoxS-PYL1

tttacggctagctcagccctaggtattatgctagcGAATTCATTAAAGAGGAGAAAGGTACCATGTCC
CATCAGAAAATTATTCAGGATCTTATCGCATGGATTGACGAGCATATTGACCAGCCGC
TTAACATTGATGTAGTCGCAAAAAAATCAGGCTATTCAAAGTGGTACTTGCAACGAAT
GTTCCGCACGGTGACGCATCAGACGCTTGGCGATTACATTCGCCAACGCCGCCTG
TTACTGGCCGCCGTTGAGTTGCGCACCACCGAGCGTCCGATTTTTGATATCGCAAT
GGACCTGGGTTATGTCTCGCAGCAGACCTTCTCCCGCGTTTTTCGCGCGGCAGTTTT

pRC042: J23107.Buj.MCP-GAI

tttacggctagctcagccctaggtattatgctagcGAATTCATTAAAGAGGAGAAAGGTACCatggggccc
gcttctaactttactcagttcgttctcgtcgacaatggcggaactggcgacgtgactgtcgccccaagcaacttcgctaacgg
gatcgctgaatggatcagctctaactcgcgttcacaggcttacaaagtaacctgtagcgttcgtcagagctctgcgcagaat
cgcaaatacaccatcaaagtcgaggtgcctaaaggcgcctggcgttcgtacttaaatatggaactaaccattccaattttcg
ccacgaattccgactgcgagcttattgttaaggcaatgcaaggtctcctaaaaagatggaaacccgattccctcagcaatcg
cagcaaactccggcatctacGGTGGCGGAGGTAGCATGAAGCGCGATCATCATCACCACCA
CCACCAGGATAAAAAAGACGATGATGATGAATGAGGAAGATGATGGAAACGGGATGT
GCTCAGAAATTGGAGCAGTTAGAAGTAATGATGAGTAACGTTCAAGAAGATGATCTT
TCACAGTTAGCGACCGAAACTGTCCACTACAACCCTGCTGAGCTTTACACTTGGTT
GGACTCCATGCTTACCGATCTTAACtgacgcaaaaaaaccccgcttcggcggggttttttcgc

pRC043: J23107.Buj.SoxS-GID1

GATCGCACTCCCGCGGATTATCGCCACCGCCTGGGTGGCGGAGGTAGCATGGCAG CCTCCGACGAGGTAAATCTTATTGAGAGTCGTACCGTCGTTCCCTTGAATACTTGGG TGTTGATCTCGAATTTCAAGGTCGCGTACAATATCTTACGCCGCCCGGATGGAACCT TTAACCGTCACCTTGCAGAATATCTGGACCGCAAAGTTACAGCAAATGCTAATCCAG TTGACGGTGTTTTCAGTTTTGACGTGCTGATTGATCGCCGTATCAACCTTCTGTCCC GAAAAACCAGTGGATGGGGACATTGTCCCTGTCATCCTTTTTTTCCACGGGGGGTC GTTCGCCCACTCGTCCGCCAACAGTGCGATCTACGACACTTTATGTCGTCGTCTTG TCGGTCTTTGCAAATGCGTGGTCGTTTCCGTGAATTACCGTCGCGCTCCGGAGAAC CCCTACCCATGTGCCTACGACGACGGATGGATTGCGTTAAATTGGGTTAATTCACGT AGCTGGCTGAAAAGCAAGAAGATTCGAAGGTTCACATTTTTTTAGCGGGCGATTCT TCAGGAGGGAACATCGCTCATAATGTCGCATTGCGTGCAGGAGAGTCTGGCATCGA TGTTCTGGGCAACATTTTACTGAACCCGATGTTTGGGGGGAACGAGCGCACAGAAT CCGAGAAAAGCTTGGACGGGAAGTATTTCGTGACTGTTCGCGATCGTGACTGGTAT TGGAAAGCGTTCTTGCCCGAGGGAGAGGACCGCGAGCACCCCGCATGCAACCCC TTTTCACCTCGCGGAAAATCGCTGGAGGGGGTCAGTTTCCCAAAATCTTTAGTCGT AGTAGCTGGCCTGGATCTGATCCGTGATTGGCAACTTGCGTATGCTGAAGGCCTTA AGAAGGCTGGTCAAGAAGTAAAGCTGATGCACTTAGAGAAAGCTACGGTTGGCTTT TTAATGCGGAATGCtgacgcaaaaaaccccgcttcggcggggttttttcgc

pDA010.EL222: J23106. BBaB0034.EL222

TTTACGCTAGCTCAGTCCTAGGTATAGTGCTAGCCTAGAGAAAGAGGAGAAATACT
AGATGTTGGATATGGGACAAGATCGGCCGATCGATGGAAGTGGGGCACCCGGGGC
AGACGACACACGCGTTGAGGTGCAACCGCCGGCGCAGTGGGTCCTCGACCTGAT
CGAGGCCAGCCCGATCGCATCGGTCGTGTCCGATCCGCGTCTCGCCGACAATCCG
CTGATCGCCATCAACCAGGCCTTCACCGACCTGACCGGCTATTCCGAAGAAGAATG
CGTCGGCCGCAATTGCCGATTCCTGGCAGGTTCCGGCACCGAGCCGTGGCTGAC
CGACAAGATCCGCCAAGGCGTGCGCGAGCACAAGCCGGTGCTGACTC
GAACTACAAGAAGGACGCACGCCGTTCCCGCAATGCCGTGCTCGACCCGATC
TACGATGACGACGACGACGACCTTCTCTATTTCCTCGGCAGCCAGGTCGAAGTCGACGA

CGACCAGCCCAACATGGGCATGGCGCGCGCGAACGCGCCGCGGAAATGCTCAA
GACGCTGTCGCCGCGCCAGCTCGAGGTTACGACGCTGGTGGCATCGGGCTTGCG
CAACAAGGAAGTGGCGGCCCGGCTCGGCCTGTCGGAGAAAACCGTCAAGATGCA
CCGCGGGCTGGTGATGGAAAAGCTCAACCTGAAGACCAGCGCCGATCTGGTGCG
CATTGCCGTCGAAGCCGGAATCTAAGGATCCAAACTCGAGTAAGGATCTCCAGGCA
TCAAATAAAACGAAAGGCTCAGTCGAAAGACTGGGCCTTTCGTTTTTT
GTCGGTGAACGCTCTCTACTAGAGTCACACTGGCTCACCTTCGGGTGGGCCTTTCT
GCGTTTATA

Table S7: ANOVA analysis of combinatorial promoter screens

	Sum of Squares	Degrees of Freedom	F Value	p Value
Minimal Promoter	23155.9	3	9.5	1.2e-4
UP-Element	315527.0	3	129.7	5.5e-18
Minimal Promoter & UP-Element	53678.2	9	7.4	1.0e-5
Residual	25954.2	32	-	-

## **Supplementary Methods**

## Methods S1: Plasmid Preparation for Cell-Free System

Plasmids intended for use in CFS were grown in culture volumes ~20 mL to ensure adequate yields for multiple cell-free reactions and were further purified using a PCR purification kit (Invitrogen PureLink, Cat. K310001), eluted into nuclease-free water. Plasmid concentrations were quantified via spectrophotometry (Nanodrop 2000c, Cat. ND-2000C).

## Methods S2: CFS Blue-light CRISPRa/i modeling

The model was implemented using the text-based model definition language Antimony for Python 3.7. We introduced blue-light regulation as a piecewise function that modulates transcription of the sgRNA required for CRISPRi. We used linear functions of different slopes to capture the fast dimerization of the EL222 protein and binding to the DNA upon blight exposure as well as the slow unbinding in the absence of blue-light. Specifically, we the sgRNA basal transcription constant is modified with the following function:

$$\frac{k_{\max}}{t_{oN}} \Big( t - t_{delay} \Big) \ \ if \ \ t_{delay} < t < t_{delay} + t_{oN}$$
 
$$k_{\max} \ if \ \ t_{delay} + t_{oN} < t < t_{delay} + t_{oN} + t_{expose}$$
 
$$\frac{-k_{\max}}{t_{oFF}} \Big( t - (t_{delay} + t_{oN} + t_{expose}) \ \ if \ \ t_{delay} + t_{oN} + t_{expose} < t < t_{delay} + t_{oN} + t_{expose} + t_{oFF}$$

Where  $k_{max}$  represents the transcription rate constant when EL222 is fully bound to the promoter, and  $t_{delay}$ ,  $t_{oN}$ ,  $t_{expose}$ , and  $t_{oFF}$  represent the time delay for light exposure, the time for

EL222 dimerization and binding, the exposure time to light, and the time for EL222 unbinding upon removing the light source, respectively.

## Methods S3: Quantification and Statistical Analysis

## E. coli data analysis:

Dynamic range:

Dynamic range was calculated as the ratio of measured RFP outputs without induction (0 nM aTc, or dark) and with induction (200nM aTc, or light):

$$DR = \frac{B^{\alpha_1} - B^0}{B^{\alpha_2} - B^0}$$

where:

*B* is RFP/OD<sub>600</sub> measured at endpoint  $\alpha_1$  is activated expression, with induction  $\alpha_2$  is basal expression, without induction  $\alpha_3$  is no RFP expression

#### Pareto optimality:

To identify the best-performing promoter variants belonging to the Pareto front, we compared the basal and activated RFP expression levels of each variant to all other variants. A variant belongs to the Pareto front if no other variant had both lower basal and higher activated expression levels:

$$v_{o} \in P(V)$$
 if there is no  $v$  such that  $(v^{a} > v_{o}^{a} \& v^{b} < v_{o}^{b})$  for all  $v \in V$ 

where:

V is the set of all promoter variants

 $\boldsymbol{v_{_{o}}}$  is a variant in  $\boldsymbol{V}$ 

 $v_{_{o}}^{^{a}}$ ,  $v_{_{o}}^{^{b}}$  are the activated and basal expression levels of said variant

P(V) is the set of promoter variants belonging to the Pareto front

## Cell-free data analysis

Production Rate:

Throughout this work, we define production rate as:

$$\overset{\cdot}{B}^{\alpha}(t) = \frac{dB^{\alpha}}{dt} = \frac{B^{\alpha}(t+30) - B^{\alpha}(t)}{30}$$

where:

B is the measured RFP

 $\alpha$  specifies the circuit topology and relevant plasmid concentrations

Relative Production Rates:

Relative production rates of CRISPRa mediated outputs were calculated as the ratio of CRISPRa mediated production rates divided by unregulated production rates. For CRISPRa the contribution due to unregulated basal expression was subtracted from measured output levels due to CRISPRa. This was done to isolate the timing of CRISPRa mediated gene expression from the comparatively early contribution of basal expression, and to allow observation of CRISPRa mediated gene expression dynamics under conditions where basal expression of reporter constructs dominates. Throughout this work, relative production rates are abbreviated as Rel. RFP Prod. Rate and are calculated as:

$$\dot{B}_{\Gamma}^{\alpha}(t) = \frac{\dot{B}(t) - \dot{B}(t)}{\dot{B}(t)}$$

where:

α is a specific CRISPRa/i circuit

 $\Gamma$  is constitutive expression

Fold change:

Fold change was calculated as the ratio of RFP values generated by CRISPRa in the presence of input scRNA compared to RFP values generated in the absence of input scRNA.

$$FC^{\alpha}(y) = \frac{B^{\alpha+}(t) - B^{\Gamma}(t)}{B^{\alpha-}(t) - B^{\Gamma}(t)}$$

where:

 $\alpha$  + is CRISPRa with y nM input scRNA

 $\alpha$  – is CRISPRa without input scRNA

 $\Gamma$  is constitutive expression

Time to maximum expression rate:

To calculate the time to maximum expression rate, the contribution due to unregulated basal expression was subtracted from measured RFP levels due to CRISPRa. This was done to isolate the timing of CRISPRa mediated gene expression from the comparatively early contribution of leak, and to allow observation of CRISPRa mediated gene expression dynamics under conditions where basal expression of reporter constructs dominates. The time to maximum expression is denoted as  $t_{max}$ .

$$t = t_{max} when B_{\Gamma}^{\alpha}(t) = max(B_{\Gamma}^{\alpha}(t))$$

where:

α is a specific CRISPRa/i circuit

 $\Gamma$  is constitutive expression

Change in time to maximum expression rate ( $\Delta t_{max}$ ) is calculated by finding the difference in time to reach maximum production rate between the with and without input conditions.

$$\Delta t_{max} = t_{max}^{\alpha +} - t_{max}^{\alpha -}$$

Signal propagation efficiency:

Propagation efficiency of the CRISPRa cascade in CFS was calculated as the maximum fold change in cascade output ± input divided by the fold change provided by CRISPRa in the input layer at the same time point.

propagation = 
$$100 \cdot \frac{max(FC^{\alpha}(y))}{FC^{\beta}(y)}$$

where:

 $\alpha$  is CRISPRa cascade with y nM of scRNAs  $\beta$  is CRISPRa with y nM of scRNAs

Signal delay:

Signal delay is calculated as the difference in time to reach the maximum fold change of the cascade between the cascade output and input layer.

$$t^{\alpha} = t_{max}^{\alpha} FC \text{ when } FC^{\alpha}(y) = max(FC^{\alpha}(y))$$

$$t^{\beta} = t_{max}^{\beta} FC \text{ when } FC^{\beta}(y) = max(FC^{\alpha}(y))$$

$$delay = t_{max}^{\beta}FC - t_{max}^{\alpha}FC$$

where:

 $\alpha$  is CRISPRa cascade with y nM of scRNAs  $\beta$  is CRISPRa with y nM of scRNAs

## Methods S4: Relationship between signal delay and signal propagation

We define fraction of signal propagation at the *nth* node to be the product of the fraction of signal propagated at the previous nodes, namely:

$$fSP_n = \prod_{i}^{n} fSP_i$$

where the fraction of signal propagated by each node i is a function of the characteristic relative fold-change of node i, as well as the time of the reaction at which the signal propagates through node i:

$$fSP_i = rFC_i \cdot e^{\frac{-(\theta_i + t_o)}{\tau}}$$

where  $t_o$  is the reaction boot up time, and  $\tau$  is the characteristic time of the system. While seemingly simple, the exponential term accounts for the complex dynamics of cell-free expression and gRNA competition, and favors expression from earlier nodes.

The time of the reaction at which the signal propagates through the *nth* node can be estimated based on the fraction of the signal propagated through the *nth* node and the relative lifetime of the reaction:

$$\theta_n = rLT \cdot (1 - fSP_n)$$

where the relative lifetime of the reaction is the difference between the time to maximum fold activation of a one-layer cascade and the end of the reaction. With these equations and the characteristic relative fold-change of each node, both the signal delay and probation can be calculated iteratively.

Based on kinetic data, we set  $t_o$  and rLT to be ~2 hrs and ~5 hrs, respectively. In order to estimate  $\tau$ , we fit the model to empirical signal propagation and delay data by minimizing the sum of residuals using the Nelder-Mead algorithm.

## Methods S5: Cell-Free Gene Expression Reaction

Cell-free gene expression reactions were assembled on ice from the CFS and purified DNA. A master mix with common plasmids across reactions was prepared, and 1.5 µL per reaction allocated into PCR tubes. Plasmids which were varied across reactions were added in the remaining 1 µL. For reactions containing ABA (Sigma, A4906) or GA, .1 µL of the small molecules were added alongside the plasmids. For reactions involving more than 5 plasmids, plasmids were mixed with an acoustic liquid handler robot (Echo Labcyte 525). The CFS was pipette mixed and added to each PCR tube in 7.5 µL for a final volume of 10 µL. PCR tubes were vortexed, spun-down using a mini benchtop centrifuge, and placed on ice. Triplicates of 2.5 µL for each reaction were pipetted into individual wells of a 96-well V-bottom plate (Costar, Cat. 3363). The plate was sealed (Costar, Cat. 3080) and analyzed on a BioTek Synergy HTX plate reader at 29 °C. mRFP1 fluorescence (ex. 540 nm, em. 600 nm) of cell-free reactions were measured every 10 min from the bottom of the plate. All reactions were run in batch mode.

#### Methods S6: Plasmid and Library Construction

All PCR amplification of plasmids and fragments used Phusion DNA polymerase in GC buffer. Primers were synthesized by IDT and resuspended into nuclease-free water. All PCR reactions were treated with DpnI for longer than 1 hour and purified using Qiagen gel extraction kits. Plasmid assembly was achieved using 5X In-Fusion HD mastermix (Takara).

Assembled plasmids and libraries were transformed into chemically competent NEB Turbo *E. coli* and plated onto LB-agar plates with either 100 µg/mL carbenicillin or 25 µg/mL chloramphenicol. Transformed cells were grown overnight ~16 hours at 37 °C.

Single colonies were picked from plates and grown overnight in LB shaking at 37 °C with appropriate concentrations of relevant antibiotics.

## Methods S7: Optogenetic setup

The samples were placed at 37 °C or 29 °C in an incubator (Thermo Forma Orbital Shaker, Model #435) with the illumination source placed atop the incubator and irradiating inwards. The distance between the illumination source and the *E. coli* deepwell plates was 14 cm. CFS reactions were placed inside the incubator at 29 °C at a distance of 6 cm with the bottom of the wells facing the illumination source. In both cases, the dark conditions were kept inside a cardboard box inside the incubator. Endpoint plate reader measurements were conducted using a BioTek Synergy HTX.

## Methods S8: E. coli experiments culturing and quantification conditions

Transformed *E. coli* were outgrown for 1 hour shaking at 37 °C and plated onto LB-agar with carbenicillin and chloramphenicol. Plates were grown overnight at 37 °C. Experiments were conducted by picking three individual colonies into 400 µL Teknova EZ-RDM with 0.2% glucose and appropriate antibiotics in 96 well plates, covering with breathable membrane (Breathe Easier cat# Z763624) and shaking overnight at 37 °C at 1200 RPM on a Heidolph Titramax 1000. For inducible experiments, overnight cultures are subsequently diluted 1:40 into a fresh plate of EZ-RDM and supplemented with appropriate concentrations of aTc. Plate reader measurements were conducted using a BioTek Synergy HTX with a black flat bottom plate (Ref# 3631) using 100 µL of culture.